USING CHEMICAL AND PROTEOMICS APPROACHES TO STUDY THE FUNCTIONS OF SIRT6 AND KRAS

A Dissertation

Presented to the Faculty of the Graduate School

of Cornell University

In Partial Fulfillment of the Requirements for the Degree of

Doctor of Philosophy

by

Xiaoyu Zhang

December 2017

USING CHEMICAL AND PROTEOMICS APPROACHES TO STUDY THE FUNCTIONS OF SIRT6 AND KRAS

Xiaoyu Zhang, Ph. D.

Cornell University 2017

Sir2 (silencing information regulator 2) family of enzymes (or sirtuins) are nicotinamide adenine dinucleotide (NAD^+)-dependent protein lysine deacylases and play a variety of roles in biological systems. SIRT6 is one of the seven mammalian sirtuins and has diverse biological functions such as maintaining genomic stability, controlling glucose homeostasis and suppressing tumor growth. Enzymatically, SIRT6 has been shown to have lysine deacetylation, lysine defatty-acylation and mono-adenosine diphosphate (ADP)-ribosyltransferase activities. However, the contribution of each activity to the various functions of SIRT6 is poorly understood.

In Chapter 2, I describe the dissection of functional contribution of the defatty-acylase activity of SIRT6 by utilizing a SIRT6 mutant (Gly60Ala), which has efficient defatty-acylase activity but no detectable deacetylase and mono-ADP-ribosyltransferase activities. Using this mutant, I found that SIRT6's defatty-acylase activity regulates the secretion of numerous proteins in mouse embryonic fibroblasts. Interestingly, SIRT6 defatty-acylase activity regulates the sorting of many ribosomal proteins into exosomes for secretion.

In Chapter 3, I found that SIRT6 defatty-acylase activity contributes to its tumor suppressor function. To identify SIRT6 defatty-acylation targets, I utilized a fatty acid reporter to metabolically label the proteome followed by affinity enrichment and mass spectrometry analysis. I found that R-Ras2 is a SIRT6 defatty-acylation target that accounts for its tumor suppressor function. Mechanistically, lysine fatty-acylation of

R-Ras2 promotes its plasma membrane localization and increases its interaction with PI3K. The increase in R-Ras2 and PI3K association leads to elevated Akt activation and increased cell proliferation.

In Chapter 4, I describe an interactome study of KRas4a and KRas4b, which led to the identification of many previously unknown KRas4a and KRas4b interacting proteins. Interestingly, I found that KRas4a interacts more with Raf1 than KRas4b does, which may contribute to the more anchorage-independent colony formation in KRas4a transformed NIH 3T3 cells than in KRas4b transformed NIH 3T3 cells. Moreover, mTOR was identified as a KRas4a/b interaction protein. Different from well-established mTORC1 and mTORC2, KRas4a/b forms a new mTOR complex without raptor or rictor in cells.

BIOGRAPHICAL SKETCH

Xiaoyu Zhang was born in Shenyang, China. He graduated and received a Bachelor's degree from Zhejiang University in 2008, majored in Pharmaceutical Science. His undergraduate research work was focused on isolation and characterization of natural products with NAD(P)H dehydrogenase-inducing activities. This work was conducted under the guidance of Prof. Zhongjun Ma. After graduation, he continued the research work in Prof. Zhongjun Ma's laboratory as a master student by studying naturally occurring electrophiles with chemopreventive activities. He received a Master's degree from Zhejiang University in 2011. He won Chu Kochen Scholarship in 2010 and Eli Lilly Asia Outstanding Graduate Thesis Award in 2011. In 2012, he began graduate study in Department of Chemistry and Chemical Biology at Cornell University and joined in Prof. Hening Lin's laboratory, where he studied sirtuins and Ras proteins. His thesis entitled "Using Chemical and Proteomics Approaches to Study the Functions of SIRT6 and KRas" was supervised by Prof. Hening Lin.

Dedicated to my newborn daughter, Chloe Jingxi Zhang.

Thank you for coming to this world.

There is no love greater than a parent’s love for their child.

ACKNOWLEDGMENTS

First, I am deeply grateful to my advisor, Prof. Hening Lin, for 5 years inspiration and motivation. None of my achievements would have been possible without his guidance, advice and support. Needless to say, he set a perfect example for me to love science, word hard, think deeply, and read broadly. His successful career also motivates me to move forward every day. I hope that one day I can make as deep impact in the chemical biology field as him.

I would also like to thank my committee, Prof. Richard Cerione and Prof. Maurine Linder, for providing me invaluable advice in the past 5 years. Prof. Cerione brings me to the world of extracellular vesicles, which leads to my first important publication. I have also learned a lot about Ras proteins and signaling transduction from his class 'Chemistry of signaling transduction'. Prof. Linder has given me lots of valuable suggestions and also provided me many useful resources when I conducted the research on protein lipidation. I feel very lucky that Prof. Cerione and Prof. Linder advised my thesis work. What I have learned from them will influence my research life for many years.

I would like to thank our lab manager Xuan Lu. Xuan is very responsible and has done a lot for the lab, making the whole lab always running well. Xuan is also a good friend of mine and helps me a lot outside the lab. I am truly thankful for her support and help.

I would like to thank all of my labmates, present and past. Specifically, I would like to thank Dr. Hong Jiang and Dr. Bin He. When I first joined the lab, they helped me adapt to the new environment. I also worked with them on my first project. I would like to thank Dr. Marc Antonyak from Prof. Cerione's lab, who taught me how to

isolate exosomes and microvesicles. I would like to thank David Kim for working with me in purifying and studying the enzymatic activities of sirtuins. It is a true pleasure to work with him. I would like to thank the rest of the Lin group members-Dr. Min Dong, Dr. Jing Hu, Dr. Qingjie Zhao, Dr. Colleen Kuemmel, Dr. Sushabhan Sadhukhan, Dr, Zhi Li, Dr. Ying-Ling Chiang, Dr. Ji Cao, Dr. Ian Price, Dr. Min Yang, Dr. Sha Li, Dr. Shuai Zhang, Dr. Chien-Sheng (Jason) Chen, Dr. Xiaoyang Su, Dr. Anita Zhu, Dr. Jonanthan Shrimp, Dr. Pornpun (Polly) Aramsangtienchai, Dr. Zhen Tong, Dr. Zhewang Lin, Ornella Nelson, Xiao Chen, Seth Miller, Nicole Spiegelman, Yugang Zhang, Miao Wang, Lu Zhang, Arash Latifkar, Jun Young (Nick) Hong, Tatsiana Kosciuk, Se In Son, Patricia Tolbert, Irma Fernandez, Sonny Komaniecki-for all their help.

I would like to thank my previous advisor Prof. Zhongjun Ma at Zhejiang University. If I did not meet Prof. Ma when I was an undergraduate student, I would not pursue my career in science. He guided me to my path in chemistry and biology.

I would like to thank my dear friends Zheqian Zhang and Shaowei Cui. When I first came to US, they helped me a lot to adapt to the new life. I could not imagine how difficult my first year would be without their help. I feel very lucky I have such good friends like them.

Finally, I would like to thank my parents, Junhui Guo and Longfu Zhang, for their support in everything throughout my life, and my wife, Hui Jing, for her love, understanding and support since I met her. Nothing is greater than being a family with them in my life.

TABLE OF CONTENTS

Biographical Sketch iii

Dedication iv

Acknowledgements v

Table of Contents vii

List of Figures ix

List of Tables xii

Chapter 1: An overview of SIRT6 and Ras proteins

Introduction of SIRT6 1

Enzymatic activities of SIRT6 1

Structural and biochemical features of SIRT6 4

Biological functions of SIRT6 and the underlying molecular mechanisms 7

Introduction of Ras proteins 9

RAS mutations in human cancer 11

Structural and biochemical features of Ras proteins 12

Signaling of Ras proteins 17

Summary of my thesis research 19

References 20

Chapter 2: Identifying the functional contribution of the defatty-acylase activity of SIRT6

Abstract 27

Introduction 28

Results and discussion 29

Methods 59

References 71

Chapter 3: SIRT6 regulates Ras-related protein R-Ras2 by lysine defatty-acylation

Abstract 74

Introduction 75

Results and discussion 76

Methods 94

References 102

Chapter 4: Global map of KRas4a and KRas4b interacting proteins

Abstract 106

Introduction 107

Results and discussion 110

Methods 135

References 141

Conclusions and Future Directions

Discussion 145

References 150

Appendix A: Permission for reproduction (Chapter 2) 151

Appendix B: Permission for reproduction (Chapter 3) 152

LIST OF FIGURES

1.1 NAD^+-dependent protein lysine deacylation reaction of SIRT6 2

1.2 Proposed mechanism of SIRT6 deacylation reaction 3

1.3 Proposed mechanism of SIRT6 mono-ADP-ribosyltransferase activity 3

1.4 Structure of human SIRT6 in complex with ADP-ribose (PDB: 3PKI) 5

1.5 Key hydrophobic residues in SIRT6 hydrophobic pocket (PDB: 3ZG6) that accommodate the myristoyl group 6

1.6 Ras superfamily of small GTPases act as binary molecular switches 11

1.7 Multiple sequence alignment of KRas4a (P01116), KRas4b (P01116-2), HRas (P01112), and NRas (P01111) 13

1.8 Structure of HRas in complex with GTP analog GppNHp (PDB: 5P21) 15

1.9 HRas crystal structure (PDB: 5P21) showing the positions of Ser17, Thr35, Gly12, Gly13, and Gln61 16

1.10 HRas and GAP complex showing the arginine finger (Arg789) on GAP (PDB: 1WQ1) 16

1.11 Proposed mechanism of GTP hydrolysis of HRas 17

1.12 Overview of Ras effector pathways 17

2.1 *In vitro* deacetylation and defatty-acylation activities of SIRT6 WT and mutants 30

2.2 *In vitro* defatty-acylase activities of SIRT6 WT and mutants on different fatty-acyl peptide substrates 31

2.3 *In vitro* deacylase activity assay using SIRT6 purified from HEK 293T cells 32

2.4 Steady-state kinetic study of SIRT6 WT and G60A on H3K9 myristoyl and H3K9 acetyl peptides 35

2.5 *In vitro* mono-ADP-ribosyltransferase activity assay of SIRT6 WT and

mutants 37

2.6 Mechanistic study on how SIRT6 G60A maintains defatty-acylation but loses deacetylation 38

2.7 The dissociation constants of SIRT6 WT and G60A for NAD^+ with or without 1 mM Ac-H3K9, and saturation binding curves of SIRT6 WT, S56Y, G60A, R65A and H133Y binding to NAD^+ 39

2.8 Measurement of SIRT6 WT, G60A and H133Y binding to NAD^+ using concentrators with 10 kDa cutoff membranes 40

2.9 In-cell validation of the deacetylase and defatty-acylase activities of SIRT6 WT and mutants 44

2.10 Identification of secreted proteins regulated by SIRT6 46

2.11 Analysis of secreted proteins by SILAC 48

2.12 Validation of secreted proteins that are regulated by SIRT6 52

2.13 In-gel fluorescence showing Alk14 labeling of endogenous COL5A1 and COL6A1 in *Sirt6* WT and KO MEFs 52

2.14 Sub-cellular localization of overexpressed SIRT6 WT, G60A and H133Y in *Sirt6* KO MEFs 53

2.15 SIRT6 defatty-acylase activity inhibits ribosomal protein sorting to the exosomes 55

3.1 Identification of defatty-acylation targets of SIRT6 that contribute to its function in cell proliferation 79

3.2 Validation of R-Ras2 as the defatty-acylation target of SIRT6 82

3.3 R-Ras2 is fatty-acylated on C-terminal lysine residues 84

3.4 Lysine fatty-acylation targets R-Ras2 to plasma membrane 87

3.5 SIRT6 defatty-acylase activity is required for regulating R-Ras2 lysine fatty-acylation and subcellular localization 88

3.6 Raf-RBD binding assay showed that both overexpressed and endogenous R-Ras2 did not bind Raf RBD-conjugated argarose beads 90

3.7 Lysine fatty-acylation of R-Ras2 activates PI3K-Akt pathway and promotes cell proliferation in MEFs 92

4.1 Identify KRas4a and 4b interacting proteins in HEK293T cells by SILAC and AP-MS 113

4.2 KRas4b interacts with v-ATPase a2 and eIF2Bδ through its C-terminal HVR116

4.3 KRas4a has more RAF1 interaction than KRas4b in cells 120

4.4 mTOR interacts with KRas4a and 4b 124

4.5 Identify KRas and mTOR binding region by DSSO crosslinker 127

4.6 KRas4a/b interact with mLST8 128

4.7 KRas4a/b and mTOR form a complex without of raptor and rictor 130

4.8 A proposed KRas4b-mTOR interaction model 133

4.9 HRas, KRas4a and KRas4b increase the phosphorylation of some well-studied mTORC1 and mTORC2 substrates to the similar extents 135

4.10 Purification of endogenous mTOR from HEK 293T cells 139

5.1 Identification of proteins that regulate the sorting of ribosomal proteins (RPs) into the exosomes by RNAi screening 147

5.2 Potential KRas4a/b effector proteins that server as GEFs for other small GTPases 149

LIST OF TABLES

1.1 Catalytic efficiencies of SIRT6 on different acyl peptides 6

2.1 The k_{cat}, K_m and k_{cat}/K_m values for SIRT6 WT and G60A demyristoylase and deacetylase activities 34

2.2 The list of secreted proteins (Group 1) that are regulated by SIRT6 49

2.3 The list of secreted proteins (Group 2, 3, 4) that are regulated by SIRT6 50

CHAPTER 1

AN OVERVIEW OF SIRT6 AND RAS PROTEINS

My thesis work is focused on demonstrating the physiological relevance of SIRT6 defatty-acylase activity, and investigating the novel signaling outputs of KRas4a and KRas4b. In this chapter, I review the research progress of SIRT6 and Ras proteins, including their enzymatic activities, structural and biochemical features, and biological functions.

Introduction of SIRT6

Sir2 (silencing information regulator 2) family of enzymes (or sirtuins) are a class of proteins that exist in bacteria, archaea, and eukaryotes and possess multiple enzymatic activities, including nicotinamide adenine dinucleotide (NAD^+)-dependent protein lysine deacylase and mono-ADP ribosyltransferase activities[1-10]. In mammals, there are seven sirtuins (SIRT1-7), they have different enzymatic activities, subcellular localizations, and biological functions[11-13]. Mammalian SIRT6 was initially reported as a NAD^+-dependent protein lysine deacetylase[1] and played important roles in maintaining genomic stability[14]. Later, numerous studies showed that SIRT6 has many other pivotal biological functions such as promoting DNA repair[15,16], regulating glucose homeostasis[17], suppressing tumorgenesis[18], and increasing lifespan[19,20]. SIRT6 knockout (KO) mice are born normally, but around 3 weeks after birth they develop lymphopenia, loss of subcutaneous fat, suffer from severe metabolic defects, and die before 4 weeks of age[14]. Clearly, SIRT6 has very important biological functions.

Enzymatic activities of SIRT6

SIRT6 was first characterized as a NAD^+-dependent histone deacetylase that targets

histone H3 lysine K9, K18, and K56[1,21-23]. Later studies showed that SIRT6 deacetylation targets also include non-histone proteins such as CtIP[16] and GCN5[24]. Recently, SIRT6 was found to possess lysine defatty-acylase activity that targets TNFα lysine K19, 20[8], suggesting that SIRT6 has multiple enzymatic activities. Similar to other sirtuins, SIRT6 utilizes NAD^+ for its deacylation reaction that yields deacylated peptide/protein product, *O*-acyl-ADP ribose and nicotinamide (**Figure 1.1**). Sirtuin-catalyzed deacylation is thought to undergo several different intermediates (**Figure 1.2**). In the first step, the acyl lysine residue attacks the anomeric carbon of ribose, generating nicotinamide and 1'-*O*-alkylamidate intermediate. In the second step, a catalytic histidine (His133 for SIRT6) serves as general base to deprotonate the 2'-hydroxyl group of ribose, which promotes an intramolecular nucleophilic attack and forms a 1',2'-cyclic ADP-ribose intermediate. The 1',2'-cyclic intermediate reacts with water and forms 2'-*O*-acyl-ADP ribose and 3'-*O*- acyl-ADP ribose as final products.

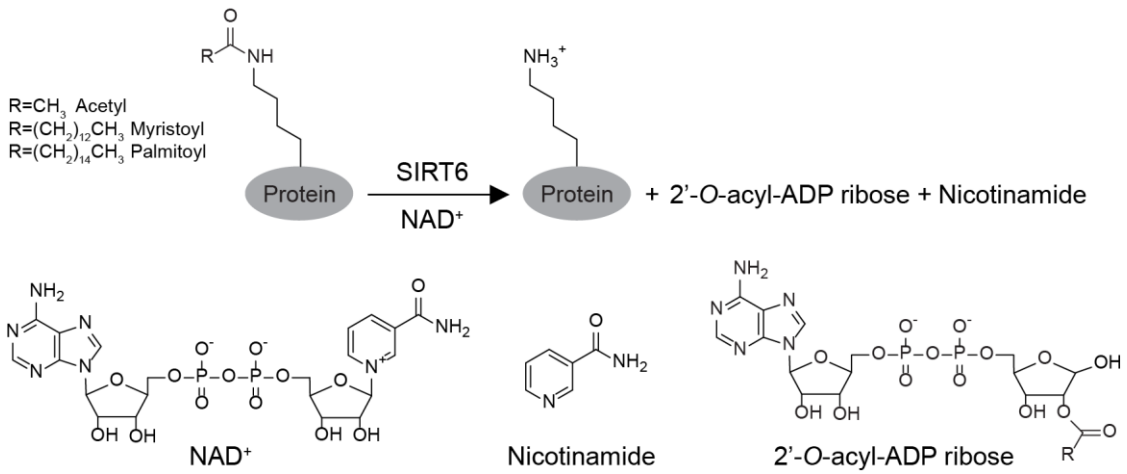

Figure 1.1. NAD^+-dependent protein lysine deacylation reaction of SIRT6.

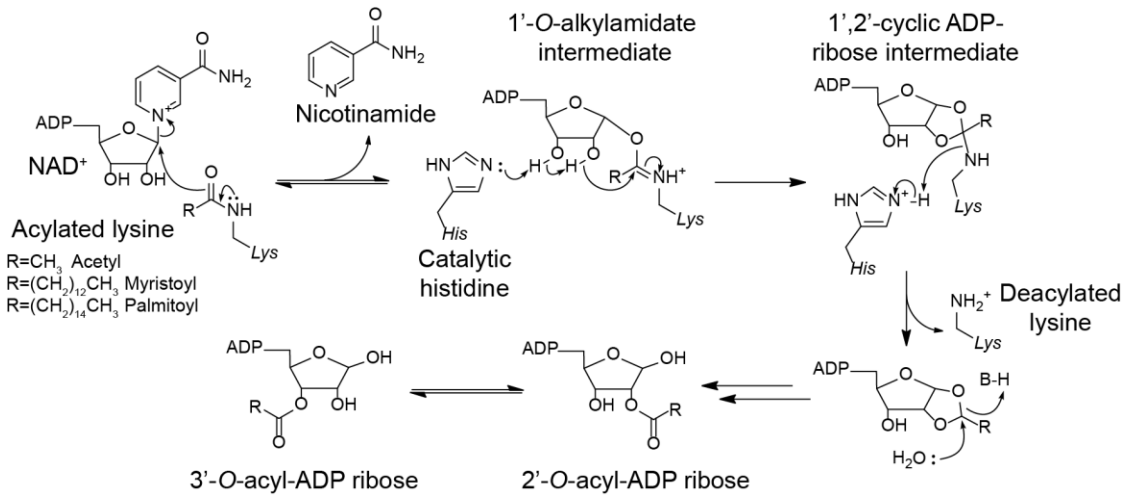

Figure 1.2. Proposed mechanism of SIRT6 deacylation reaction.

Besides lysine deacylase activities, SIRT6 was also reported to have mono-ART activity that targets itself, PARP1 and KAP1[15,25,26]. However, several *in vitro* studies showed that this activity is weak[27,28], suggesting that this activity could depend on specific substrates or conditions. Currently, biochemical studies that uncover the mechanism of SIRT6 mono-ART activity is still lacking, but it is thought to have the same mechanism as proteins from the poly-(ADP-ribose) polymerase family, with SIRT6 mediating the attack of nucleophilic amino acids to the anomeric carbon of the ribose, generating nicotinamide and mono-ADP-ribose covalently modified proteins (**Figure 1.3**). However, the identity of the nucleophilic amino acids is not known.

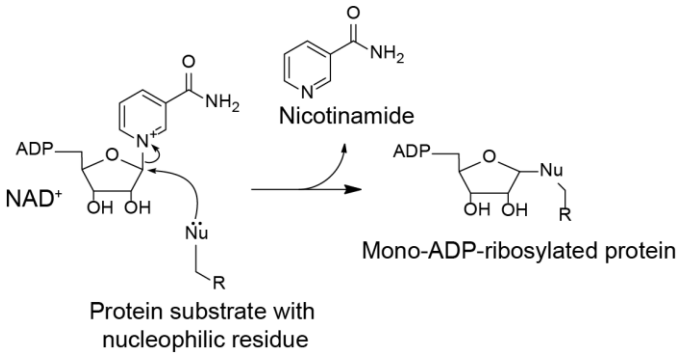

Figure 1.3. Proposed mechanism of SIRT6 mono-ADP-ribosyltransferase activity.

Structural and biochemical features of SIRT6

Human SIRT6 has 355 amino acids. It has a conserved catalytic core with N- and C-terminal extensions (NTE and CTE). Biochemical studies showed that NTE is important for both its catalytic activity and chromatin association, and CTE is required for proper nucleus localization[29].

Several crystal structures of SIRT6 were reported to provide important insights into the mechanism for its deacylase activity and substrate specificity. The first SIRT6 crystal structure at 2.0 Å resolution was reported in 2011[30]. Denu and coworkers used human SIRT6 (3-318) construct purified from *Escherichia coli* (*E.Coli*) for crystallization because it has higher yield (10-20 mg per liter) than full length protein without diminishing the deacetylase activity. Similar to other sirtuins, SIRT6 has two domains: a large Rossmann fold domain and a small Zn^{2+}-binding motif (**Figure 1.4**). The Rossmann fold domain (residues 25-128 and 191-266) consists of a six parallel β sheets surrounded by six α helices (two on one side and four on the other side). The Zn^{2+}-binding motif (residues 129-190) is structurally more variable and consists of three antiparallel β sheets and two loops. The two loops provide four cysteine residues that bind to Zn^{2+}. The Zn^{2+} in SIRT6 does not directly participate in catalysis and plays a structural role. The NAD^+ binding pocket is largely conserved between SIRT6 and other sirtuins. One interesting feature of SIRT6 structure is that SIRT6 can bind to NAD^+ without binding to acetylated substrate, which is different from other sirtuins that require peptide substrate binding prior to NAD^+ binding. Although there are many SIRT6 crystal structures reported, there is no SIRT6 crystal structure co-crystalized with acetyl peptide substrate. Indeed, in the first SIRT6 structure paper, the authors attempted to co-crystallize SIRT6 with acetyl H3K9 peptide and NAD^+ but did not observe the acetyl H3K9 peptide in SIRT6 structure[30], suggesting the weak binding

between SIRT6 and its acetyl substrate.

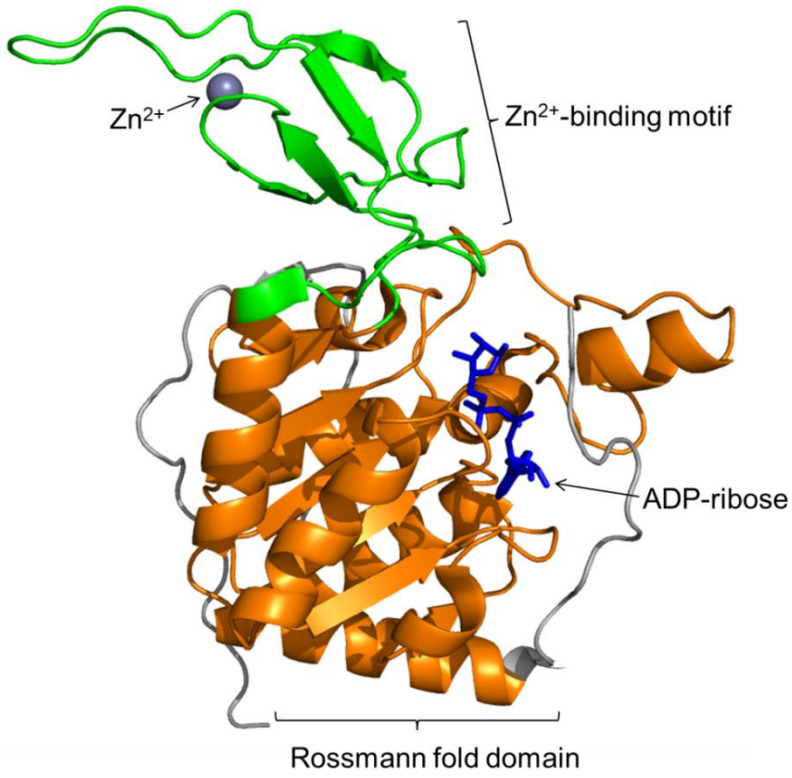

Figure 1.4. Structure of human SIRT6 in complex with ADP-ribose (PDB: 3PKI). *Green*, Zn^{2+} binding motif. *Orange*, Rossman fold domain. The image was made using PyMOL.

In 2013, our group reported that SIRT6 is a lysine defatty-acylase[8]. *In vitro* kinetic studies showed that SIRT6 can remove myristoyl and palmitoyl groups more efficiently than acetyl groups from lysine residue (**Table 1.1**). Co-crystal structure of SIRT6 with myristoyl H3K9 peptide and ADP-ribose reveals a large hydrophobic pocket near the active site. The accommodated myristoyl group forms van der Waals interactions with several hydrophobic residues in the pocket, including Ala 11, Pro 60, Phe 62, Trp 69, Pro 78, Phe 80, Phe 84, Val 113, Leu 130, Leu 184, and Ile 217

(**Figure 1.5**). This structure explains why SIRT6 is a better lysine defatty-acylase than lysine deacetylase *in vitro*-SIRT6 can bind fatty-acyl lysine much better, leading to decreased K_m values and thus increased catalytic efficiency (**Table 1.1**).

Table 1.1 Catalytic efficiencies of SIRT6 on different acyl peptides[8]

Acyl peptide	k_{cat} (s^{-1})	K_m (μM)	k_{cat}/K_m (s^{-1} M^{-1})
Acetyl H3K9	0.00396 ± 0.0006	810 ± 160	4.8
Myristoyl H3K9	0.00496 ± 0.0004	3.4 ± 0.9	1.4×10^3
Palmitoyl H3K9	0.00276 ± 0.0002	0.9 ± 0.4	3.0×10^3
Myristoyl TNFα K19	0.00206 ± 0.0002	2.4 ± 0.6	8.3×10^2
Myristoyl TNFα K20	0.00506 ± 0.0004	4.5 ± 1.1	1.1×10^3

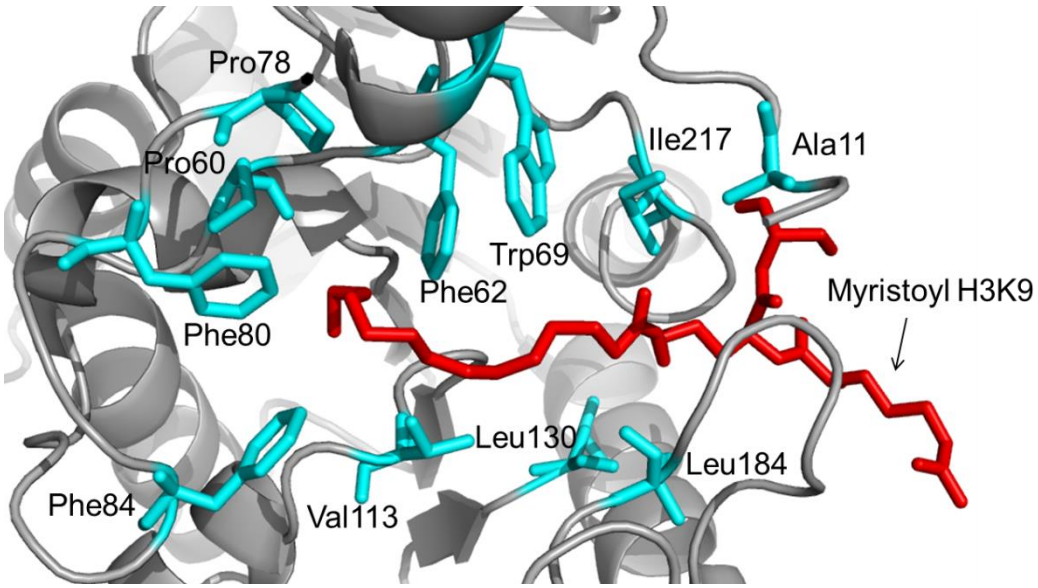

Figure 1.5. Key hydrophobic residues in SIRT6 hydrophobic pocket (PDB: 3ZG6) that accommodate the myristoyl group. The image was made using PyMOL.

The weak deacetylase activity of SIRT6 *in vitro* originally raised a concern about the physiological relevance of SIRT6's deacetylation *in vivo*. Two later studies

investigated this topic and found that SIRT6 deacetylase activity can be significantly enhanced by nucleosome or free fatty acids *in vitro*[31,32], suggesting the physiological relevance of SIRT6 deacetylation might depend on specific context. These findings are also consistent with other features of SIRT6. For example, SIRT6 has been characterized as a chromatin regulator, indicating that it needs to associate with nucleosome to exhibit histone deacetylation. In addition, the large hydrophobic pocket in SIRT6 may accommodate the free fatty acids, the binding of free fatty acids may induce a conformation change that allow it to bind acetyl peptide better, which may explain the activation effect of free fatty acids on SIRT6 deacetylation. Also, free fatty acids inhibit SIRT6 defatty-acylase activity[31], suggesting that free fatty acids may be important physiological molecules that switch SIRT6 to a lysine deacetylase. A recent study showed that nucleosome can activate SIRT6 defatty-acylase activity *in vitro*[33], suggesting that nucleosome and free fatty acids may use different mechanisms to activate SIRT6. Currently, there are still many questions to be addressed, such as how nucleosome and free fatty acids activate SIRT6 deacetylase activity, and why SIRT6 can only deacetylate histone H3K9, K18 and K56, but not other residues of histone H3 and other histones. Future structural studies may help answer these questions.

Biological functions of SIRT6 and the underlying molecular mechanisms

The diverse biological functions of SIRT6 were initially discovered from transgenic mice either deleting or overexpressing SIRT6. SIRT6 KO mice suffer from severe metabolic defects and develop lymphopenia, osteopenia and hypoglycemia[14]. They die around 4 weeks of age after birth[14]. Conversely, SIRT6 overexpression increases lifespan in male mice[20]. Neural-specific SIRT6 KO mice show postnatal growth retardation after birth and ultimately become obese at 6 months[34]. Hepatic-specific SIRT6 KO mice have increased low-density lipoprotein (LDL)-cholesterol, while

SIRT6 overexpression in high fat diet (HFD)-fed mice lowers LDL-cholesterol[35]. The mechanistic studies showed that SIRT6 regulates different signaling pathways through both deacetylase and defatty-acylase activities to achieve its diverse biological functions.

Silencing transcription. SIRT6 acts as a gene silencer by deacetylating histone H3K9, K18, and K56 at promoter regions that co-represses several transcriptional factors, including HIF-1α[17], Myc[18], c-Jun[36], FoxO3[35] and NF-κB[19]. Transcriptional suppression plays important roles in SIRT6's biological functions. For example, SIRT6 maintains glucose homeostasis by suppressing HIF-1α controlled transcription via H3K9 deacetylation[17]. SIRT6 acts as a tumor suppressor by suppressing MYC controlled transcription via H3K56 deacetylation[19].

DNA repair and genome stability. SIRT6 is a key player in DNA repair. It is reported that SIRT6 is important for both base excision repair (BER)[14] and DNA double-strand breaks (DSBs) repair[16]. Although the underlying mechanism of SIRT6's function in DNA repair is not fully understood, it is thought that SIRT6 promotes DNA end resection by deacetylating CtIP[16]. It is reported that SIRT6 also promotes DNA repair by mono-ADP-ribosylating PARP1 and increases PARP1 activity[15]. Another study suggests that SIRT6 recruits the chromatin remodeler SNF2H to DSBs and deacetylates H3K56, which serves as an early step in the DNA damage response[37]. Besides the role in DNA repair, SIRT6 is also known to maintain telomeric chromatin structure by deacetylating H3K9[1]. SIRT6 depletion causes telomere dysfunction with end-to-end chromosomal fusions, which further leads to the cellular senescence. At telomeric chromatin, SIRT6 stabilizes Werner syndrome ATP-dependent helicase (WRN) by deacetylating H3K9 and prevents replication-associated telomere defects.

Glucose and lipid homeostasis. SIRT6-deficient mice have increased glucose uptake and decreased insulin secretion[14,17], suggesting a crucial role of SIRT6 in glucose

homeostasis. It is found that SIRT6 suppresses glycolysis by repressing HIF-1α controlled transcription via H3K9 deacetylation[17]. SIRT6 also inhibits gluconeogenesis by different mechanisms. One study shows that SIRT6 interacts with Forkhead box protein O1 (FoxO1), a key transcription factor that activates gluconeogenesis. This interaction causes FoxO1 deacetylation and export to the cytoplasm to be inactive[38]. Another study finds that SIRT6 activates the acetyltransferase GCN5, likely by deacetylating it on K549, which further induces acetylation on its substrate peroxisome proliferator-activated receptor γ coactivator 1-α (PGC-1α). PGC-1α is a transcriptional co-activator that regulates the genes involved in gluconeogenesis, and lysine acetylation is known to suppress PGC-1α activity[24]. In addition to regulating glucose metabolism, SIRT6 also plays important roles in lipid homeostasis. SIRT6 overexpression in mice results in reduced cholesterol and triglyceride levels. Mechanistically, SIRT6 represses lipogenic transcription factors Sterol regulatory element binding proteins 1 and 2 (SREBP1 and SREBP2) by both suppressing SREBP1/2 transcriptions and inhibiting their cleavage[39].

Defatty-acylation regulated biological functions. Compared with the biological functions attributed by SIRT6 deacetylase activity, the cellular functions attributed by SIRT6's defatty-acylation have just started to be uncovered. No other defatty-acylation substrate or function of SIRT6 was known before my thesis work. One of the major focuses of my thesis work was to uncover new functions and new substrates for the defatty-acylation activity of SIRT6.

Introduction of Ras proteins

The Ras superfamily of small guanosine triphosphatases (GTPases) consists of over 150 members in humans[40]. There are five major branches of the Ras superfamily on the basis of their sequence and functional similarities: Ras, Rho, Rab, Ran, and Arf.

These proteins serve as essential players for numerous biological processes, including cell growth, membrane trafficking, nuclear export/import, and cytoskeletal dynamics[40,41]. Small GTPases act as binary switches. They are active in the guanosine triphosphate (GTP)-bound state and inactive in the guanosine diphosphate (GDP)-bound state (**Figure 1.6**). Guanine nucleotide exchange factors (GEFs) promote the exchange of GDP with GTP, thereby serving as the activators of small GTPases[42]. On the other hand, small GTPases have very low intrinsic GTP hydrolysis activity, but it can be significantly accelerated by GTPase-activating proteins (GAPs)[42]. In the GTP-bound state, small GTPases can interact with and activate different effector proteins (**Figure 1.6**), which contribute to different functional outputs. In addition, Ras superfamily of small GTPases are regulated by diverse post-translational modifications (PTMs), such as cysteine farnesylation, cysteine palmitoylation, and serine phosphorylation. These PTMs play important roles in both subcellular localizations and signaling transduction[41]. As the founding members of Ras superfamily of small GTPases, Ras proteins (HRas, NRas, KRas4a, and KRas4b) have been the subject of intense research because of their high mutation rates and relevance in human cancer[43]. Activated Ras proteins interact with distinct downstream effector proteins, such as Raf, phosphatidylinositol 3-kinase (PI3K), and Ral guanine nucleotide dissociation stimulator (RalGDS)[44]. These effector proteins regulate diverse cellular functions such as cell proliferation, survival, and differentiation[44].

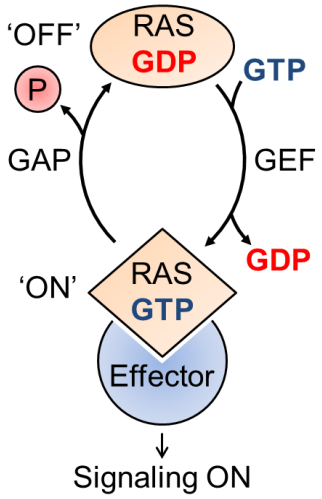

Figure 1.6. Ras superfamily of small GTPases act as binary molecular switches.

RAS mutations in human cancer

In humans, there are three RAS genes (HRAS, NRAS, and KRAS) encoding four Ras proteins: HRas, NRas, KRas4a, and KRas4b (KRas4a and KRas4b are two alternative splice variants from KRAS gene). They constitute the most frequently mutated oncogenes in human cancer[43]. RAS constitutively active mutations are found in 60-90% of pancreatic cancer, 36% of colorectal cancer, and 19% of lung cancer[45,46]. Overall, approximately 30% of all tumor samples have RAS mutations (COSMIC, the Catalogue Of Somatic Mutations In Cancer). It is well established that mutant Ras proteins are cancer drivers. Additional generic mutations (such as p53 and APC) are often found to cooperate with mutant Ras to fully transform cells[47,48]. Once the tumor is established, continuous expression of mutant Ras proteins is also important for maintaining the tumor[49].

RAS genes have different mutation frequencies and distributions[45]. Among all RAS-driven cancers, KRAS is the most frequently mutated RAS (86%), followed by NRAS (11%) and HRAS (3%) (COSMIC database). Pancreatic, colon, and rectal cancers have been found to have high KRAS mutation rate. Specifically, pancreatic ductal

adenocarcinoma (PDAC), which accounts for ~90% of all pancreatic cancers, have almost 100% KRAS mutations. Lung adenocarcinoma (LAC), which accounts for one third of all lung cancers, also possesses almost 100% KRAS mutations. Conversely, NRAS is the most frequently mutated RAS in cutaneous melanomas (94%) and acute myelogenous leukaemias (AML, 59%). Although HRAS is the least frequently mutated RAS, it has been shown that in bladder and head and neck squamous cell carcinomas (HNSCC), HRAS mutations are predominant (57% in bladder cancer and 86% in HNSCC).

RAS mutation usually occurs on a single amino acid. 98% of these mutations are found on one of three residues: Gly12, Gly13, and Gln61. These mutations block GAP-mediated (Gly12 and Gly13 mutations) or Ras intrinsic (Gln61 mutation) GTP hydrolysis, resulting in GTP-locked state of Ras proteins[50]. Gly12 mutation is mainly found on KRAS and HRAS, while Gln61 mutation is predominant on NRAS. For Gly12 mutation, the substituted residues differ in different cancers. For example, Gly12Asp (G12D) is the predominant mutant in PDAC, Gly12-Cys (G12C) is the predominant mutation in non-small cell lung cancer (NSCLC)[43].

Structural and biochemical features of Ras proteins

Ras proteins have a highly conserved catalytic domain (residues 1-166) and C-terminal hypervariable region (HVR, residues 167-189 on HRas, NRas and KRas4a, residues 167-188 on KRas4b). The catalytic domains of four Ras proteins share high sequence identity (89%), while the C-terminal HVR have low sequence identity (8%) (**Figure 1.7**). The C-termini of all Ras proteins end with a CAAX motif (C, cysteine; A, aliphatic amino acid; X, any amino acid). After synthesis on ribosomes, Ras proteins undergo a three-step processing on the CAAX motif to form mature Ras proteins. The cysteine residue on the CAAX motif is first modified by a C15 farnesyl

isoprenoid lipid (farnesylation), which is catalyzed by cytosolic farnesyltransferase (FTase).Then RAS-converting enzyme 1 (RCE1) catalyzes the proteolytic removal of the AAX tripeptide. Finally, isoprenylcysteine methyltransferase (ICMT) catalyzes carboxylmethylation of the newly formed C-terminal farnesylated cysteine[41]. Cysteine farnesylation of Ras proteins is important for membrane targeting[41]. However, biochemical studies suggest that farnesylation itself cannot provide enough binding affinities to fully target membranes[51,52]. A second membrane targeting signal is needed. HRas, NRas, and KRas4a utilize cysteine palmitoylation in the HVR as the second membrane targeting signal[53,54], while KRas4b is thought to use a poly-basic lysine cluster in the HVR as the second membrane targeting signal[55].

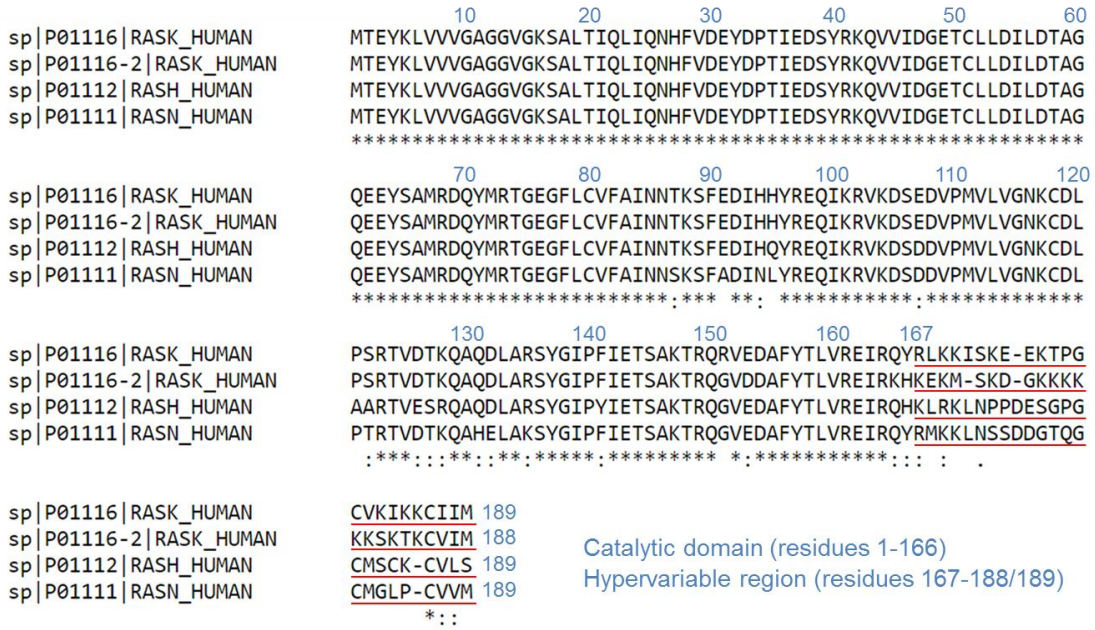

Figure 1.7. Multiple sequence alignment of KRas4a (P01116), KRas4b (P01116-2), HRas (P01112), and NRas (P01111). Alignment was made using Clustal Omega.

The first Ras structure (HRas) was reported in 1988[56], which showed HRas catalytic domain in complex with GDP. Later, several papers reported HRas catalytic domains

in complex with a GTP analog GppNHp (5'-Guanylyl imidodiphosphate) (**Figure 1.8**), thus providing more structural information of Ras proteins[57-59]. Currently, there are many reported Ras protein structures, including different Ras mutants and Ras in complex with different effector proteins[59-62]. However, there is only one reported crystal structure of NRas (PDB: 3CON) and no reported KRas4a structure. Of note, most crystal structures of Ras proteins are for catalytic domains only, because the C-terminal HVR is too flexible to show electron density. Recently, the first crystal structure of full-length KRas4b protein was reported (PDB: 5TAR)[63]. The full-length KRas4b was co-crystalized with phosphodiesterase-δ (PDEδ), which has been reported to bind to farnesyl group on Ras proteins and stabilize them[64].

The crystal structures of HRas reveal three functional regions that serve as binding sites for GTP/GDP, Mg^{2+}, and effector proteins: P-loop (residues 10-17), switch I (residues 30-38), and switch II (residues 59-76) (**Figure 1.8**). These three regions have 100% sequence identity across the four Ras proteins. Switch I and II are also the regions that change conformation during GDP-GTP cycling, therefore contributing to the effector binding. The Mg^{2+} is coordinated with oxygen atoms of the β- and γ-phosphates and also interacts with Thr35 (from switch I) and Ser17 (from P-loop) (**Figure 1.9**).

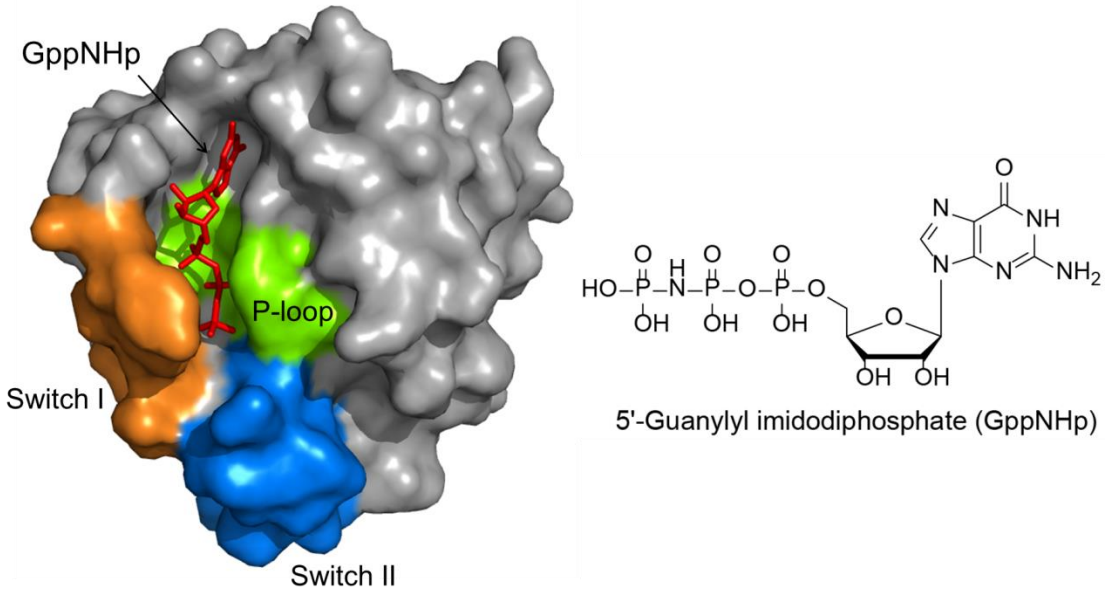

Figure 1.8. Structure of HRas in complex with GTP analog GppNHp (PDB: 5P21). *Green*, P-loop (residues 10-17); *orange*, switch I (residues 30-38); *blue*, switch II (residues 59-76). The images were made using PyMOL.

Biochemical and structure studies have shown that mutation of Ser17 to Asn (S17N) abolishes Mg^{2+} binding capacity of Ras protein (and thus nucleotide binding capacity) and therefore serves as a dominant negative control to study Ras signaling and functions[65]. Two of the three most frequently oncogenic mutated residues, Gly12 and Gly13, are located in the P-loop, while another frequently mutated residue Gln61 is located in the switch II region (**Figure 1.9**). The catalytic arginine finger of GAP is placed adjacent to Gly12/13 to stabilize the α- and β-phosphates of GTP to promote GTP hydrolysis[66,67] (**Figure 1.10**). Mutation of Gly12 or Gly13 to any residue other than proline would sterically block the access of GAP arginine finger to GTP and therefore lock Ras proteins in the GTP-bound state. Gln61 is the catalytic amino acid that positions the water molecule for attacking γ-phosphate (**Figure 1.11**), it also helps to stabilize the transition state of GTP hydrolysis reaction[68]. Mutation of Q61 would

block intrinsic and GAP-mediated GTP hydrolysis[67].

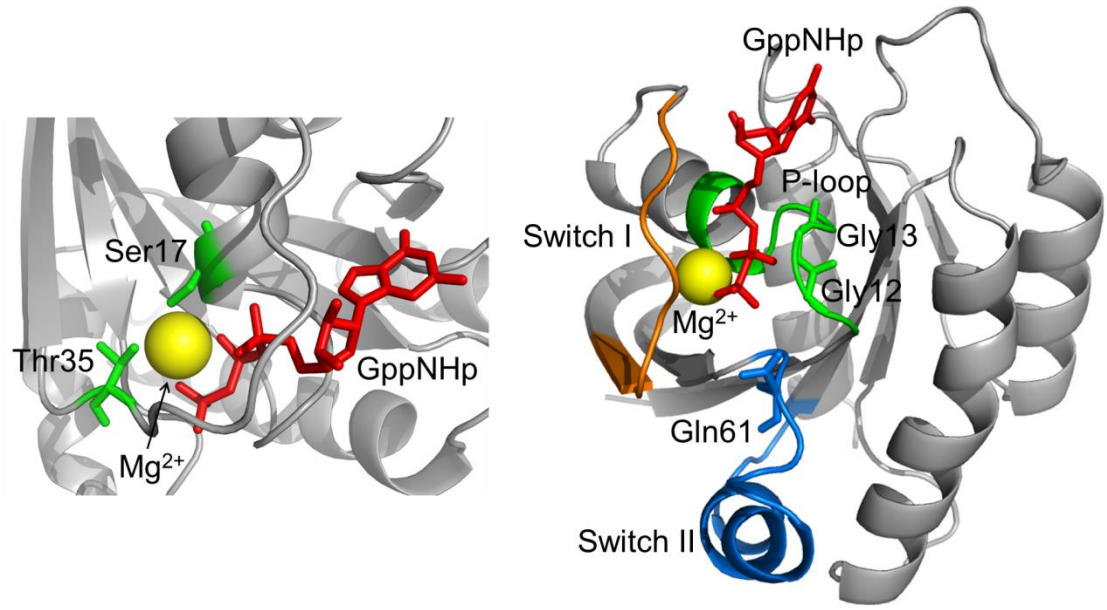

Figure 1.9. HRas crystal structure (PDB: 5P21) showing the positions of Ser17, Thr35, Gly12, Gly13, and Gln61. The images were made using PyMOL.

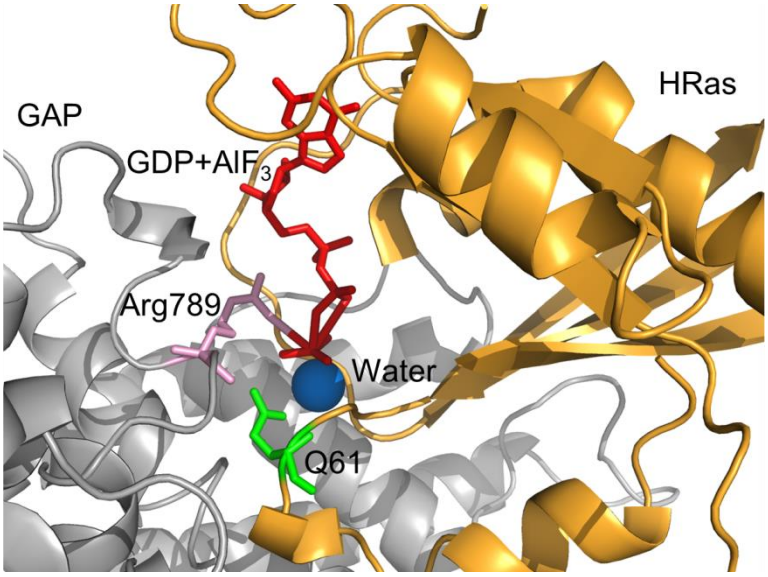

Figure 1.10. HRas and GAP complex showing the arginine finger (Arg789) on GAP (PDB: 1WQ1). The images were made using PyMOL.

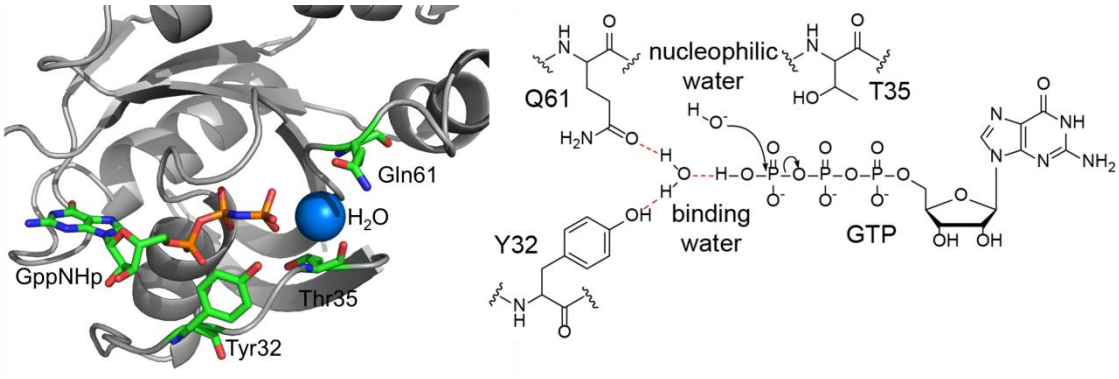

Figure 1.11. Proposed mechanism of GTP hydrolysis of HRas. The images were made using PyMOL (PDB: 5P21).

Signaling of Ras proteins

Ras proteins are known to regulate diverse signaling pathways by interacting with different effector proteins, including Raf, PI3K, and RalGDS (**Figure 1.12**). All reported Ras effector proteins share a conserved Ras binding domain (RBD). Biochemical studies show that GTP-binding induces a conformational change on switch I and allows Ras-GTP to strongly interact with RBD with high affinity (K_d value is in the range of 0.01-3 μM)[69].

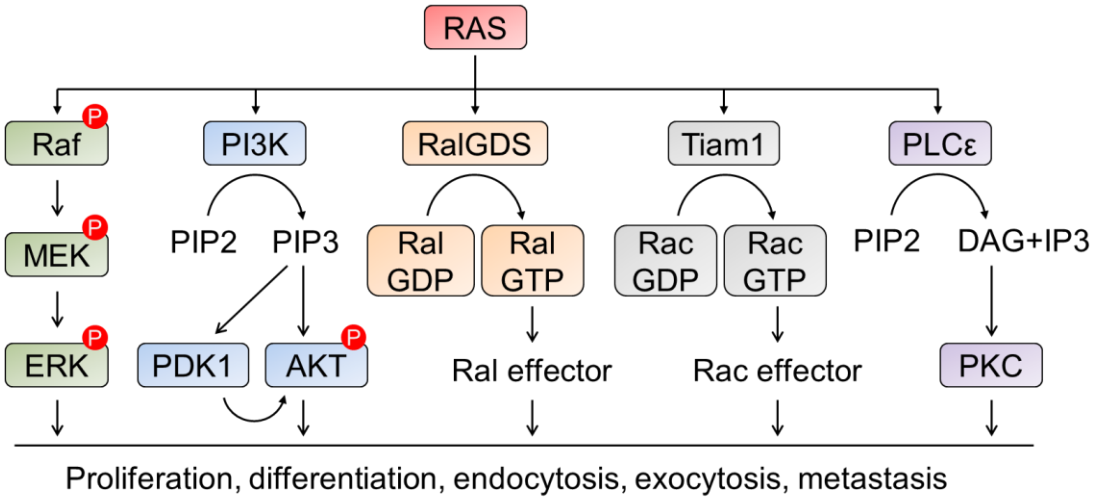

Figure 1.12. Overview of Ras effector pathways.

Ras-Raf-MEK-ERK pathway. The first well-established Ras signaling pathway is Ras-Raf-MEK-ERK pathway. In mammals, Raf family contains three proteins: A-Raf, B-Raf and C-Raf (also known as Raf1), all of which have been reported to bind GTP-loaded Ras proteins[70,71]. Early studies showed that C-Raf contains a RBD (residues 55-131) that binds to GTP-bound HRas[70,71]. The binding between Ras and Raf recruits Raf to the membrane and also promotes Raf dimerization, which is the active form of B-Raf and C-Raf. Activated Raf further phosphorylates and activates its substrate MEK1/2, and activated MEK1/2 phosphorylates and activates ERK1/2. Active ERK1/2 is the kinase that phosphorylates a number of transcription factors, which play important roles in diverse cellular processes, such as cell cycle progression, differentiation, protein translation, and evasion from cell death[72]. One well studied ERK substrate is transcription factor E26 oncogene homology 1-like gene 1 (ELK-1), ERK phosphorylates and activates ELK-1, leading to increased cell proliferation[73].

Ras-PI3K-Akt pathway. After the discovery of the Ras-Raf-MEK-ERK pathway, more effector pathways of Ras proteins were discovered. Phosphatidylinositol 3-kinase (PI3K) is a heterodimer that comprises a p110 catalytic subunit and a p85 regulatory subunit[74]. The p110 catalytic subunit is highly conserved among different classes of PI3K proteins and contains a RBD, which binds GTP-bound Ras. Several biochemical studies show that PI3K can directly bind to Ras in a GTP-dependent manner[75,76]. The binding between PI3K and Ras is weaker than that between Raf and Ras. The K_d value for PI3Kγ-HRas-GppNHp binding is 3.2 ± 0.5 μM[61] (The K_d value for RafRBD-HRas-GppNHp binding is 0.018 μM[77]). The binding of GTP-bound Ras to PI3K leads to the recruitment of PI3K to the plasma membrane, where it converts phosphatidylinositol-4,5-bisphosphate (PIP2) to phosphatidylinositol-3,4,5-bisphosphate (PIP3). The newly formed PIP3 recruits both 3-phosphoinositide-

dependent kinase 1 (PDK1) and Akt to the plasma membrane, where PDK1 phosphorylates and activates Akt. Activated Akt can further activate mammalian target of rapamycin (mTOR) by phosphorylating its substrate tuberous sclerosis proteins TSC1/2, which is the GAP of another GTPase Rheb. The activated mTOR then increases protein translation and thus promotes cell survival and proliferation.

Ras-RalGDS-Ral pathway. Ral guanine nucleotide dissociation stimulator (RalGDS) is another well studied Ras effector protein that mediates Ras-driven tumor formation[78-80]. RBD is located at the C-terminus of RalGDS which serves as the binding site for Ras proteins. It is thought that RalGDS RBD and Raf RBD interact with the similar regions on Ras proteins, suggesting that they may compete for binding to Ras proteins. RalGDS is the GEF of another two small GTPases, RalA and RalB. After RalA and RalB are activated by RalGDS, they can further interact with and activate their effectors, such as Sec5[81,82], RalBP1[83] and ZONAB[84]. These effector proteins regulate a number of biological functions, such as endocytosis, exocytosis, and metastasis[81,84,85].

Other effector proteins. Other Ras effector proteins also play important roles in Ras-mediated biological functions (**Figure 1.12**). Some effector proteins are GEFs for other Ras family proteins, such as T cell lymphoma invasion and metastasis 1 (Tiam1), a GEF for Rac GTPases[86], and Ras and Rab interactor (RIN), a GEF for Rab GTPase[87]. Phospholipase C-ε (PLCε) is another reported Ras effector protein[88], it converts PIP2 to inositol triphosphate (IP3) and diacylglycerol (DAG). IP3 interacts with its receptor on the endoplasmic reticulum (ER), which releases calcium to the cytosol[89]. DAG recruits and activates protein kinase C (PKC), which plays important roles in several signaling cascades[90].

Summary of my thesis research

SIRT6 was initially identified as a NAD^+-dependent lysine deacetylase. This activity has been widely studied in the past decade. In contrast, SIRT6 lysine defatty-acylase is a newly discovered enzymatic activity and its physiological relevance is still under appreciated. Investigating the function of SIRT6's lysine defatty-acylation activity and dissecting the functional contributions of SIRT6 deacetylase and defatty-acylase activities is the focus of my thesis work, which will be discussed in Chapter 2 and 3.

My work on SIRT6 also led me to the Ras family of proteins. Among four Ras proteins, KRas has been well established as a tumor driver and its signaling and biological functions are also widely studied. However, most studies of KRas focus on one of its isoforms, KRas4b, and the biological significance of the other isoform KRas4a is still poorly understood. I have investigated and compared the signaling and biological functions of KRas4a and KRas4b by studying the state-dependent KRas4a and KRas4b interactome, which will be discussed in Chapter 4.

REFERENCES

1 Michishita, E. *et al.* SIRT6 is a histone H3 lysine 9 deacetylase that modulates telomeric chromatin. *Nature* **452**, 492-496, doi:10.1038/nature06736 (2008).

2 Rack, J. G. *et al.* Identification of a Class of Protein ADP-Ribosylating Sirtuins in Microbial Pathogens. *Molecular cell* **59**, 309-320, doi:10.1016/j.molcel.2015.06.013 (2015).

3 Barber, M. F. *et al.* SIRT7 links H3K18 deacetylation to maintenance of oncogenic transformation. *Nature* **487**, 114-118, doi:10.1038/nature11043 (2012).

4 Du, J. *et al.* Sirt5 is a NAD-dependent protein lysine demalonylase and desuccinylase. *Science* **334**, 806-809, doi:10.1126/science.1207861 (2011).

5 Haigis, M. C. *et al.* SIRT4 inhibits glutamate dehydrogenase and opposes the effects of calorie restriction in pancreatic beta cells. *Cell* **126**, 941-954, doi:10.1016/j.cell.2006.06.057 (2006).

6 Hirschey, M. D. *et al.* SIRT3 regulates mitochondrial fatty-acid oxidation by reversible enzyme deacetylation. *Nature* **464**, 121-125, doi:10.1038/nature08778 (2010).

7 Imai, S., Armstrong, C. M., Kaeberlein, M. & Guarente, L. Transcriptional silencing and longevity protein Sir2 is an NAD-dependent histone deacetylase. *Nature* **403**, 795-800, doi:10.1038/35001622 (2000).

8 Jiang, H. *et al.* SIRT6 regulates TNF-alpha secretion through hydrolysis of long-chain fatty acyl lysine. *Nature* **496**, 110-113, doi:10.1038/nature12038 (2013).
9 North, B. J., Marshall, B. L., Borra, M. T., Denu, J. M. & Verdin, E. The human Sir2 ortholog, SIRT2, is an NAD+-dependent tubulin deacetylase. *Molecular cell* **11**, 437-444 (2003).
10 Tong, Z. *et al.* SIRT7 Is Activated by DNA and Deacetylates Histone H3 in the Chromatin Context. *ACS chemical biology* **11**, 742-747, doi:10.1021/acschembio.5b01084 (2016).
11 Nakagawa, T. & Guarente, L. SnapShot: sirtuins, NAD, and aging. *Cell metabolism* **20**, 192-192 e191, doi:10.1016/j.cmet.2014.06.001 (2014).
12 Guarente, L. Franklin H. Epstein Lecture: Sirtuins, aging, and medicine. *The New England journal of medicine* **364**, 2235-2244, doi:10.1056/NEJMra1100831 (2011).
13 Herskovits, A. Z. & Guarente, L. Sirtuin deacetylases in neurodegenerative diseases of aging. *Cell research* **23**, 746-758, doi:10.1038/cr.2013.70 (2013).
14 Mostoslavsky, R. *et al.* Genomic instability and aging-like phenotype in the absence of mammalian SIRT6. *Cell* **124**, 315-329, doi:10.1016/j.cell.2005.11.044 (2006).
15 Mao, Z. *et al.* SIRT6 promotes DNA repair under stress by activating PARP1. *Science* **332**, 1443-1446, doi:10.1126/science.1202723 (2011).
16 Kaidi, A., Weinert, B. T., Choudhary, C. & Jackson, S. P. Human SIRT6 promotes DNA end resection through CtIP deacetylation. *Science* **329**, 1348-1353, doi:10.1126/science.1192049 (2010).
17 Zhong, L. *et al.* The histone deacetylase Sirt6 regulates glucose homeostasis via Hif1alpha. *Cell* **140**, 280-293, doi:10.1016/j.cell.2009.12.041 (2010).
18 Sebastian, C. *et al.* The histone deacetylase SIRT6 is a tumor suppressor that controls cancer metabolism. *Cell* **151**, 1185-1199, doi:10.1016/j.cell.2012.10.047 (2012).
19 Kawahara, T. L. *et al.* SIRT6 links histone H3 lysine 9 deacetylation to NF-kappaB-dependent gene expression and organismal life span. *Cell* **136**, 62-74, doi:10.1016/j.cell.2008.10.052 (2009).
20 Kanfi, Y. *et al.* The sirtuin SIRT6 regulates lifespan in male mice. *Nature* **483**, 218-221, doi:10.1038/nature10815 (2012).
21 Michishita, E. *et al.* Cell cycle-dependent deacetylation of telomeric histone H3 lysine K56 by human SIRT6. *Cell cycle* **8**, 2664-2666, doi:10.4161/cc.8.16.9367 (2009).
22 Tasselli, L. *et al.* SIRT6 deacetylates H3K18ac at pericentric chromatin to prevent mitotic errors and cellular senescence. *Nature structural & molecular biology* **23**, 434-440, doi:10.1038/nsmb.3202 (2016).
23 Yang, B., Zwaans, B. M., Eckersdorff, M. & Lombard, D. B. The sirtuin SIRT6 deacetylates H3 K56Ac in vivo to promote genomic stability. *Cell cycle* **8**, 2662-2663, doi:10.4161/cc.8.16.9329 (2009).
24 Dominy, J. E., Jr. *et al.* The deacetylase Sirt6 activates the acetyltransferase GCN5 and suppresses hepatic gluconeogenesis. *Molecular cell* **48**, 900-913,

doi:10.1016/j.molcel.2012.09.030 (2012).
25 Van Meter, M. *et al.* SIRT6 represses LINE1 retrotransposons by ribosylating KAP1 but this repression fails with stress and age. *Nature communications* **5**, 5011, doi:10.1038/ncomms6011 (2014).
26 Liszt, G., Ford, E., Kurtev, M. & Guarente, L. Mouse Sir2 homolog SIRT6 is a nuclear ADP-ribosyltransferase. *The Journal of biological chemistry* **280**, 21313-21320, doi:10.1074/jbc.M413296200 (2005).
27 Kugel, S. *et al.* Identification of and Molecular Basis for SIRT6 Loss-of-Function Point Mutations in Cancer. *Cell reports* **13**, 479-488, doi:10.1016/j.celrep.2015.09.022 (2015).
28 Du, J., Jiang, H. & Lin, H. Investigating the ADP-ribosyltransferase activity of sirtuins with NAD analogues and 32P-NAD. *Biochemistry* **48**, 2878-2890, doi:10.1021/bi802093g (2009).
29 Tennen, R. I., Berber, E. & Chua, K. F. Functional dissection of SIRT6: identification of domains that regulate histone deacetylase activity and chromatin localization. *Mechanisms of ageing and development* **131**, 185-192, doi:10.1016/j.mad.2010.01.006 (2010).
30 Pan, P. W. *et al.* Structure and biochemical functions of SIRT6. *The Journal of biological chemistry* **286**, 14575-14587, doi:10.1074/jbc.M111.218990 (2011).
31 Feldman, J. L., Baeza, J. & Denu, J. M. Activation of the protein deacetylase SIRT6 by long-chain fatty acids and widespread deacylation by mammalian sirtuins. *The Journal of biological chemistry* **288**, 31350-31356, doi:10.1074/jbc.C113.511261 (2013).
32 Gil, R., Barth, S., Kanfi, Y. & Cohen, H. Y. SIRT6 exhibits nucleosome-dependent deacetylase activity. *Nucleic acids research* **41**, 8537-8545, doi:10.1093/nar/gkt642 (2013).
33 Wang, W. W., Zeng, Y., Wu, B., Deiters, A. & Liu, W. R. A Chemical Biology Approach to Reveal Sirt6-targeted Histone H3 Sites in Nucleosomes. *ACS chemical biology* **11**, 1973-1981, doi:10.1021/acschembio.6b00243 (2016).
34 Schwer, B. *et al.* Neural sirtuin 6 (Sirt6) ablation attenuates somatic growth and causes obesity. *Proc Natl Acad Sci U S A* **107**, 21790-21794, doi:10.1073/pnas.1016306107 (2010).
35 Tao, R., Xiong, X., DePinho, R. A., Deng, C. X. & Dong, X. C. FoxO3 transcription factor and Sirt6 deacetylase regulate low density lipoprotein (LDL)-cholesterol homeostasis via control of the proprotein convertase subtilisin/kexin type 9 (Pcsk9) gene expression. *The Journal of biological chemistry* **288**, 29252-29259, doi:10.1074/jbc.M113.481473 (2013).
36 Sundaresan, N. R. *et al.* The sirtuin SIRT6 blocks IGF-Akt signaling and development of cardiac hypertrophy by targeting c-Jun. *Nat Med* **18**, 1643-1650, doi:10.1038/nm.2961 (2012).
37 Toiber, D. *et al.* SIRT6 recruits SNF2H to DNA break sites, preventing genomic instability through chromatin remodeling. *Molecular cell* **51**, 454-468, doi:10.1016/j.molcel.2013.06.018 (2013).
38 Zhang, P. *et al.* Tumor suppressor p53 cooperates with SIRT6 to regulate

gluconeogenesis by promoting FoxO1 nuclear exclusion. *Proc Natl Acad Sci U S A* **111**, 10684-10689, doi:10.1073/pnas.1411026111 (2014).
39 Elhanati, S. *et al.* Multiple regulatory layers of SREBP1/2 by SIRT6. *Cell reports* **4**, 905-912, doi:10.1016/j.celrep.2013.08.006 (2013).
40 Wennerberg, K., Rossman, K. L. & Der, C. J. The Ras superfamily at a glance. *Journal of cell science* **118**, 843-846, doi:10.1242/jcs.01660 (2005).
41 Ahearn, I. M., Haigis, K., Bar-Sagi, D. & Philips, M. R. Regulating the regulator: post-translational modification of RAS. *Nature reviews. Molecular cell biology* **13**, 39-51, doi:10.1038/nrm3255 (2011).
42 Vigil, D., Cherfils, J., Rossman, K. L. & Der, C. J. Ras superfamily GEFs and GAPs: validated and tractable targets for cancer therapy? *Nature reviews. Cancer* **10**, 842-857, doi:10.1038/nrc2960 (2010).
43 Cox, A. D., Fesik, S. W., Kimmelman, A. C., Luo, J. & Der, C. J. Drugging the undruggable RAS: Mission possible? *Nature reviews. Drug discovery* **13**, 828-851, doi:10.1038/nrd4389 (2014).
44 Mitin, N., Rossman, K. L. & Der, C. J. Signaling interplay in Ras superfamily function. *Current biology : CB* **15**, R563-574, doi:10.1016/j.cub.2005.07.010 (2005).
45 Prior, I. A., Lewis, P. D. & Mattos, C. A comprehensive survey of Ras mutations in cancer. *Cancer research* **72**, 2457-2467, doi:10.1158/0008-5472.CAN-11-2612 (2012).
46 Ryan, D. P., Hong, T. S. & Bardeesy, N. Pancreatic adenocarcinoma. *The New England journal of medicine* **371**, 2140-2141, doi:10.1056/NEJMc1412266 (2014).
47 Hingorani, S. R. *et al.* Trp53R172H and KrasG12D cooperate to promote chromosomal instability and widely metastatic pancreatic ductal adenocarcinoma in mice. *Cancer cell* **7**, 469-483, doi:10.1016/j.ccr.2005.04.023 (2005).
48 Haigis, K. M. *et al.* Differential effects of oncogenic K-Ras and N-Ras on proliferation, differentiation and tumor progression in the colon. *Nature genetics* **40**, 600-608, doi:10.1038/ng.115 (2008).
49 Singh, A. *et al.* A gene expression signature associated with "K-Ras addiction" reveals regulators of EMT and tumor cell survival. *Cancer cell* **15**, 489-500, doi:10.1016/j.ccr.2009.03.022 (2009).
50 Ostrem, J. M. & Shokat, K. M. Direct small-molecule inhibitors of KRAS: from structural insights to mechanism-based design. *Nature reviews. Drug discovery* **15**, 771-785, doi:10.1038/nrd.2016.139 (2016).
51 Shahinian, S. & Silvius, J. R. Doubly-lipid-modified protein sequence motifs exhibit long-lived anchorage to lipid bilayer membranes. *Biochemistry* **34**, 3813-3822 (1995).
52 Silvius, J. R. & l'Heureux, F. Fluorimetric evaluation of the affinities of isoprenylated peptides for lipid bilayers. *Biochemistry* **33**, 3014-3022 (1994).
53 Roy, S. *et al.* Individual palmitoyl residues serve distinct roles in H-ras trafficking, microlocalization, and signaling. *Molecular and cellular biology* **25**, 6722-6733, doi:10.1128/MCB.25.15.6722-6733.2005 (2005).

54 Rocks, O. *et al.* An acylation cycle regulates localization and activity of palmitoylated Ras isoforms. *Science* **307**, 1746-1752, doi:10.1126/science.1105654 (2005).
55 Hancock, J. F., Paterson, H. & Marshall, C. J. A polybasic domain or palmitoylation is required in addition to the CAAX motif to localize p21ras to the plasma membrane. *Cell* **63**, 133-139 (1990).
56 de Vos, A. M. *et al.* Three-dimensional structure of an oncogene protein: catalytic domain of human c-H-ras p21. *Science* **239**, 888-893 (1988).
57 Pai, E. F. *et al.* Refined crystal structure of the triphosphate conformation of H-ras p21 at 1.35 A resolution: implications for the mechanism of GTP hydrolysis. *The EMBO journal* **9**, 2351-2359 (1990).
58 Milburn, M. V. *et al.* Molecular switch for signal transduction: structural differences between active and inactive forms of protooncogenic ras proteins. *Science* **247**, 939-945 (1990).
59 Krengel, U. *et al.* Three-dimensional structures of H-ras p21 mutants: molecular basis for their inability to function as signal switch molecules. *Cell* **62**, 539-548 (1990).
60 Huang, L., Hofer, F., Martin, G. S. & Kim, S. H. Structural basis for the interaction of Ras with RalGDS. *Nature structural biology* **5**, 422-426 (1998).
61 Pacold, M. E. *et al.* Crystal structure and functional analysis of Ras binding to its effector phosphoinositide 3-kinase gamma. *Cell* **103**, 931-943 (2000).
62 Fetics, S. K. *et al.* Allosteric effects of the oncogenic RasQ61L mutant on Raf-RBD. *Structure* **23**, 505-516, doi:10.1016/j.str.2014.12.017 (2015).
63 Dharmaiah, S. *et al.* Structural basis of recognition of farnesylated and methylated KRAS4b by PDEdelta. *Proc Natl Acad Sci U S A* **113**, E6766-E6775, doi:10.1073/pnas.1615316113 (2016).
64 Chandra, A. *et al.* The GDI-like solubilizing factor PDEdelta sustains the spatial organization and signalling of Ras family proteins. *Nature cell biology* **14**, 148-158, doi:10.1038/ncb2394 (2011).
65 Nassar, N., Singh, K. & Garcia-Diaz, M. Structure of the dominant negative S17N mutant of Ras. *Biochemistry* **49**, 1970-1974, doi:10.1021/bi9020742 (2010).
66 Trahey, M. & McCormick, F. A cytoplasmic protein stimulates normal N-ras p21 GTPase, but does not affect oncogenic mutants. *Science* **238**, 542-545 (1987).
67 Scheffzek, K. *et al.* The Ras-RasGAP complex: structural basis for GTPase activation and its loss in oncogenic Ras mutants. *Science* **277**, 333-338 (1997).
68 Buhrman, G., Holzapfel, G., Fetics, S. & Mattos, C. Allosteric modulation of Ras positions Q61 for a direct role in catalysis. *Proc Natl Acad Sci U S A* **107**, 4931-4936, doi:10.1073/pnas.0912226107 (2010).
69 Spoerner, M., Herrmann, C., Vetter, I. R., Kalbitzer, H. R. & Wittinghofer, A. Dynamic properties of the Ras switch I region and its importance for binding to effectors. *Proc Natl Acad Sci U S A* **98**, 4944-4949, doi:10.1073/pnas.081441398 (2001).
70 Ghosh, S. & Bell, R. M. Identification of discrete segments of human Raf-1

kinase critical for high affinity binding to Ha-Ras. *The Journal of biological chemistry* **269**, 30785-30788 (1994).
71 Vojtek, A. B., Hollenberg, S. M. & Cooper, J. A. Mammalian Ras interacts directly with the serine/threonine kinase Raf. *Cell* **74**, 205-214 (1993).
72 Samatar, A. A. & Poulikakos, P. I. Targeting RAS-ERK signalling in cancer: promises and challenges. *Nature reviews. Drug discovery* **13**, 928-942, doi:10.1038/nrd4281 (2014).
73 Cruzalegui, F. H., Cano, E. & Treisman, R. ERK activation induces phosphorylation of Elk-1 at multiple S/T-P motifs to high stoichiometry. *Oncogene* **18**, 7948-7957, doi:10.1038/sj.onc.1203362 (1999).
74 Huang, C. H. *et al.* The structure of a human p110alpha/p85alpha complex elucidates the effects of oncogenic PI3Kalpha mutations. *Science* **318**, 1744-1748, doi:10.1126/science.1150799 (2007).
75 Rubio, I., Rodriguez-Viciana, P., Downward, J. & Wetzker, R. Interaction of Ras with phosphoinositide 3-kinase gamma. *The Biochemical journal* **326 (Pt 3)**, 891-895 (1997).
76 Fritsch, R. *et al.* RAS and RHO families of GTPases directly regulate distinct phosphoinositide 3-kinase isoforms. *Cell* **153**, 1050-1063, doi:10.1016/j.cell.2013.04.031 (2013).
77 Thapar, R., Williams, J. G. & Campbell, S. L. NMR characterization of full-length farnesylated and non-farnesylated H-Ras and its implications for Raf activation. *Journal of molecular biology* **343**, 1391-1408, doi:10.1016/j.jmb.2004.08.106 (2004).
78 Hofer, F., Fields, S., Schneider, C. & Martin, G. S. Activated Ras interacts with the Ral guanine nucleotide dissociation stimulator. *Proc Natl Acad Sci U S A* **91**, 11089-11093 (1994).
79 Kikuchi, A., Demo, S. D., Ye, Z. H., Chen, Y. W. & Williams, L. T. ralGDS family members interact with the effector loop of ras p21. *Molecular and cellular biology* **14**, 7483-7491 (1994).
80 White, M. A., Vale, T., Camonis, J. H., Schaefer, E. & Wigler, M. H. A role for the Ral guanine nucleotide dissociation stimulator in mediating Ras-induced transformation. *The Journal of biological chemistry* **271**, 16439-16442 (1996).
81 Moskalenko, S. *et al.* The exocyst is a Ral effector complex. *Nature cell biology* **4**, 66-72, doi:10.1038/ncb728 (2002).
82 Fukai, S., Matern, H. T., Jagath, J. R., Scheller, R. H. & Brunger, A. T. Structural basis of the interaction between RalA and Sec5, a subunit of the sec6/8 complex. *The EMBO journal* **22**, 3267-3278, doi:10.1093/emboj/cdg329 (2003).
83 Cantor, S. B., Urano, T. & Feig, L. A. Identification and characterization of Ral-binding protein 1, a potential downstream target of Ral GTPases. *Molecular and cellular biology* **15**, 4578-4584 (1995).
84 Frankel, P. *et al.* RalA interacts with ZONAB in a cell density-dependent manner and regulates its transcriptional activity. *The EMBO journal* **24**, 54-62, doi:10.1038/sj.emboj.7600497 (2005).

85 Wu, Z. *et al.* RalBP1 is necessary for metastasis of human cancer cell lines. *Neoplasia* **12**, 1003-1012 (2010).
86 Lambert, J. M. *et al.* Tiam1 mediates Ras activation of Rac by a PI(3)K-independent mechanism. *Nature cell biology* **4**, 621-625, doi:10.1038/ncb833 (2002).
87 Wang, Y. *et al.* The RAS effector RIN1 directly competes with RAF and is regulated by 14-3-3 proteins. *Molecular and cellular biology* **22**, 916-926 (2002).
88 Song, C. *et al.* Regulation of a novel human phospholipase C, PLCepsilon, through membrane targeting by Ras. *The Journal of biological chemistry* **276**, 2752-2757, doi:10.1074/jbc.M008324200 (2001).
89 Hanson, C. J., Bootman, M. D. & Roderick, H. L. Cell signalling: IP3 receptors channel calcium into cell death. *Current biology : CB* **14**, R933-935, doi:10.1016/j.cub.2004.10.019 (2004).
90 Huang, K. P. The mechanism of protein kinase C activation. *Trends Neurosci* **12**, 425-432 (1989).

CHAPTER 2

IDENTIFYING THE FUNCTIONAL CONTRIBUTION OF THE DEFATTY-ACYLASE ACTIVITY OF SIRT6[a]

Abstract

Mammalian sirtuin 6 (SIRT6) exhibits many pivotal functions and multiple enzymatic activities, but the contribution of each activity to the various functions is unclear. We identified a SIRT6 G60A mutant that possesses efficient defatty-acylase activity, but has significantly decreased deacetylase activity *in vitro* and no detectable deacetylase activity in cells. The G60A mutant has decreased ability to bind NAD^+, but the presence of fatty-acyl lysine peptides restores NAD^+ binding, explaining the retention of the defatty-acylase activity. Using this mutant, we found that SIRT6's defatty-acylase activity regulates the secretion of numerous proteins. Interestingly, many ribosomal proteins were secreted via exosomes from *Sirt6* KO mouse embryonic fibroblasts, and these exosomes increased NIH 3T3 cell proliferation compared with control exosomes. Our data supports that distinct activities of SIRT6 regulate different pathways, and that the G60A mutant is a useful tool to study the contribution of the defatty-acylase activity to SIRT6's various functions.

[a] This is a revised version of our published paper: Zhang, X. et al. Identifying the functional contribution of the defatty-acylase activity of SIRT6. ***Nat. Chem. Biol.***, 12 (2016) 614-620.

Introduction

Mammalian sirtuin 6 (SIRT6) belongs to the Sir2 (silencing information regulator 2) family of enzymes (or sirtuins), which were initially reported as nicotinamide adenine dinucleotide (NAD^+)-dependent protein lysine deacetylases. SIRT6 has attracted a lot of interest because it has pivotal biological functions in regulating genome stability[1,2], DNA repair[3,4], metabolism[5,6], and longevity[7,8]. There are three reported enzymatic activities of SIRT6: deacetylation[2,9], defatty-acylation[10,11], and mono-adenosine diphosphate (ADP)-ribosylation[4,12]. SIRT6 has poor deacetylase activity *in vitro*, but the deacetylase activity can be significantly enhanced by nucleosomes or fatty acids *in vitro*[10,13]. SIRT6 is also reported to exhibit ADP-ribosyltransferase (ART) activity, but this activity is very weak *in vitro*[14] and the physiological relevance of this activity has not been independently validated by other laboratories. We and others have recently identified lysine defatty-acylation as an efficient enzymatic activity of SIRT6[10,11]. Sirt6 knockout (KO) mice exhibit many phenotypes. They develop lymphopenia, loss of subcutaneous fat, and suffer from severe metabolic defects[1,5]. Now that we know SIRT6 has multiple enzymatic activities, an important question emerges: What is the contribution of each activity to the various functions of SIRT6?

Here we report that a point mutant of SIRT6, Gly60Ala (G60A), maintains efficient defatty-acylase activity but shows no detectable deacetylase activity in cells and no ART activity in vitro. Utilizing this G60A mutant, we were able to identify the contribution of defatty-acylation to several functions of SIRT6. We found that the defatty-acylase activity plays little role in regulating gene transcription while it is important for regulating the secretion of many proteins. In particular, in *Sirt6* KO mouse embryonic fibroblasts (MEFs), many ribosomal proteins were secreted via exosomes and their secretion was blocked by SIRT6 WT or the G60A mutant re-expression. We believe this SIRT6 G60A mutant will be a valuable tool for probing

many of the other biological functions of SIRT6.

Results and discussion

SIRT6 G60A is a lysine defatty-acylase *in vitro*

To find a SIRT6 mutant that only has one of the three catalytic activities, we first tested four reported mutants used in other studies: S56Y, G60A, R65A, and H133Y[4]. S56, G60, R65 are either in or close to the active site of SIRT6, and H133 is the catalytic base necessary for deacylation and is conserved among all seven mammalian sirtuins. It is reported that SIRT6 S56Y and H133Y lack both deacetylase and ART activities, whereas G60A only shows deacetylase activity, and SIRT6 R65A only shows ART activity. We decided to test whether any of these SIRT6 mutants purified from *Escherichia coli* (*E.coli*) showed lysine defatty-acylase activities using a H3K9 myristoyl peptide. One of the mutants, SIRT6 G60A, exhibited approximately 50% of SIRT6 WT defatty-acylase activity, but none of the other three mutants showed defatty-acylase activities (**Figure 2.1a**). We also tested other fatty-acyl peptides (H3K9 palmitoyl, TNFα myristoyl and H3K9 octanoyl), and the results showed that SIRT6 G60A had robust defatty-acylase activities on different peptide substrates (**Figure 2.2a-f**).

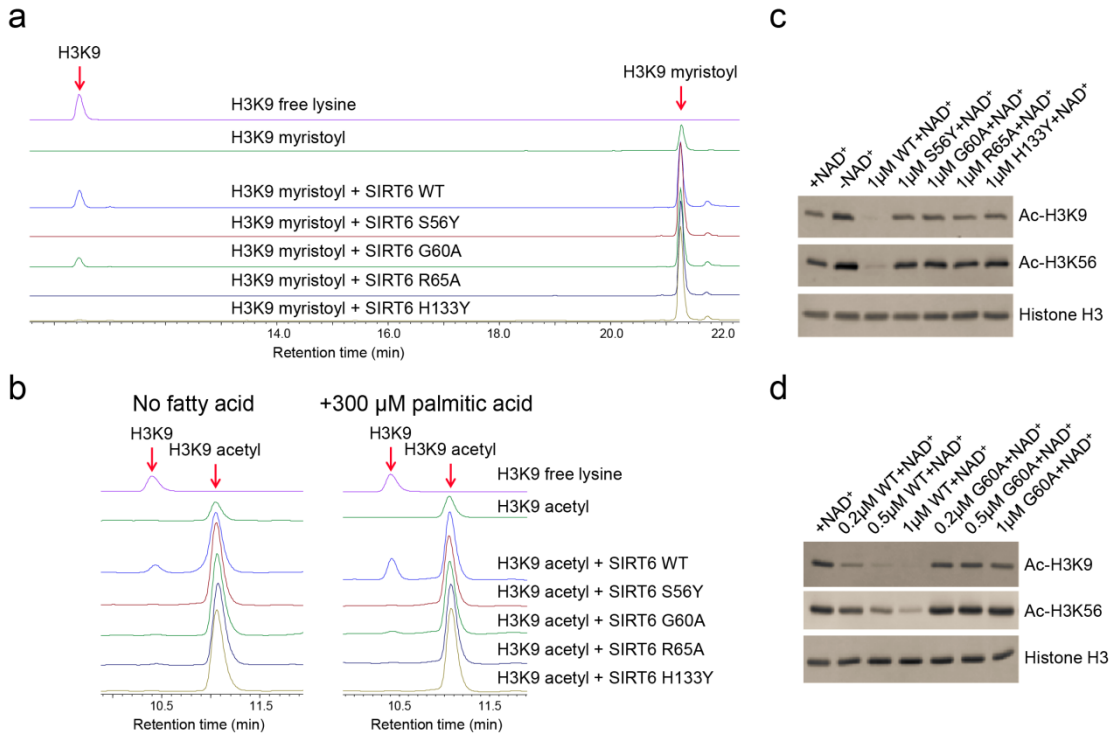

Figure 2.1. *In vitro* deacetylation and defatty-acylation activities of SIRT6 WT and mutants. (a) The defatty-acylase activities of SIRT6 WT and mutants analyzed using a H3K9 myristoyl peptide. SIRT6 (1 μM) was incubated with 25 μM Myr-H3K9 and 1 mM NAD^+ at 37˚C for 20 min. (b) The deacetylase activities of SIRT6 WT and mutants analyzed using a H3K9 acetyl peptide. SIRT6 (4 μM) was incubated with 25 μM Ac-H3K9 and 1 mM NAD^+ at 37˚C for 4 hours (left). Alternatively, 2 μM SIRT6 was incubated with 25 μM Ac-H3K9, 1 mM NAD^+, and 300 μM palmitic acid at 37˚C for 2 hours (right). (c) Deacetylation of H3K9 and K56 on chromatin histones by SIRT6 WT and G60A. SIRT6 WT or mutants (1 μM) was incubated with chromatin fractions isolated from HEK293T cells in the presence of 1 mM NAD^+ at 37˚C for 120 min. (d) Deacetylation of H3K9 and H3K56 on chromatin histones with different concentrations of SIRT6 WT and G60A. SIRT6 at different concentrations was incubated with chromatin fractions isolated from HEK293T cells in the presence of 1 mM NAD^+ at 37˚C for 120 min.

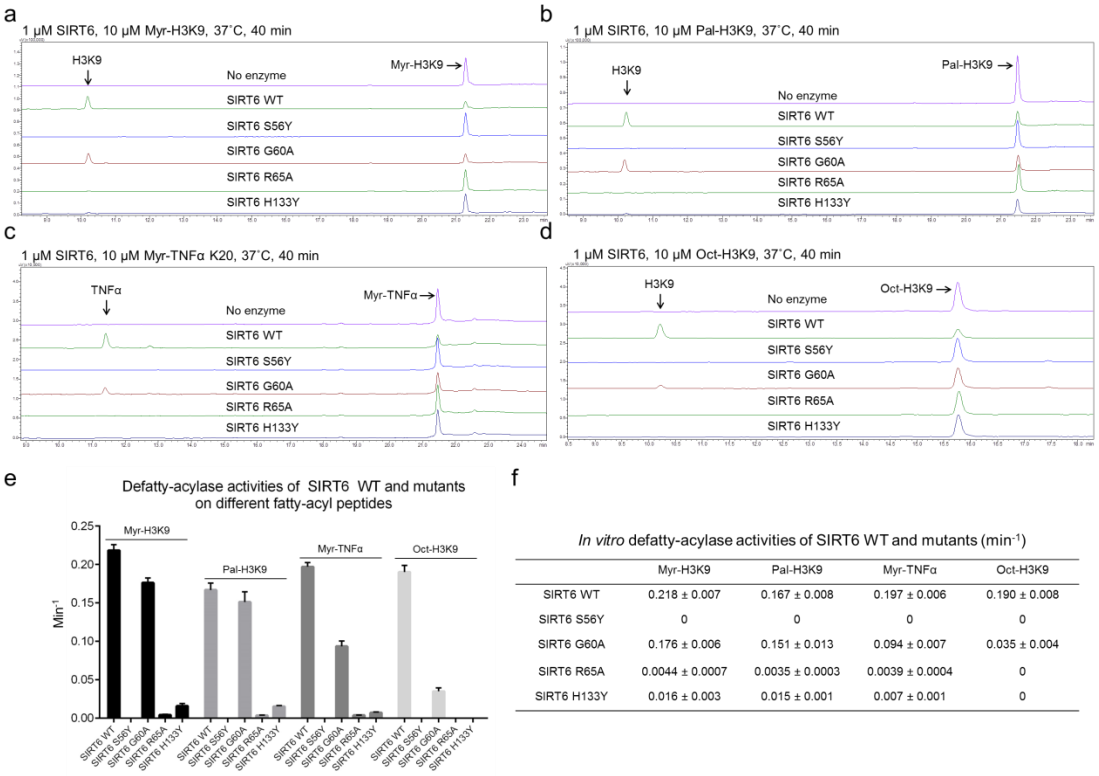

In vitro defatty-acylase activities of SIRT6 WT and mutants (min^{-1})

	Myr-H3K9	Pal-H3K9	Myr-TNFα	Oct-H3K9
SIRT6 WT	0.218 ± 0.007	0.167 ± 0.008	0.197 ± 0.006	0.190 ± 0.008
SIRT6 S56Y	0	0	0	0
SIRT6 G60A	0.176 ± 0.006	0.151 ± 0.013	0.094 ± 0.007	0.035 ± 0.004
SIRT6 R65A	0.0044 ± 0.0007	0.0035 ± 0.0003	0.0039 ± 0.0004	0
SIRT6 H133Y	0.016 ± 0.003	0.015 ± 0.001	0.007 ± 0.001	0

Figure 2.2. *In vitro* defatty-acylase activities of SIRT6 WT and mutants on different fatty-acyl peptide substrates. (a) Defatty-acylase activities of SIRT6 WT and mutants on H3K9 myristoyl peptide. (b) Defatty-acylase activities of SIRT6 WT and mutants on H3K9 palmitoyl peptide. (c) Defatty-acylase activities of SIRT6 WT and mutants on TNFα myristoyl peptide. (d) Defatty-acylase activities of SIRT6 WT and mutants on H3K9 octanoyl peptide. (e, f) Conversion rates of SIRT6 WT and mutants on different fatty-acyl peptides. Error bars indicate s.d. from the mean for three replicates. The equation used for calculating the conversion rate is:

$$\text{Conversion rate} = \frac{\text{Conversion\%} \times \text{peptide substrate concentration (μM)}}{\text{reaction time (min)} \times \text{SIRT6 concentration (μM)}}$$

We then tested the deacetylase activities of SIRT6 WT and mutants using a H3K9 acetyl peptide as substrate. We did not observe any deacetylase activity for any of the

mutants (**Figure 2.1b**). To ensure that we did not miss any weak deacetylase activity, we added 300 μM palmitic acid in the reactions because it was recently reported that fatty acid can increase SIRT6 deacetylase activity *in vitro*[10]. With 300 μM palmitic acid, 2 μM SIRT6 WT was able to hydrolyze 22% of 25 μM H3K9 acetyl peptide in 2 hours (**Figure 2.1b**). However, SIRT6 G60A only converted approximately 1.8% of H3K9 acetyl peptide to H3K9 peptide, which was close to our HPLC detection limit (**Figure 2.1b**). To further confirm this result, we also purified SIRT6 WT and mutants from HEK293T cells and tested their activities. SIRT6 G60A from HEK293T cells showed comparable defatty-acylase activity with WT (25.6% *versus* 34.8% substrate conversion) but undetectable deacetylase activity (**Figure 2.3a-d**).

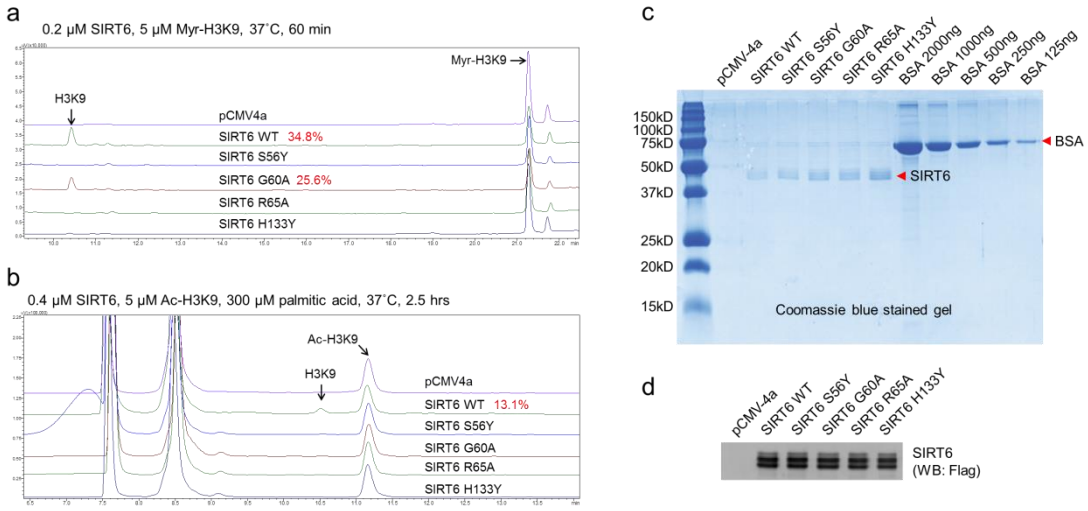

Figure 2.3. *In vitro* deacylase activity assay using SIRT6 purified from HEK 293T cells. (a) Defatty-acylase activities of SIRT6 WT, S56Y, G60A, R65A, and H133Y on a H3K9 myristoyl peptide. SIRT6 (0.2 μM) was incubated with 5 μM Myr-H3K9 and 1 mM NAD^+ at 37˚C for 60 min. (b) Deacetylase activities of SIRT6 WT, S56Y, G60A, R65A, and H133Y on a H3K9 acetyl peptide. SIRT6 (0.4 μM) was incubated with 5 μM Ac-H3K9 and 1 mM NAD^+ in the presence of 300 μM palmitic acid at 37˚C for 2.5 hours. (c) SDS-PAGE analysis of SIRT6 WT and mutants purified from

HEK293T cells. (d) Western blot analysis of SIRT6 WT and mutants purified from HEK293T cells.

To make quantitative comparisons, we performed kinetic studies for SIRT6 WT and G60A on H3K9 myristoyl and H3K9 acetyl peptides. The k_{cat}/K_m of the demyristoylation activity of SIRT6 WT was 9,100 $M^{-1}s^{-1}$, which was 3.4-fold higher than that of SIRT6 G60A (2,700 $M^{-1}s^{-1}$ **Table 2.1** and **Figure 2.4a**). The decreased catalytic efficiency was due to decreased k_{cat} (1.9-fold) and increased K_m (1.8-fold). The k_{cat}/K_m of the deacetylation activity of SIRT6 WT was 3.4 $M^{-1}s^{-1}$. This catalytic efficiency is approximately 19-fold better than that of SIRT6 G60A (0.18 $M^{-1}s^{-1}$, **Table 2.1** and **Figure 2.4b**). When we used 300 μM palmitic acid to activate SIRT6 deacetylase activity, the k_{cat}/K_m for deacetylation of SIRT6 WT was 101 $M^{-1}s^{-1}$, ~30 times faster than that for deacetylation in the absence of palmitic acid (**Table 2.1** and **Figure 2.4c**). However, 300 μM palmitic acid only increased the k_{cat}/K_m for deacetylation of SIRT6 G60A 3.6 times (0.65 $M^{-1}s^{-1}$, **Table 2.1**). Therefore, in the presence of 300 μM palmitic acid, the catalytic efficiency of SIRT6 WT deacetylation was approximately 155-fold better than that of SIRT6 G60A.

Table 2.1. The k_{cat}, K_m and k_{cat}/K_m values for SIRT6 WT and G60A demyristoylase and deacetylase activities. Each value is the mean of three replicates ± s.d. n.d.: The k_{cat} and K_m values cannot be accurately determined because V~[S] curve is linear, thus only k_{cat}/K_m value can be achieved. PA: palmitic acid.

Proteins	k_{cat} (s^{-1})	K_m (μM)	k_{cat}/K_m ($M^{-1}s^{-1}$)
H3K9 myristoyl peptide			
SIRT6 WT	0.00815 ± 0.00027	0.9 ± 0.1	9.1×10^3
SIRT6 G60A	0.00439 ± 0.00011	1.6 ± 0.1	2.7×10^3
H3K9 acetyl peptide			
SIRT6 WT	0.00109 ± 0.00003	316 ± 8	3.4
SIRT6 G60A	n.d.	n.d.	~0.18
SIRT6 WT+PA	0.00099 ± 0.00001	9.8 ± 0.2	101.0
SIRT6 G60A+PA	n.d.	n.d.	~0.65

a

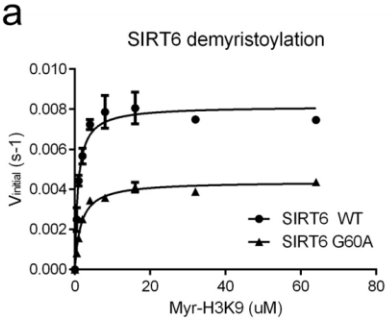

	k_{cat} (s^{-1})	K_m (μM)	k_{cat}/K_m ($M^{-1}s^{-1}$)
SIRT6 WT	0.00815 ± 0.00027	0.9 ± 0.1	9.1×10^3
SIRT6 G60A	0.00439 ± 0.00011	1.6 ± 0.1	2.7×10^3

b

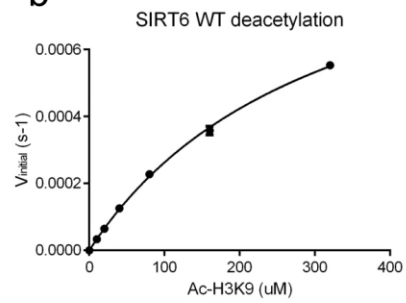

	k_{cat} (s^{-1})	K_m (μM)	k_{cat}/K_m ($M^{-1}s^{-1}$)
SIRT6 WT	0.00109 ± 0.00003	316 ± 8	3.4

c

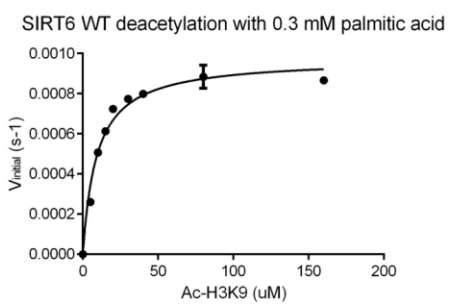

	k_{cat} (s^{-1})	K_m (μM)	k_{cat}/K_m ($M^{-1}s^{-1}$)
SIRT6 WT+PA	0.00099 ± 0.00001	9.8 ± 0.2	101.0

d

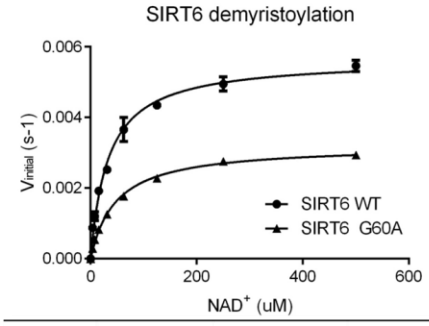

	k_{cat} (s^{-1})	$K_{m,NAD+}$ (μM)	$k_{cat}/K_{m,NAD+}$ ($M^{-1}s^{-1}$)
SIRT6 WT	0.0057 ± 0.0002	33 ± 2	173
SIRT6 G60A	0.0031± 0.0003	47 ± 9	66

e

In steady-state of Michaelis-Menten kinetics,

$$E + S \underset{k_{-1}}{\overset{k_1}{\rightleftarrows}} ES \overset{k_2}{\rightarrow} E + P$$

where *E* is the enzyme, *S* is the substrate, *ES* is the enzyme substrate complex, and *P* is the product.

Based on the definition of K_m and K_d values, $K_m = \frac{k_{-1}+k_2}{k_1}$ $K_d = \frac{k_{-1}}{k_1}$

Therefore, $K_m = \frac{k_{-1}}{k_1} + \frac{k_2}{k_1} = K_d + \frac{k_2}{k_1}$

In steady-state, the enzyme and substrate form complex quickly and slowly generate product, suggesting $k_1 >> k_2$, Thus the K_d value is smaller but close to the K_m value.

Figure 2.4. Steady-state kinetic study of SIRT6 WT and G60A on H3K9 myristoyl

and H3K9 acetyl peptides. (a) Initial velocity ($v_{initial}$) versus Myr-H3K9 concentration (with 1 mM NAD^+) showing SIRT6 WT and G60A demyristoylation kinetics. (b) Initial velocity ($v_{initial}$) versus Ac-H3K9 concentration without fatty acid (with 1 mM NAD^+) showing SIRT6 WT deacetylation kinetics. (c) Initial velocity ($v_{initial}$) versus Ac-H3K9 concentration with 300 μM palmitic acid (with 1 mM NAD^+) showing SIRT6 WT deacetylation kinetics. PA: palmitic acid. (d) Initial velocity ($v_{initial}$) versus NAD^+ concentration (with 25 μM Myr-H3K9) showing NAD^+ kinetics of SIRT6 WT and G60A on H3K9 myristoyl peptide. Error bars indicate s.d. from the means for three replicates. (e) Equations showing how to use the $K_{m,NAD+}$ value to estimate the K_d value.

We then used physiologically relevant substrates of SIRT6, histones, to test the deacetylase activities of SIRT6 WT and mutants. We isolated chromatin fractions from HEK293T cells and incubated with SIRT6 and NAD^+ *in vitro.* SIRT6 WT could almost completely deacetylate histone H3K9 and H3K56, while none of the mutants showed deacetylase activities (**Figure 2.1c**). The deacetylase activity of SIRT6 WT showed dose-dependent effects on H3K9Ac and H3K56Ac while SIRT6 G60A had no activity at any of the concentrations tested (**Figure 2.1d**).

A previous study showed that SIRT6 R65A had ART activity[4]. To confirm that SIRT6 G60A has no ART activity, we tested the ART activities of SIRT6 WT and mutants. SIRT6 WT and R65A showed weak self ADP-ribosylation activities while SIRT6 G60A had no observable ART activity (**Figure 2.5**).Therefore, we identified SIRT6 G60A as a mutant with efficient lysine defatty-acylase activity but significantly decreased lysine deacetylase activity on histone peptide, no detectable deacetylase activity on chromatin histones, and no ART activity.

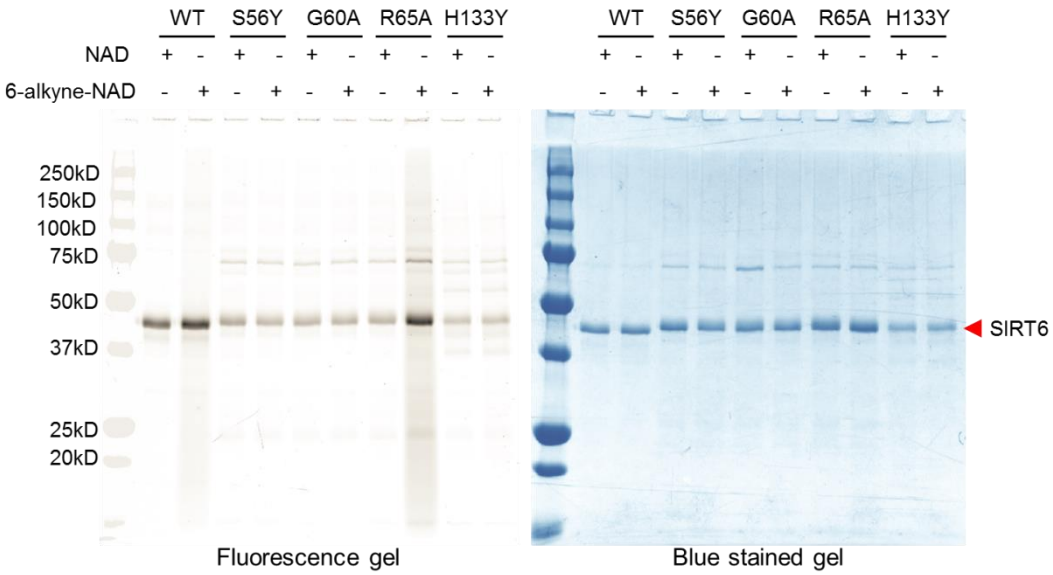

Figure 2.5. *In vitro* mono-ADP-ribosyltransferase activity assay of SIRT6 WT and mutants. 2.5 μM SIRT6 WT or mutants was incubated with 50 μM NAD^+ or 6-alkyne-NAD^+ at 30˚C for 30 min. Then click chemistry was performed by incorporating BODIPY-N_3 for fluorescence visualization.

Fatty-acyl peptides promote SIRT6 G60A binding to NAD^+

We next investigated how SIRT6 G60A could maintain defatty-acylase activity but had little deacetylase activity. G60 is on the NAD^+ binding loop (Ala58-Glu75) (**Figure 2.6a**), suggesting that the G60A mutation may change NAD^+ binding affinity. We measured the binding affinities of SIRT6 WT and mutants to NAD^+. SIRT6 contains two tryptophan residues (Trp71 and Trp188) that are close to the active site. It has been reported that SIRT6 tryptophan fluorescence signal decreases after NAD^+ binding[15]. Thus, we determined the dissociation constants (K_d) of SIRT6 WT and mutants for NAD^+ by measuring the tryptophan fluorescence. In the absence of any acyl lysine peptide, the K_d values of SIRT6 WT and H133Y for NAD^+ were 16.7 ± 1.5 μM and 3.2 ± 0.7 μM, respectively (**Figure 2.7**), which were similar to the reported values[15]. However, the K_d value of SIRT6 G60A for NAD^+ was 564 ± 84 μM (**Figure**

2.7), suggesting that the G60A mutation significantly decreased NAD^+ binding. We employed another method to confirm that the G60A mutation decreased NAD^+ binding. In this assay, the SIRT6 and NAD^+ solution was filtered with a 10 kDa cutoff membrane. Thus NAD^+ that bound to SIRT6 was retained on the membrane and the unbound NAD^+ would pass through the membrane. When 10 μM SIRT6 WT or the H133Y mutant was incubated with 10 μM NAD^+, 34 ± 3% and 59 ± 3% of NAD^+ were bound to SIRT6, respectively (**Figure 2.8**). However, almost no NAD^+ was bound to SIRT6 G60A (2.0 ± 0.7%, **Figure 2.8**), again suggesting that SIRT6 G60A bound NAD^+ very weakly.

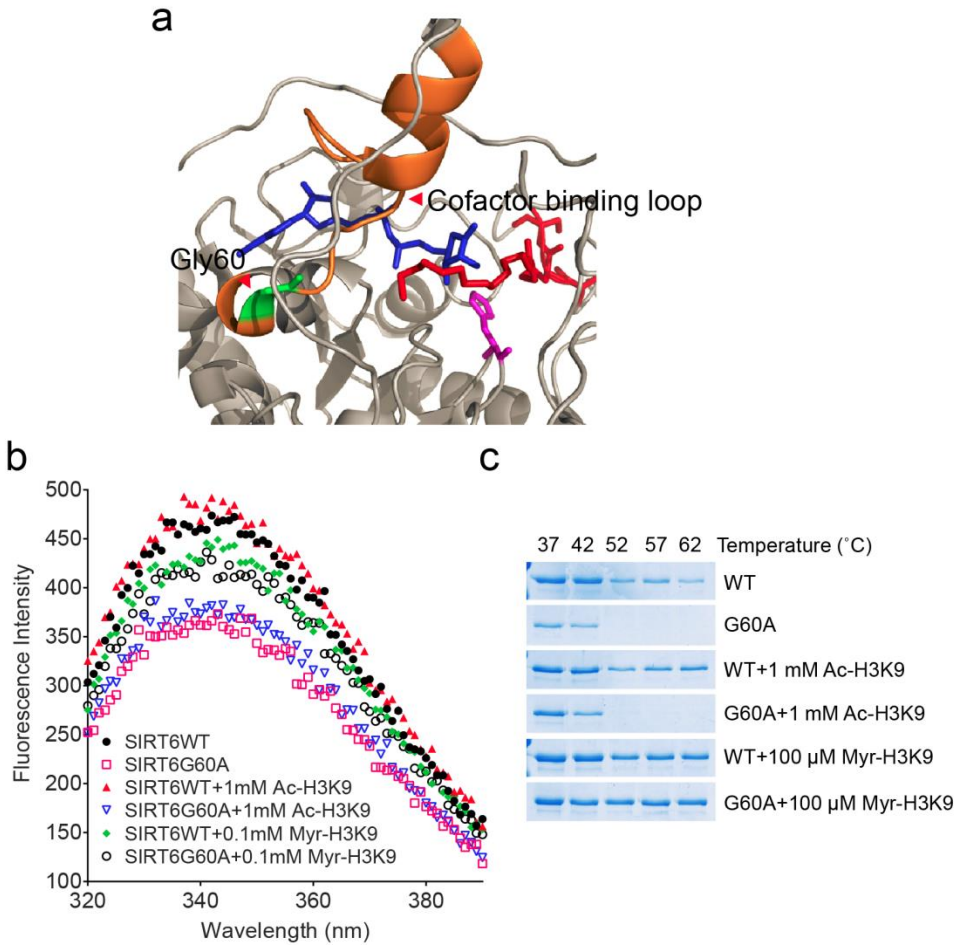

Figure 2.6. Mechanistic study on how SIRT6 G60A maintains defatty-acylation but

loses deacetylation. (a) The location of G60A in the NAD^+ binding loop (Ala58-Glu75) on the crystal structure of SIRT6 (PDB: 3ZG6). (b) Tryptophan fluorescence emission spectra of 3 μM of SIRT6 WT or G60A with or without saturating amount of Ac-H3K9 (1 mM) or Myr-H3K9 (0.1 mM). Each spectrum was repeated three times. (c) Thermal shift assay showing that SIRT6 G60A was stabilized by Myr-H3K9 (0.1 mM) but not by Ac-H3K9 (1 mM).

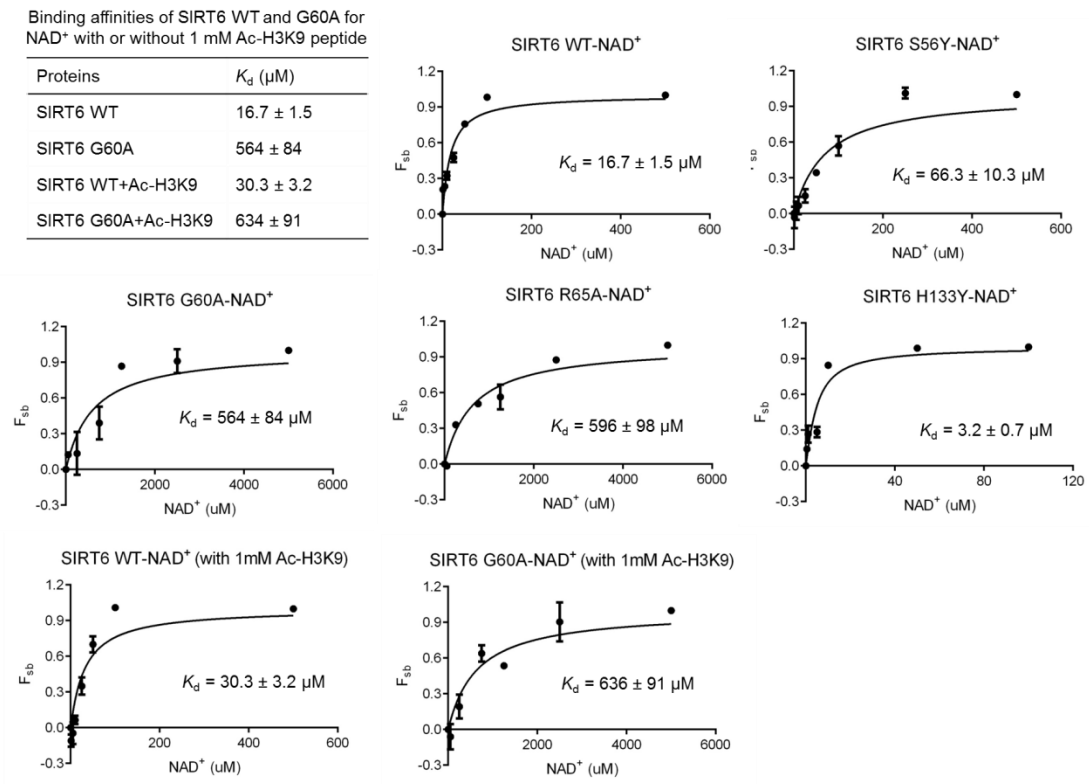

Figure 2.7. The dissociation constants of SIRT6 WT and G60A for NAD^+ with or without 1 mM Ac-H3K9, and saturation binding curves of SIRT6 WT, S56Y, G60A, R65A and H133Y binding to NAD^+. 0-500 μM of NAD^+ were added to 5 μM of SIRT6 WT and 0-5 mM of NAD^+ were added to 5 μM of SIRT6 G60A. Saturation binding curves were fitted to a one-site binding equation. Each value is the mean of three replicates ± s.d. The K_d values were calculated after fitting the curves to a one-site binding equation. Error bars indicate s.d. from the means for three replicates.

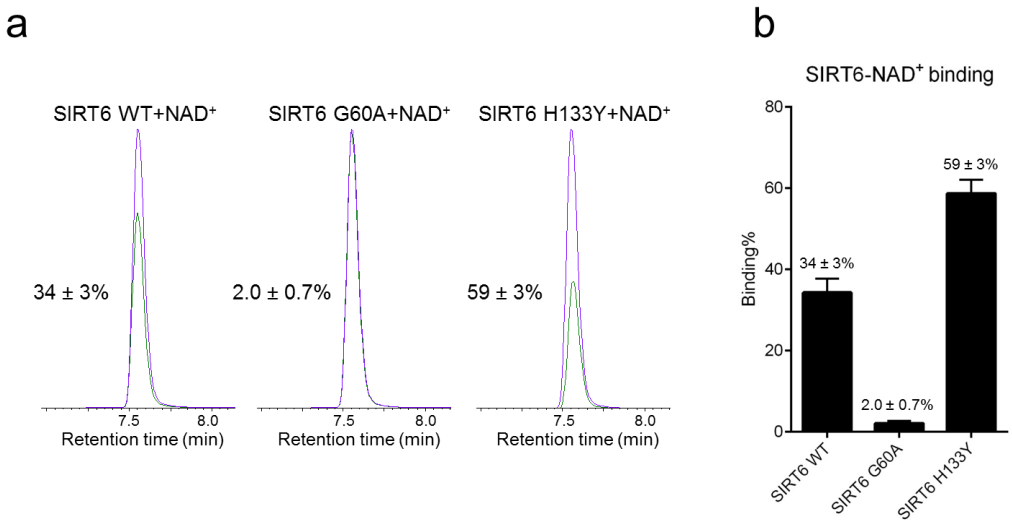

Figure 2.8. Measurement of SIRT6 WT, G60A and H133Y binding to NAD^+ using concentrators with 10 kDa cutoff membranes. (a) The HPLC trace showing SIRT6 binding to NAD^+. Purple HPLC trace is NAD^+ without SIRT6, green HPLC trace is NAD^+ with SIRT6. The percentages are the differences of area between the two peaks and represent how much NAD^+ is bound to SIRT6. For SIRT6 G60A, the purple and green traces are largely overlapped. (b) The histogram showing NAD^+ binding percentage for each protein. Error bars indicate s.d. from the means for three replicates.

To probe how SIRT6 G60A could maintain defatty-acylation but had little deacetylase activity, we further measured the binding affinities of SIRT6 WT and G60A for NAD^+ in the presence of acetyl or myristoyl peptides. In the presence of 1 mM H3K9 acetyl peptide, the K_d values of SIRT6 WT or G60A for NAD^+ were 30.3 ± 3.2 μM and 634 ± 91 μM, respectively (**Figure 2.7**), similar to that without the acetyl peptide. The weak affinity of G60A mutant for NAD^+ in the presence of acetyl peptide explained

the significantly decreased deacetylase activity of G60A. We then aimed to measure the binding affinities of SIRT6 WT and G60A for NAD^+ in the presence of the H3K9 myristoyl peptide. However, due to the efficient defatty-acylase activities of SIRT6 WT and G60A, NAD^+ would be consumed quickly in the presence of the myristoyl peptide. Thus we measured NAD^+ kinetics and used the $K_{m,NAD+}$ value to estimate the K_d value. In steady-state, the K_d value is smaller than the K_m value and we can use the K_m value as an upper estimate for the K_d value (**Figure 2.4e**). The $K_{m,NAD+}$ value of SIRT6 WT was 33 ± 2 μM (**Figure 2.4d**), similar to the K_d value of SIRT6 WT for NAD^+ without the myristoyl peptide. Strikingly, the $K_{m,NAD+}$ value of SIRT6 G60A was 47 ± 9 μM (**Figure 2.4d**), which was much lower than the K_d value of SIRT6 G60A for NAD^+ without the myristoyl peptide. The significantly decreased $K_{m,NAD+}$ value suggested that in the presence of fatty-acyl substrates, SIRT6 G60A could bind NAD^+ tightly and perform defatty-acylation.

Tryptophan fluorescence emission spectra of SIRT6 WT and G60A without any substrate suggested that the G60A mutation changed the conformation of the active site (**Figure 2.6b**). Thermal shift assays revealed that SIRT6 G60A had decreased thermal stability (**Figure 2.6c**). These data suggested that the G60A mutation induces a conformational change that affects SIRT6 stability. The structural changes may affect the NAD^+ binding pocket, leading to loss of NAD^+ binding ability. Furthermore, the altered stability and fluorescence of G60A were not affected by 1 mM H3K9 acetyl peptide (**Figure 2.6b, c**). However, when we added 0.1 mM H3K9 myristoyl peptide, the stability and fluorescence of G60A became similar to those of SIRT6 WT (**Figure 2.6b, c**), suggesting that fatty-acyl substrates could restore the conformation of SIRT6 G60A similar to that of WT and allow SIRT6 G60A to regain high NAD^+ binding ability.

SIRT6 G60A catalyzes only defatty-acylation in cells

We next validated the activity of SIRT6 G60A in cells by detecting the acylation levels of known targets of SIRT6. We chose acetyl-H3K9 and acetyl-H3K56 as cellular readouts for deacetylation since it has been reported that overexpression of flag-tagged SIRT6 is able to decrease acetyl-H3K9 and acetyl-H3K56 levels in 293T cells[16]. We used CRISPR to generate SIRT6 KO in 293T cells (**Figure 2.9a**) and then overexpressed flag-tagged SIRT6 WT and mutants. Only expression of SIRT6 WT was able to decrease H3K9 and H3K56 acetylation levels (**Figure 2.9b**). The cellular results were therefore consistent with the *in vitro* activity assay results and supported that SIRT6 G60A has no detectable deacetylase activity in cells.

For defatty-acylation, we used TNFα as the cellular readout. We stably expressed SIRT6 WT and the different mutants in *Sirt6* KO mouse embryonic fibroblasts (MEFs) and then transiently transfected TNFα into these cells. The fatty-acylation levels on TNFα were then detected using a fatty acid probe, Alk14, as previously reported[11]. Both SIRT6 WT and G60A expression decreased TNFα lysine fatty-acylation (**Figure 2.9c**), while none of the other mutants did. This result demonstrated that SIRT6 G60A exhibits defatty-acylase activity in cells.

SIRT6 promotes TNFα secretion by defatty-acylation

We previously reported that SIRT6 defatty-acylates TNFα and promotes its secretion. With the G60A mutant available, we further tested whether the defatty-acylase activity of SIRT6 is sufficient for the regulation of TNFα secretion. We stably expressed SIRT6 WT, G60A and H133Y in *Sirt6* KO MEFs and examined TNFα secretion in these cells. SIRT6 WT and G60A expression in *Sirt6* KO MEFs promoted TNFα secretion, while SIRT6 H133Y expression in *Sirt6* KO MEFs had no effect on TNFα secretion (**Figure 2.9d**). These results supported that the regulation of TNFα secretion

is achieved through the defatty-acylase activity of SIRT6, which is consistent with our previous report.

SIRT6 suppresses gene transcription by deacetylation

SIRT6 can suppress the transcription activities of various transcription factors, such as NF-κB, HIF-1α and c-Myc. To investigate whether the defatty-acylase activity of SIRT6 contributes to the transcriptional regulation, we chose several genes (IAP2, GLS, RPL3 and MnSOD) that are known to be regulated by SIRT6 and detected their mRNA levels after overexpression of SIRT6 WT or G60A in *Sirt6* KO MEFs. For all the genes tested, SIRT6 WT overexpression could restore the transcriptional suppression while SIRT6 G60A could not (**Figure 2.9e**). This result suggests that the defatty-acylase activity does not contribute to SIRT6's role in transcriptional regulation of these genes.

It is reported that SIRT6 can suppress glycolysis by inhibiting HIF-1α transcriptional activity. Because of the glycolysis suppression function, *Sirt6* KO MEFs are more sensitive to glucose starvation than WT MEFs. Using the sensitivity to glucose starvation, we tested different SIRT6 mutants to find out whether the defatty-acylase activity contributes to this phenotype. SIRT6 WT expression in *Sirt6* KO MEFs rescued glucose starvation-caused cell death, while neither SIRT6 G60A nor H133Y did (**Figure 2.9f**). Given that SIRT6 G60A has defatty-acylase activity but lacks ART activity and has no detectable deacetylase activity in cells, this result suggests that the defatty-acylase activity is not important for suppressing glucose starvation induced cell death. However, since SIRT6 G60A has weaker lysine defatty-acylase activity and lower stability than SIRT6 WT, we could not completely rule out that the failure of SIRT6 G60A to restore this phenotype is due to decreased protein stability or decreased defatty-acylase activity.

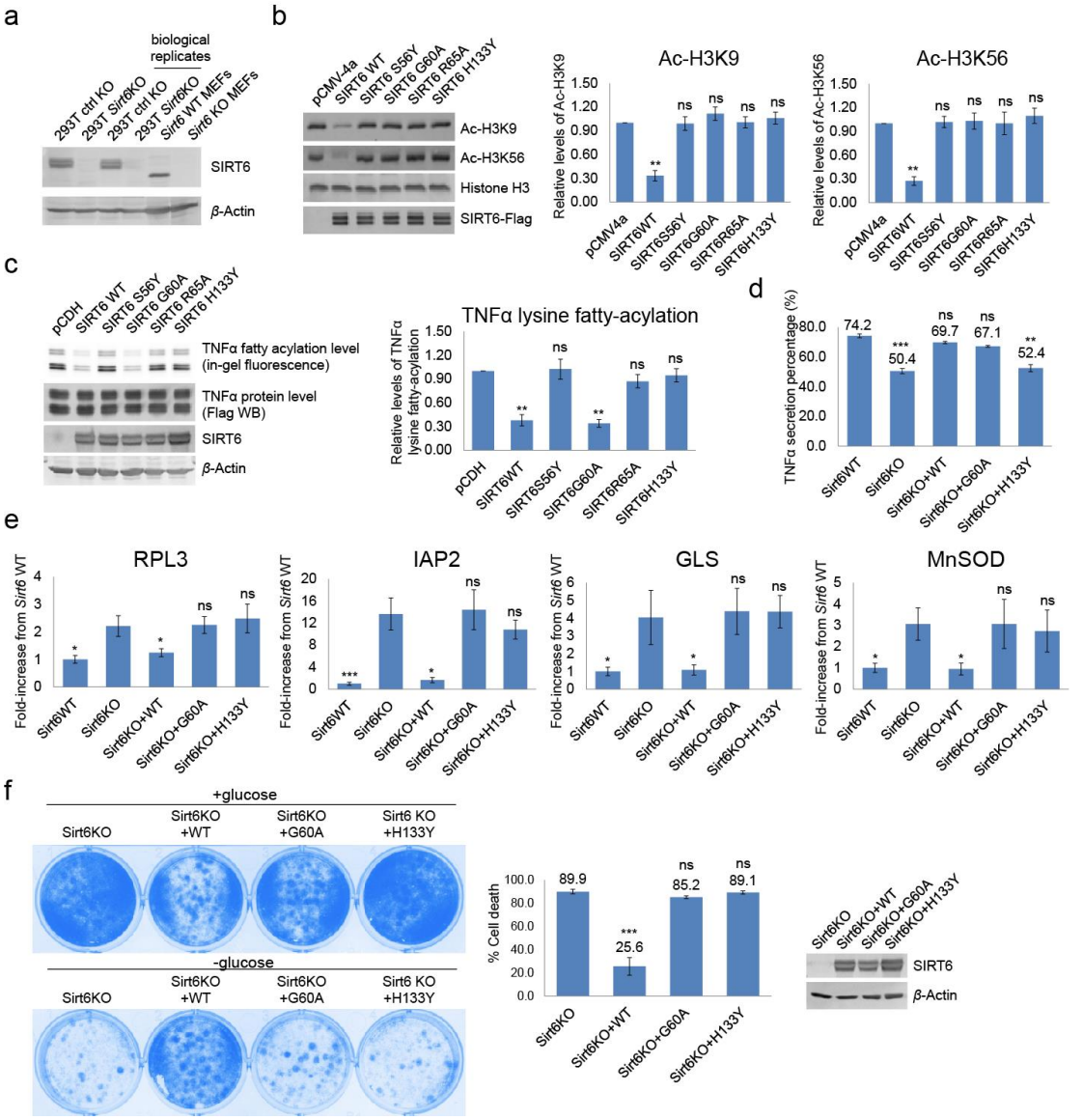

Figure 2.9. In-cell validation of the deacetylase and defatty-acylase activities of SIRT6 WT and mutants. (a) Western blot of endogenous SIRT6 in HEK293T control KO and Sirt6KO cells. (b) Left: Western blot analysis of H3K9 and H3K56 acetylation levels in HEK293T *Sirt6* KO cells after transient transfection of SIRT6 WT or mutants. Middle and right: quantification of the Western blot results. Values with error bars indicate mean ± s.d. of three replicates. $^{**}p < 0.01$, for comparing pCMV4a with all the other groups. "ns", not significant. (c) Left: In-gel fluorescence

showing TNFα lysine fatty-acylation levels in *Sirt6* KO MEFs expressing SIRT6 WT or mutants. Right: quantification of the fluorescence gel. Values with error bars indicate mean ± s.d. of three replicates. $^{**}p < 0.01$ for comparing pCDH with all the other groups. (d) Secretion of TNFα in MEFs with or without SIRT6 WT and mutants. Values with error bars indicate mean ± s.d. of three replicates. $^{**}p < 0.01$ and $^{***}p < 0.005$ for comparing SIRT6 WT with all the other groups. (e) Real-time PCR analysis of RPL3, IAP2, GLS and MnSOD in MEFs with or without Sirt6WT and mutants. Values with error bars indicate mean ± s.d. of three replicates. $^{*}p < 0.05$ and $^{***}p < 0.005$ for comparing Sirt6KO with all the other groups. (f) Cell viability was assayed and calculated by crystal violet staining. Values with error bars indicate mean ± s.d. of three replicates. *** indicates $p < 0.005$, which is for comparing Sirt6KO with all the other groups. ns, not significant. Right: Western blot showing SIRT6 WT, G60A, and H133Y levels in the cells used for the cell viability assay.

SIRT6 regulates the secretion of many proteins

Given that SIRT6 promotes TNFα secretion by defatty-acylation, we wondered whether its defatty-acylase activity regulates the secretion of other proteins. We first detected total secreted proteins in *Sirt6* WT and KO MEFs. As shown in **Figure 2.10a**, the patterns of total secreted proteins in *Sirt6* WT and KO MEFs were different. In contrast, the patterns of total cellular proteins were similar in *Sirt6* WT and KO MEFs (**Figure 2.10a**). This result suggests that SIRT6 likely regulates the secretion of many proteins.

By performing SILAC (stable isotope labeling with amino acids in cell culture) in *Sirt6* WT and KO MEFs (**Figure 2.10b**), we identified the secreted proteins that are regulated by SIRT6. We identified 497 secreted proteins with minimal 2 peptides. Among them, 106 proteins showed high (>1.5) Heavy/Light (H/L) ratios, suggesting

that SIRT6 decreased the secreted amounts of these proteins, while 117 proteins showed low H/L ratios (<0.667), suggesting SIRT6 increased the secreted amounts of these proteins.

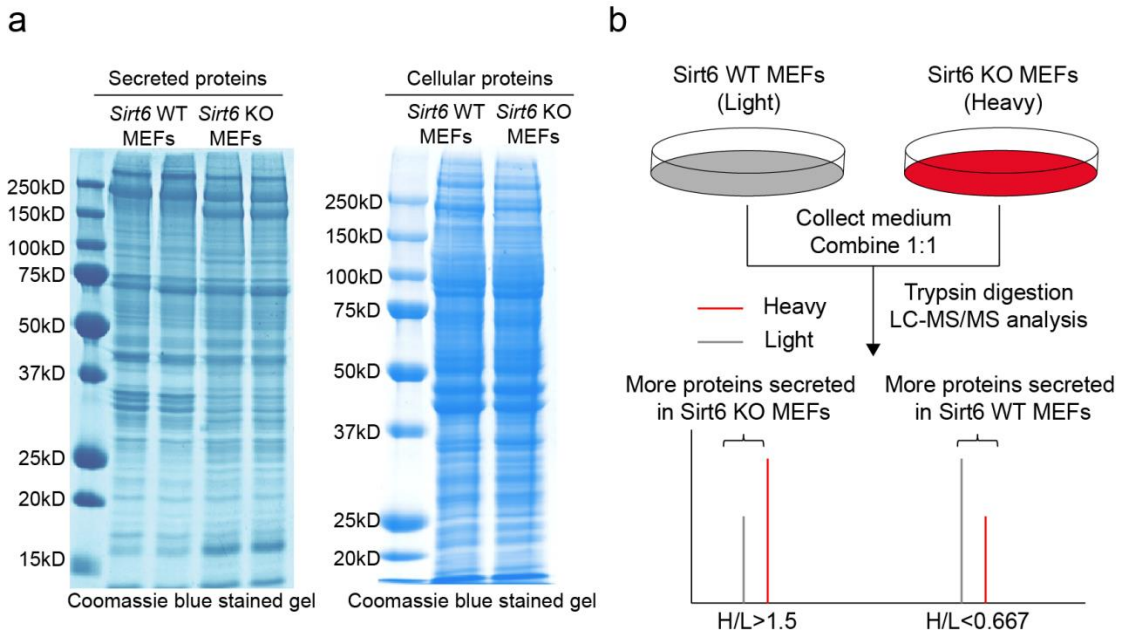

Figure 2.10. Identification of secreted proteins regulated by SIRT6. (a) The Coomassie blue stained gel of total secreted (left) and intracellular (right) proteins in *Sirt6* WT and KO MEFs. For secreted proteins, the two lanes for each cell line were biological replicates. (b) Schematic overview of the SILAC design.

To further confirm that the secreted proteins with high or low H/L ratios were indeed regulated by SIRT6 and to find out which activity of SIRT6 is important for regulating these secreted proteins, we stably expressed SIRT6 WT, G60A, or H133Y in *Sirt6* KO MEFs and performed another three SILAC experiments: SILAC1 was *Sirt6* KO MEFs vs. *Sirt6* KO MEFs expressing SIRT6 WT; SILAC2 was *Sirt6* KO MEFs vs. *Sirt6* KO MEFs expressing SIRT6 G60A; SILAC3 was *Sirt6* KO MEFs vs. *Sirt6* KO MEFs expressing SIRT6 H133Y (**Figure 2.11a**).

We identified 395 proteins with at least 2 peptides detected in all three SILAC experiments. We further filtered the data using the following criteria: H/L ratio in control SILAC3 was close to 1 (0.8-1.25), which served as a quality control as SIRT6 H133Y expression should not change the secreted protein levels. After the filtering, 225 secreted proteins were left. These proteins were further divided into the five groups (**Figure 2.11a**): (1) H/L > 1.5 in both SILAC1 and SILAC2 (50 proteins; SIRT6 defatty-acylase activity decreased the secreted levels of these proteins); (2) H/L < 0.667 in both SILAC1 and SILAC2 (12 proteins; SIRT6 defatty-acylase activity increased the secreted levels of these proteins); (3) H/L > 1.5 in SILAC1, H/L is ~1 (0.8-1.25) in SILAC2 (6 proteins; SIRT6 deacetylase/ART activity decreased the secreted levels of these proteins); (4) H/L < 0.667 in SILAC1, H/L is ~1 (0.8-1.25) in SILAC2 (7 proteins; SIRT6 deacetylase/ART activity increased the secreted levels of these proteins); (5) H/L is ~ 1 (0.8-1.25) in both SILAC1 and SILAC2 (SIRT6 does not regulate the secreted levels of these proteins). Theoretically there should not be proteins that show high H/L ratios in SILAC1 but low H/L ratios in SILAC2 (or vice versa). The analysis of the SILAC data showed that no proteins fell into this category (**Figure 2.11b**). There were 75 proteins in Group 1 to 4 (**Table 2.2** and **Table 2.3**), suggesting SIRT6 regulates 33% (75 out of 225) of the secreted proteins identified. Datasets of SILAC1 and SILAC2 proteins with altered secretion levels (H/L>1.5 and H/L<0.667) were also analyzed by DAVID Functional Annotation Tool (**Figure 2.11c**). Based on the datasets analysis, SIRT6 defatty-acylase activity likely regulates pathways involved in ribosome, ECM-receptor interaction, focal adhesion, systemic lupus erythematosus, and cytokine-cytokine receptor interaction, while SIRT6 deacetylase/ART activity likely regulates pathways involved in glycolysis/gluconeogenesis, glutathione metabolism, cysteine and methionine metabolism, and metabolism of xenobiotics by cytochrome P450.

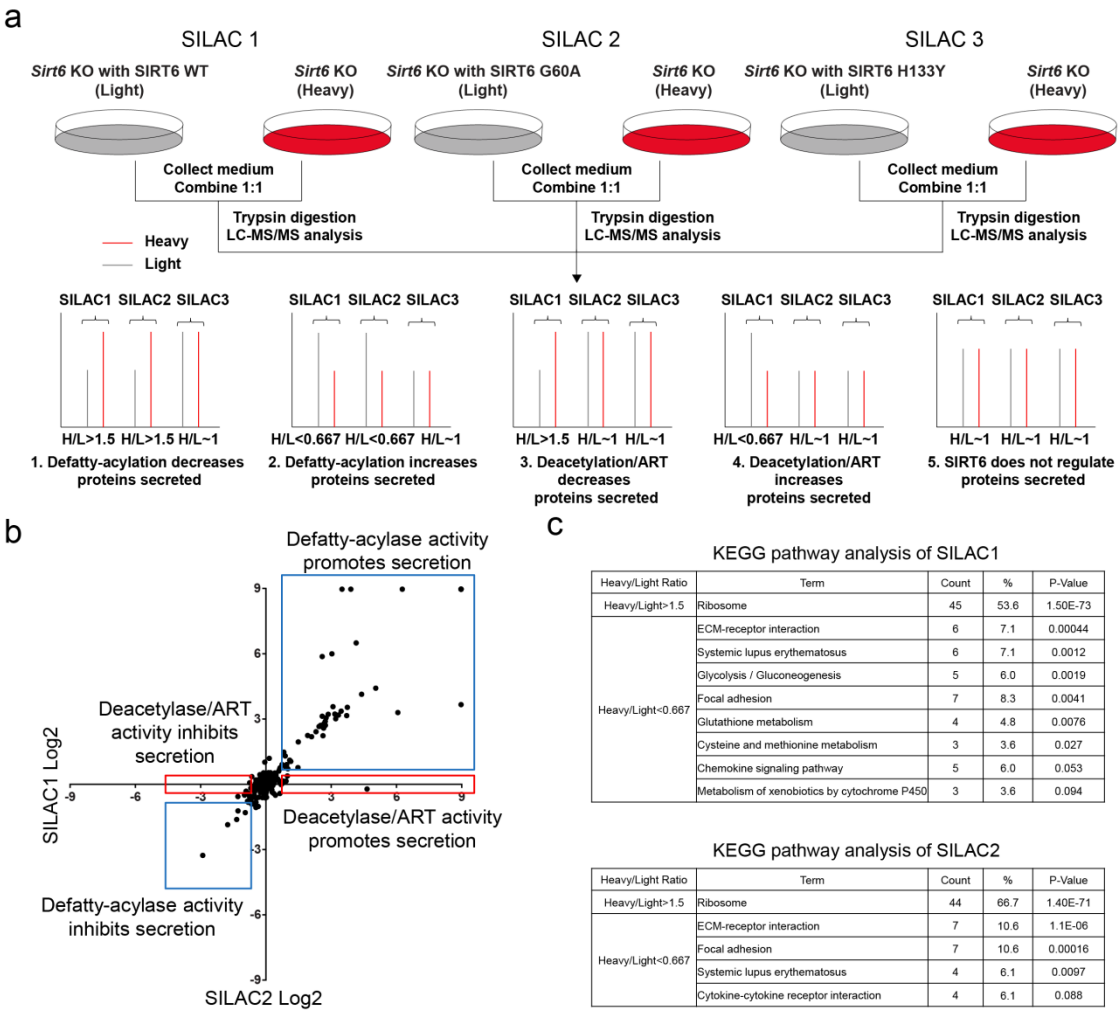

Heavy/Light Ratio	Term	Count	%	P-Value
Heavy/Light>1.5	Ribosome	45	53.6	1.50E-73
Heavy/Light<0.667	ECM-receptor interaction	6	7.1	0.00044
	Systemic lupus erythematosus	6	7.1	0.0012
	Glycolysis / Gluconeogenesis	5	6.0	0.0019
	Focal adhesion	7	8.3	0.0041
	Glutathione metabolism	4	4.8	0.0076
	Cysteine and methionine metabolism	3	3.6	0.027
	Chemokine signaling pathway	5	6.0	0.053
	Metabolism of xenobiotics by cytochrome P450	3	3.6	0.094

Heavy/Light Ratio	Term	Count	%	P-Value
Heavy/Light>1.5	Ribosome	44	66.7	1.40E-71
Heavy/Light<0.667	ECM-receptor interaction	7	10.6	1.1E-06
	Focal adhesion	7	10.6	0.00016
	Systemic lupus erythematosus	4	6.1	0.0097
	Cytokine-cytokine receptor interaction	4	6.1	0.088

Figure 2.11. Analysis of secreted proteins by SILAC. (a) Schematic overview of the SILAC design. (b) Log2-transformation of H/L ratios of proteins identified from SILAC1 (x-axis) and SILAC2 (y-axis) experiments are plotted. Proteins regulated by the defatty-acylase activity of SIRT6 (Group 1 and 2) are in the blue rectangles. Proteins regulated by the deacetylase/ART activity of SIRT6 (Group 3 and 4) are in the red rectangles. (c) KEGG pathway analysis of SILAC1 and SILAC2 proteins with H/L>1.5 and H/L<0.667. Data was analyzed by DAVID Functional Annotation Tool (https://david.ncifcrf.gov/).

Table 2.2. The list of secreted proteins (Group 1) that are regulated by SIRT6

Description	Heavy/Light of SILAC pair1 (KO/WT)	Heavy/Light of SILAC pair2 (KO/GA)	Heavy/Light of SILAC pair3 (KO/HY)
SIRT6 defatty-acylase activity decreases the secreted levels			
PREDICTED: 60S ribosomal protein L13-like	500.000	500.000	1.007
60S ribosomal protein L4	500.000	500.000	1.006
60S ribosomal protein L13a	500.000	500.000	0.966
60S ribosomal protein L15	500.000	500.000	0.901
60S ribosomal protein L18a	500.000	500.000	0.897
60S ribosomal protein L14	500.000	12.664	0.930
60S ribosomal protein L21	77.012	500.000	1.037
40S ribosomal protein S9	66.855	9.832	1.127
60S ribosomal protein L7a	33.071	21.374	0.914
60S ribosomal protein L7	21.103	17.593	0.989
60S ribosomal protein L18	17.727	90.388	1.018
60S ribosomal protein L27a	14.972	500.000	0.946
40S ribosomal protein S8	13.389	11.629	1.091
40S ribosomal protein S6	13.109	8.929	1.178
60S ribosomal protein L3	11.309	500.000	0.934
60S ribosomal protein L24	10.976	10.280	0.970
40S ribosomal protein S4, X isoform	10.085	9.064	1.112
60S ribosomal protein L10	9.228	8.077	0.948
60S ribosomal protein L6	8.990	9.377	0.961
60S ribosomal protein L27	8.485	11.848	1.026
40S ribosomal protein S14	8.182	63.813	1.102
40S ribosomal protein S26	7.268	9.316	1.075
PREDICTED: 40S ribosomal protein S25-like	6.794	8.288	1.134
40S ribosomal protein S11	6.644	6.550	1.168
40S ribosomal protein S17	6.631	7.423	1.166
60S ribosomal protein L17	6.483	6.412	0.976
40S ribosomal protein S2	6.379	6.921	1.099
40S ribosomal protein S3a	6.290	5.999	1.097
40S ribosomal protein S19	6.153	4.699	1.092
40S ribosomal protein S13	6.138	6.168	1.122
40S ribosomal protein S23	6.010	58.606	1.078
60S ribosomal protein L5	6.004	8.754	1.163
40S ribosomal protein S16	5.709	6.523	1.119
40S ribosomal protein S5	5.440	6.306	1.164
40S ribosomal protein S7	4.937	5.339	1.193
40S ribosomal protein S10	4.283	4.558	1.181
60S ribosomal protein L30	3.782	4.729	0.965
40S ribosomal protein S3	2.801	3.854	1.133
10 kDa heat shock protein, mitochondrial	2.773	1.701	1.004
transitional endoplasmic reticulum ATPase	2.205	2.078	1.228
PREDICTED: 60S ribosomal protein L11 isoform X2	2.134	2.158	0.937
heat shock 70 kDa protein 4L	2.012	1.639	1.189
nuclease-sensitive element-binding protein 1	1.941	1.873	0.851
serine/arginine-rich splicing factor 3	1.870	1.724	0.962
40S ribosomal protein S20	1.851	2.464	1.076
PREDICTED: isopentenyl-diphosphate Delta-isomerase 1-like	1.771	2.785	1.199
40S ribosomal protein SA	1.676	1.878	1.229
14-3-3 protein eta	1.572	1.693	1.097
AHNAK nucleoprotein isoform 1	1.551	1.634	1.219
tubulin beta-4B chain	1.508	1.522	1.215

Table 2.3. The list of secreted proteins (Group 2, 3, 4) that are regulated by SIRT6

Description	Heavy/Light of SILAC pair1 (KO/WT)	Heavy/Light of SILAC pair2 (KO/GA)	Heavy/Light of SILAC pair3 (KO/HY)
SIRT6 defatty-acylase activity increases the secreted levels			
pigment epithelium-derived factor precursor	0.642	0.650	1.052
fibulin-2 isoform b precursor	0.636	0.554	0.875
collagen alpha-1(VI) chain precursor	0.635	0.534	1.166
72 kDa type IV collagenase precursor	0.626	0.576	1.179
serpin H1 precursor	0.569	0.565	0.802
collagen alpha-1(V) chain precursor	0.557	0.584	0.954
PREDICTED: latent-transforming growth factor beta-binding protein 4 isoform X2	0.519	0.403	0.903
protein NOV homolog precursor	0.519	0.406	1.237
platelet-derived growth factor receptor-like protein precursor	0.411	0.429	1.167
PREDICTED: EMILIN-1 isoform X2	0.395	0.326	0.875
collagen alpha-2(I) chain precursor	0.296	0.276	0.836
growth-regulated alpha protein precursor	0.134	0.104	1.092
SIRT6 deacetylase activity decreases the secreted levels			
aconitate hydratase, mitochondrial precursor	25.087	0.860	1.144
PREDICTED: basement membrane-specific heparan sulfate proteoglycan core protein isoform X5	1.900	1.110	0.924
annexin A1	1.719	1.112	0.886
PREDICTED: tenascin isoform X2	1.702	1.037	1.194
cathepsin B preproprotein	1.623	0.993	0.956
45 kDa calcium-binding protein precursor	1.541	1.076	1.057
SIRT6 deacetylase activity increases the secreted levels			
ran GTPase-activating protein 1	0.595	1.050	1.231
SUMO-activating enzyme subunit 2	0.653	0.941	1.250
GTP-binding nuclear protein Ran	0.661	0.939	1.133
coatomer subunit epsilon	0.618	0.886	1.116
splicing factor, proline- and glutamine-rich	0.663	0.851	1.140
SUMO-conjugating enzyme UBC9	0.663	0.844	1.140
L-lactate dehydrogenase B chain	0.532	0.801	1.026

To further validate the SILAC proteomic results for proteins in Group 1 to 4, we chose a few proteins from each group (**Figure 2.12a**) and detected their secreted levels and levels in total cell lysates. For Group 1 secreted proteins (RPL17, RPS7, and VCP), the secreted levels were higher in *Sirt6* KO cells than in *Sirt6* WT cells while the levels in total cell lysate were similar (**Figure 2.12b**). Overexpression of SIRT6 WT or G60A mutant in *Sirt6* KO cells decreased the secreted levels to that in *Sirt6* WT cells, suggesting that the defatty-acylase activity of SIRT6 suppresses the secretion of these proteins. We further tested their mRNA levels and found that they were similar with or without SIRT6 (**Figure 2.12c, d**). These results are consistent with the SILAC data and suggest that SIRT6 defatty-acylase activity suppresses the secretion of these proteins but not the transcription of the corresponding mRNA.

For Group 2 secreted proteins (COL6A1, COL5A1 and CXCL1), the secreted levels

were lower in *Sirt6* KO cells than in *Sirt6* WT cells while the levels in total cell lysate were similar (**Figure 2.12b**). Overexpression of SIRT6 WT or the G60A mutant in *Sirt6* KO cells restored the secreted levels to that in *Sirt6* WT cells, suggesting that the defatty-acylase activity of SIRT6 promotes the secretion of these proteins. SIRT6 KO or overexpression did not change their mRNA levels (**Figure 2.12c, d**), supporting that SIRT6 defatty-acylase activity promotes the secretion of these proteins but not the transcription of the corresponding mRNA. For the secreted proteins in Group 2, we originally thought that SIRT6 may directly defatty-acylate them and promote their secretion, similar to the regulation of TNFα secretion. We tested two of them, COL6A1 and COL5A1, but did not observe any fatty-acylation on these proteins (**Figure 2.13**), suggesting that SIRT6 may defatty-acylate other proteins which in turn control the secretion of these proteins.

a

Table 1. Representative secreted proteins regulated by SIRT6

Protein	H/L from SILAC1	H/L from SILAC2	H/L from SILAC3
1. Secreted levels that are decreased by the defatty-acylase activity of SIRT6			
RPL17	6.48	6.41	0.98
PRS7	4.94	5.34	1.19
VCP	2.21	2.08	1.23
2. Secreted levels that are increased by the defatty-acylase activity of SIRT6			
COL6A1	0.635	0.534	1.17
COL5A1	0.557	0.584	0.95
CXCL1	0.134	0.104	1.09
3. Secreted levels that are decreased by the deacetylase/ART activity of SIRT6			
Annexin A1	1.72	1.11	0.886
Tenascin	1.70	1.04	1.19
4. Secreted levels that are increased by the deacetylase/ART activity of SIRT6			
Rangap1	0.595	1.05	1.23
Ran	0.661	0.94	1.13

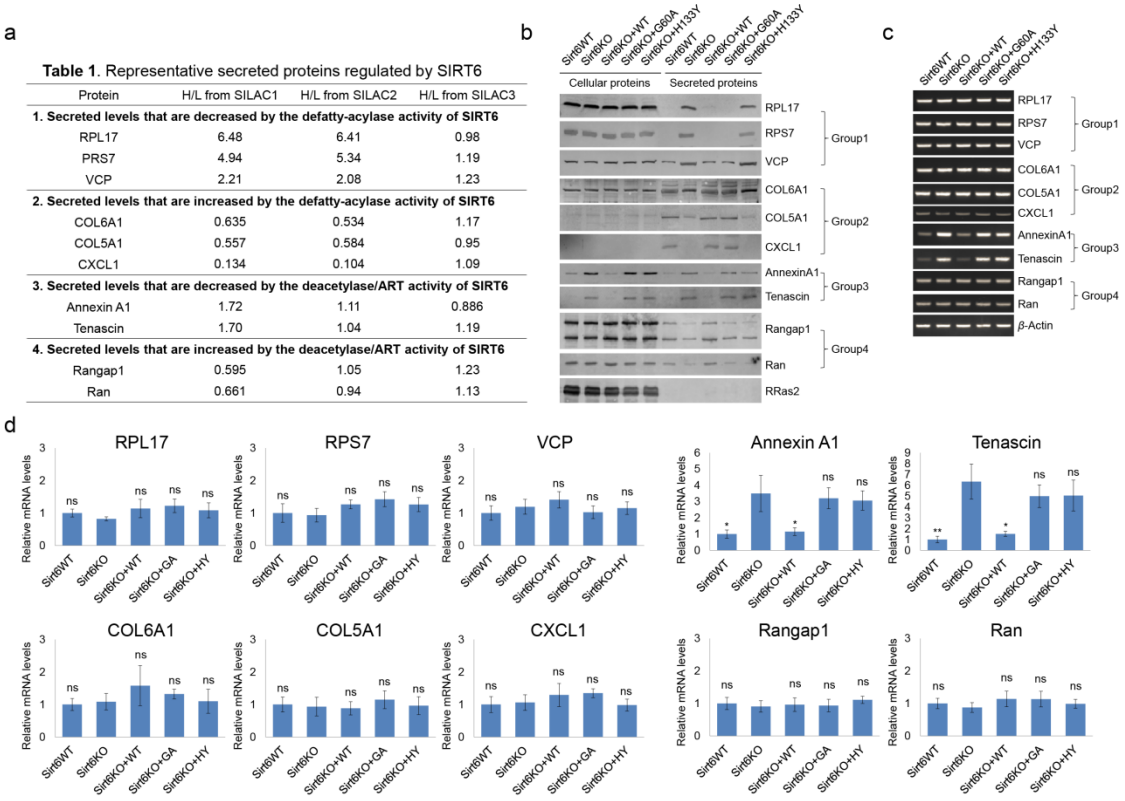

Figure 2.12. Validation of secreted proteins that are regulated by SIRT6. (a) Representative secreted proteins regulated by SIRT6. (b) Intracellular (cell lysates) and extracellular (secreted) levels of representative proteins in different cells. (c) The mRNA levels of representative proteins in *Sirt6* WT MEFs, *Sirt6* KO MEFs, and *Sirt6* KO MEFs expressing SIRT6 WT, G60A, or H133Y. (d) Quantitative real-time PCR analysis of the indicated mRNAs in *Sirt6* WT MEFs, *Sirt6* KO MEFs, and *Sirt6* KO MEFs expressing SIRT6 WT, G60A, or H133Y. Each value is the mean of three replicates ± s.d. Significance is presented as $*p < 0.05$ $**p < 0.01$, which is for comparing Sirt6KO with all the other groups. ns, not significant.

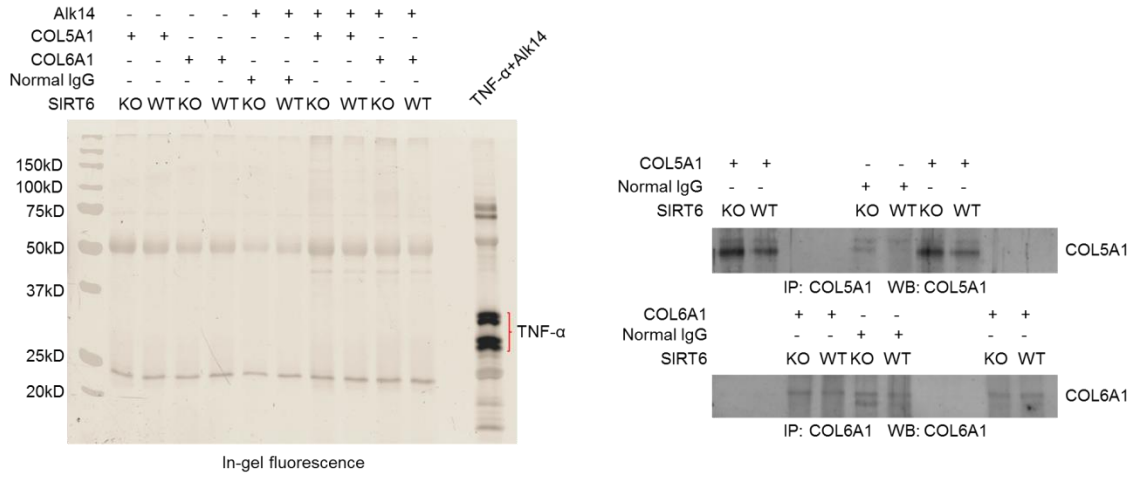

Figure 2.13. In-gel fluorescence showing Alk14 labeling of endogenous COL5A1 and COL6A1 in *Sirt6* WT and KO MEFs. Alk14 labeling of overexpressed TNFα in HEK 293T cells was shown as a positive control. Western blots showing the immunoprecipitated COL5A1 and COL6A1 are shown on the right.

Although we do not know the exact mechanisms how SIRT6 defatty-acylation regulates the secretion of Group 1 and Group 2 proteins, the sites for this function are likely organelle and plasma membranes. We performed sub-cellular fractionation and

imaging experiments and found that overexpressed SIRT6 WT, G60A and H133Y existed in the cytoplasm, nucleus, and membranes (**Figure 2.14**). Since protein lipidation is known to mediate membrane association, the defatty-acylation likely take place in organelle membranes or the plasma membrane.

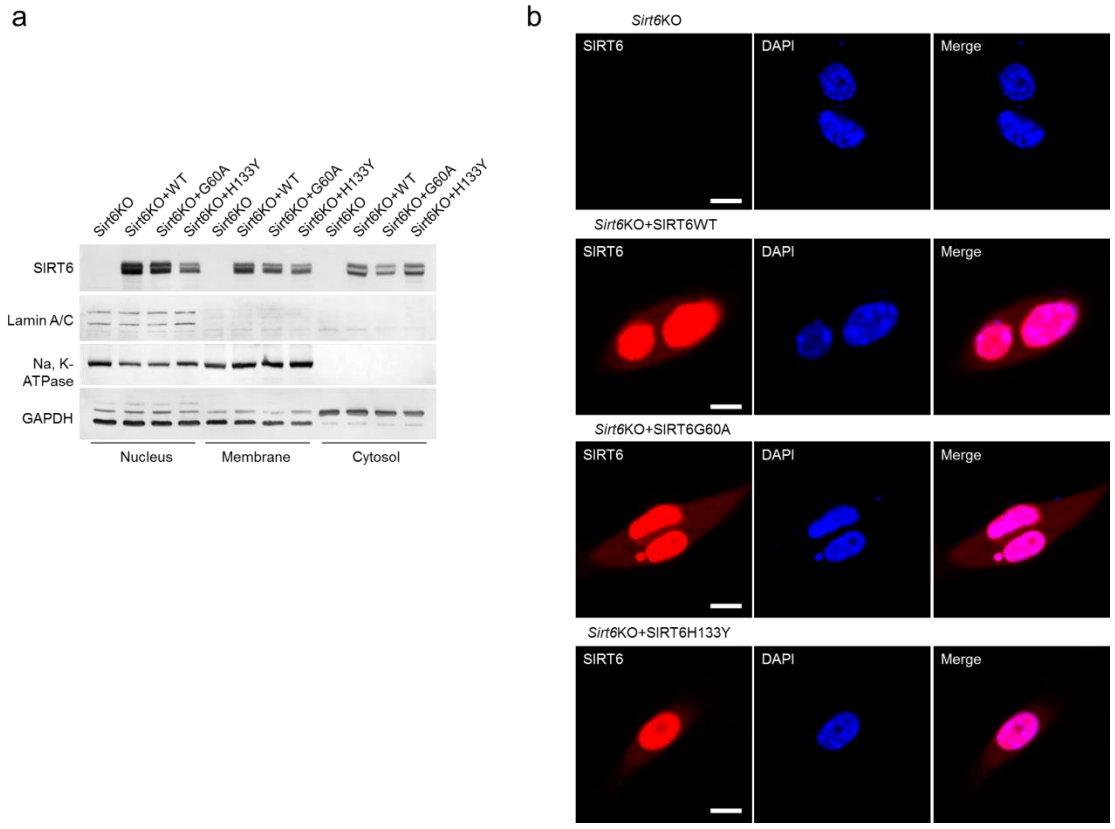

Figure 2.14. Sub-cellular localization of overexpressed SIRT6 WT, G60A and H133Y in *Sirt6* KO MEFs. (a) Western blot showing nucleus, membrane and cytosol localized SIRT6 WT, G60A and H133Y. (b) Confocal imaging showing cellular localization of overexpressed SIRT6 WT, G60A and H133Y. Scale bars, 10 μm.

For Group 3 secreted proteins (Annexin A1 and Tenascin), the secreted levels were higher in *Sirt6* KO cells than in *Sirt6* WT cells (**Figure 2.12b**). Different from Group 1 and 2 proteins, the protein levels in total cell lysate were also higher in *Sirt6* KO

cells than in *Sirt6* WT cells (**Figure 2.12b**). Only overexpression of SIRT6 WT in *Sirt6* KO cells decreased the secreted levels or the intracellular levels to that in *Sirt6* WT cells, suggesting that the deacetylase/ART activity of SIRT6 suppresses the production of Annexin A1 and Tenascin. This suppression was due to transcriptional regulation of Annexin A1 and Tenascin as the mRNA levels were regulated similarly (**Figure 2.12c, d**). These results support that SIRT6 deacetylase/ART activity (most likely the deacetylase activity) decreases the secreted levels of Group 3 proteins by suppressing their transcription.

For Group 4 secreted proteins (Rangap1 and Ran), the secreted levels were lower in *Sirt6* KO cells than in *Sirt6* WT cells (**Figure 2.12b**). Surprisingly, the protein levels in total cell lysate and the corresponding mRNA levels were similar (**Figure 2.12c, d**). Only overexpression of SIRT6 WT in *Sirt6* KO cells restored the secreted levels of Rangap1 and Ran to those in *Sirt6* WT cells, suggesting that the deacetylase/ART activity of SIRT6 promotes the secretion of these proteins. This data is consistent with the SILAC result and suggested that SIRT6 promotes the secretion of these proteins post-transcriptionally.

Ribosomal proteins are secreted via exosomes

Among the 50 proteins that are down-regulated by the defatty-acylase activity of SIRT6 (Group 1), 41 are ribosomal proteins, which are not known as classical secreted proteins. We investigated whether these ribosomal proteins were secreted through extracellular vesicles. It is known that SIRT6-deficient cells are tumorigenic[5]. Cancer cells release microvesicles and exosomes to enhance cell-cell communication and deliver oncogenic contents to other cells[17-19]. We isolated microvesicles and exosomes from *Sirt6* KO MEFs that could carry ribosomal proteins (**Figure 2.15a**). We used two ribosomal proteins (RPL17 and RPS7) as readout and found that they both existed in

exosomes, but not in microvesicles (**Figure 2.15b**). We then validated whether RPL17 and RPS7 secretion via exosomes is regulated by the defatty-acylase activity of SIRT6. We isolated exosomes from *Sirt6* KO MEFs and *Sirt6* KO MFEs expressing SIRT6 WT, G60A, or H133Y. RPL17 and RPS7 can be detected in exosomes from *Sirt6* KO MEFs and *Sirt6* KO MEFs expressing SIRT6 H133Y, but not in exosomes from *Sirt6* KO MEFs expressing SIRT6 WT or G60A mutant (**Figure 2.15c**). This data suggested that SIRT6 defatty-acylase activity inhibits ribosomal protein sorting to the exosomes. We also found that SIRT6 defatty-acylase activity affects many other proteins sorting to the exosomes (**Figure 2.15d**).

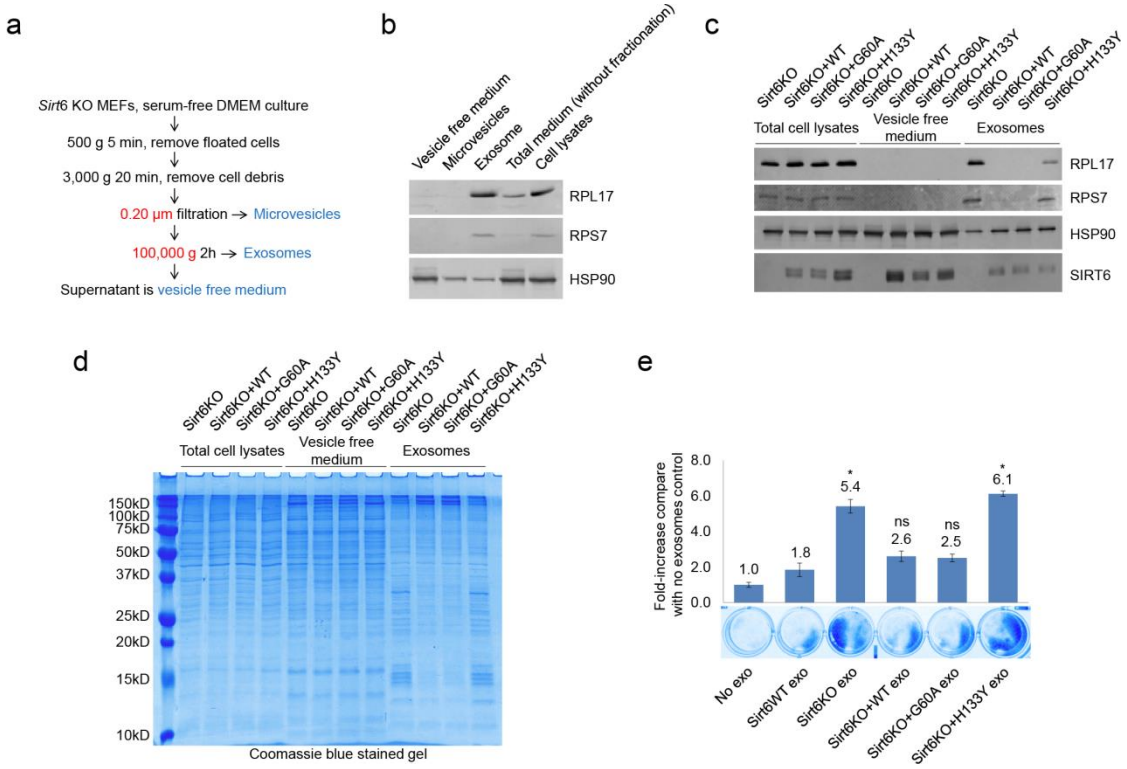

Figure 2.15. SIRT6 defatty-acylase activity inhibits ribosomal protein sorting to the exosomes. (a) Methods to isolate miscrovesicles, exosomes and vesicle-free medium from *Sirt6* KO MEFs. (b) Western blot analysis of RPL17 and RPS7 in different fractions (vesicle free medium, microvesicles, exosomes, and total cell lysates) in

Sirt6 KO MEFs. (c) Western blot analysis of RPL17 and RPS7 in exosomes from *Sirt6* KO MEFs and *Sirt6* KO MEFs expressing SIRT6 WT, G60A, or H133Y. HSP90 was used as the loading control. (d) The Coomassie blue stained gel shows total proteins from cell lysates, vesicle free medium and exosomes in *Sirt6* KO MEFs expressing pCDH vector control, SIRT6 WT, G60A, or H133Y. (e) NIH 3T3 cell proliferation after treating with the same number of exosomes from *Sirt6* WT MEFs, *Sirt6* KO MEFs and *Sirt6* KO MEFs expressing SIRT6 WT, G60A or H133Y. Cell number was determined by crystal violet staining. Error bars indicate mean ± s.d. of three replicates. *$p < 0.05$ for comparing Sirt6WT exosomes with other exosomes.

Sirt6 KO exosomes better promote cell proliferation

We further tested whether the different exosome cargo content could affect the function of exosomes. We isolated the exosomes from *Sirt6* WT MEFs, *Sirt6* KO MEFs, and *Sirt6* KO MEFs expressing SIRT6 WT, G60A, or H133Y, and then treated NIH 3T3 cells with the same number of exosomes. Compared with the cells without exosomes treatment, all exosomes-treated cells showed increased proliferation (**Figure 2.15e**). Particularly, NIH 3T3 cells treated with exosomes from *Sirt6* KO MEFs and *Sirt6* KO MEFs expressing SIRT6 H133Y had significantly higher cell proliferation rate than those treated with exosomes from *Sirt6* WT MEFs and *Sirt6* KO MEFs expressing SIRT6 WT or G60A (**Figure 2.15e**). These results suggested that the exosomes from MEFs lacking SIRT6 defatty-acylase activity had stronger ability to promote cell proliferation, likely due to the different cargo content, such as the ribosomal proteins.

In this study, we found that the SIRT6 G60A mutant exhibits efficient defatty-acylase activity. Although we observed weak deacetylase activity of SIRT6 G60A on peptide substrate *in vitro* when using high enzyme concentrations, we did not observe any

deacetylase activity on chromatin histone H3K9 and K56 *in vitro* or in cells. Our result is, at least in part, different from a previous study that identified SIRT6 G60A originally as a mutant that retained lysine deacetylase activity[4]. The previous report focused on the ART activity of SIRT6 and did not include in-depth quantitative study about deacetylase activity of SIRT6 G60A. It is possible that the deacetylase activity of the G60A mutant in the previous report is also very weak. Alternatively, slight differences in the sequences of the SIRT6 constructs used (e.g. the linker sequences between SIRT6 and the purification tags) may affect the deacetylase activity of the G60A mutant expressed. Luckily for us, our SIRT6 G60A mutant maintains efficient defatty-acylase activity but lack detectable deacetylase activity in cells and therefore is a useful tool to dissect the contribution of defatty-acylation to the various functions of SIRT6.

The unique capability of SIRT6 G60A mutant to remove fatty-acyl groups but not acetyl groups can be explained by the fact that the G60A mutation dramatically decreases the NAD^+ binding affinity, but the NAD^+ binding affinity is restored in the presence of fatty-acyl peptides. This is a very interesting phenomenon that presumably originates from the strong binding affinity of fatty-acyl peptides to SIRT6 - part of the binding energy may be used to change the SIRT6 conformation, allowing tight binding of NAD^+.

Using this mutant, we investigated the contribution of the defatty-acylase activity to the biological functions of SIRT6. In the *Sirt6* KO MEFs, if we could restore WT phenotype by expressing SIRT6 G60A, then we interpret that the defatty-acylase activity is important for that phenotype. If only expressing SIRT6 WT could restore the WT phenotype, then we interpret that the defatty-acylase activity is not important and likely the deacetylase or ART activity is important for the phenotype. However, two caveats should be pointed out. First, since SIRT6 G60A showed slightly weaker

defatty-acylase activity and lower stability than SIRT6 WT *in vitro*, overexpression of SIRT6 G60A may not be able to restore the function in *Sirt6* KO cells even if that function is regulated by defatty-acylation. Second, for any function that can be restored by expressing SIRT6 G60A, it can be argued that the remaining weak deacetylase activity is sufficient. Nonetheless, based on the test cases with known targets of SIRT6 deacetylation (histone H3 K9 and K56) and defatty-acylation (TNFα), we believe that our interpretations are reasonable.

We found that the defatty-acylase activity of SIRT6 regulates the secretion of numerous proteins. Previously, the only known biological function of the defatty-acylase activity of SIRT6 was to promote TNFα secretion. Thus, our current finding has significantly expanded the role of the defatty-acylase activity of SIRT6. Particularly, many ribosomal proteins are secreted through exosomes in *Sirt6* KO MEFs, and these exosomes can significantly increase NIH 3T3 cell proliferation compared with the exosomes from MEFs expressing SIRT6 WT or G60A. SIRT6 has previously been reported to have tumor suppression function[5]. The proliferation promoting effect of exosomes from *Sirt6* KO cells may partly explain the tumor suppression function of SIRT6. For the secreted proteins in Group 2, we noticed that the secreted levels of many collagens were up-regulated by SIRT6 defatty-acylase activity. Recently it is reported that collagens mediate extracellular matrix remodeling and are important for longevity[20]. Promoting collagen secretion by SIRT6 defatty-acylase activity may be a mechanism underlying the lifespan extension effect of SIRT6 overexpression[8].

As more and more biological functions of SIRT6 are discovered, a deep and fundamental understanding of the role of SIRT6 in biological processes is getting more desirable. We believe the SIRT6 G60A mutant with efficient defatty-acylase activity but having no detectable deacetylase activity in cells is a useful tool that will

provide important insights to help understand the role of SIRT6 in biology.

Methods

SIRT6 G60A is a lysine defatty-acylase *in vitro*

Reagents. Anti-Flag affinity gel (#A2220) and anti-Flag antibody conjugated with horseradish peroxidase (#A8592) were purchased from Sigma. Human/mouse SIRT6 antibody (#12486), histone H3 (#4499), histone H3K9 acetyl (#9671), histone H3K56 acetyl (#4243), RanGAP1 (#14675), Ran (#4462), Annexin A1 (#8691), Tenascin (#12221), VCP (#2649), HSP90 (#4877), Na,K-ATPase (#3010) and Lamin A/C (#4777) antibodies were purchased from Cell Signaling Technology. *β*-Actin (sc-4777), GAPDH (sc-20357), COL5A1 (sc-20648) and COL6A1 (sc-20649) antibodies were purchased from Santa Cruz Biotechnology. RPL17 (14121-1-AP) and RPS7 (14491-1-AP) antibodies were purchased from Proteintech. CXCL1 (PA1-29220) antibody was purchased from Thermo Fisher. Brefeldin A, palmitic acid, 3X FLAG peptide, protease inhibitor cocktail, [$^{13}C_6$, $^{15}N_2$]-L-lysine and [$^{13}C_6$, $^{15}N_4$]-L-arginine were purchased from Sigma. Sequencing grade modified trypsin and FuGene 6 transfection reagent were purchased from Promega. ECL plus western blotting detection reagent and universal nuclease for cell lysis were purchased from Thermo Scientific Pierce. Sep-Pak C18 cartridge was purchased from Waters. Amicon Ultra centrifugal filter unit with ultracel-10 membrane was purchased from EMD Millipore. *Sirt6* wild type (WT) and knockout (KO) MEFs were kindly provided by Prof. Raul Mostoslavsky at Massachusetts General Hospital Cancer Center, Harvard Medical School. Acyl peptides (H3K9 acetyl, H3K9 acetyl without tryptophan, H3K9 myristoyl, H3K9 myristoyl without tryptophan, H3K9 palmitoyl, H3K9 octanoyl, TNFα K20 myristoyl and H3K9 free lysine), Alk14, and 6-alkyne-NAD were synthesized according to reported procedures[21-23].

Cell Culture. *Sirt6* WT, KO MEFs and *Sirt6* KO MEFs expressing SIRT6 WT, S56Y, G60A, R65A, or H133Y were cultured in Dulbecco's Modified Eagle Medium (DMEM) with 10% heat inactived fetal bovine serum (FBS). Human Embryonic Kidney (HEK) 293T cells and HEK 293T SIRT6 KO cells were cultured in DMEM medium with 10% heat inactived FBS. NIH 3T3 cells were cultured in DMEM medium with 15% heat inactived FBS and MEM non-essential amino acids. All the cell lines have been tested for mycoplasma contamination and showed no mycoplasma contamination.

Cloning, expression and purification of SIRT6 WT, S56Y, G60A, R65A and H133Y from *Escherichia coli* (*E.Coli*). Full-length human SIRT6 was inserted into pET28a vector. SIRT6 S56Y, G60A, R65A and H133Y mutations were made by QuikChange. All the plasmids were transformed into *E.coli* BL21 (DE3) cells and the proteins were purified according to reported procedures[11].

Cloning, expression and purification of SIRT6 WT, S56Y, G60A, R65A and H133Y from HEK 293T cells. Full-length human SIRT6 WT or mutant was inserted into pCMV-Tag 4a vector with C-terminal Flag tag. The SIRT6 WT and different mutant plasmids were transfected into HEK 293T cells using FuGene 6 transfection reagent according to the manufacturer's protocol. pCMV-Tag 4a empty vector was used as negative control. The cells were collected at 500 g for 5 min and then lysed in Nonidet P-40 lysis buffer (25 mM Tris-HCl pH 7.4, 150 mM NaCl, 10% glycerol and 1 % Nonidet P-40) with universal nuclease (1:1000 dilution) and protease inhibitor cocktail (1:100 dilution) at 4℃ for 30 min. After centrifuging at 15,000 g for 15 min, the supernatant was collected and incubated with 20 μL of anti-Flag affinity gel at 4 ˚C for 2 h. The affinity gel was washed three times with washing buffer (25 mM Tris-HCl pH 7.4, 150 mM NaCl, 0.2% Nonidet P-40) and then eluted by 3X FLAG peptide (dissolved in 25 mM Tris-HCl pH 7.4, 150 mM NaCl and 10% glycerol). Eluted

SIRT6 proteins were buffer exchanged three times using Amicon Ultra-0.5 centrifugal filter unit with ultracel-10 membrane. SIRT6 proteins after buffer exchange were used for the deacylation assay.

SIRT6 deacylase activity assay. For the defatty-acylation assay using SIRT6 WT and mutants purified from *E. coli*, 1 μM of SIRT6 WT, S56Y, G60A, R65A or H133Y was incubated in 40 μL of reaction mixture (25 mM Tris-HCl pH 8.0, 50 mM NaCl, 1 mM DTT, 1 mM NAD^+, 25 μM H3K9 myristoyl peptide) at 37℃ for 20 min. For the deacetylation assay (no fatty acid activation) using SIRT6 WT and mutants purified from *E. coli*, 4 μM of SIRT6 WT, S56Y, G60A, R65A or H133Y was incubated in 40 μL of reaction mixture (25 mM Tris-HCl pH 8.0, 50 mM NaCl, 1 mM DTT, 1 mM NAD^+, 25 μM H3K9 acetyl peptide) at 37℃ for 4 hours. For the deacetylation assay (with fatty acid activation) using SIRT6 WT and mutants purified from *E. coli*, 2 μM of SIRT6 WT, S56Y, G60A, R65A or H133Y was incubated in 40 μL of reaction mixture (25 mM Tris-HCl pH 8.0, 50 mM NaCl, 1 mM DTT, 1 mM NAD^+, 25 μM H3K9 acetyl peptide, 300 μM palmitic acid) at 37℃ for 2 hours. To quench the reactions, 40 μL of cold acetonitrile was added into the reaction mixture. After centrifuging at 15,000 g for 15 min, the supernatant was collected and analyzed by HPLC using Kinetex 5u EVO C18 100A column (150 mm × 4.6 mm, Phenomenex). Solvents used for HPLC were water with 0.1% trifluoroacetic acid (solvent A) and acetonitrile with 0.1% trifluoroacetic acid (solvent B). The gradient for HPLC condition: 0% B for 2 min, 0-20% B in 2 min, 20-40% B in 13 min, 40-100% B in 2 min, and then 100% B for 5 min. The flow rate was 0.5 mL/min.

For the defatty-acylation assay using SIRT6 WT and mutants purified from HEK 293T cells, 0.2 μM of SIRT6 WT, S56Y, G60A, R65A or H133Y was incubated in 40 μL of reaction mixture (25 mM Tris-HCl pH 8.0, 50 mM NaCl, 1 mM DTT, 1 mM NAD^+, 5 μM H3K9 myristoyl peptide) at 37℃ for 60 min. For the deacetylation assay

using SIRT6 WT and mutants purified from HEK 293T cells, 0.4 μM of SIRT6 WT, S56Y, G60A, R65A or H133Y was incubated in 40 μL of reaction mixture (25 mM Tris-HCl pH 8.0, 50 mM NaCl, 1 mM DTT, 1 mM NAD^+, 5 μM H3K9 acetyl peptide, 300 μM palmitic acid) at 37℃ for 2.5 hours. To quench the reactions, 40 μL of cold acetonitrile was added into the reaction mixture. After centrifuging at 15,000 g for 15 min, the supernatant was collected and analyzed by HPLC using the same method described above.

Kinetics assay for SIRT6 WT and G60A on acetyl and myristoyl peptides. For the demyristoylation kinetics, 0.1 μM of SIRT6 WT or G60A was incubated with different concentrations of H3K9 myristoyl peptides (0.5-64 μM) in 40 μL of reaction mixture (25 mM Tris-HCl pH 8.0, 50 mM NaCl, 1 mM DTT, 1 mM NAD^+) at 37˚C for 10 min (SIRT6 WT) or 15 min (SIRT6 G60A). For the deacetylation kinetics without fatty acid, 6 μM of SIRT6 WT or 15 μM of SIRT6 G60A was incubated with different concentrations of H3K9 acetyl peptides (10-320 μM) in 40 μL of reaction mixture (25 mM Tris-HCl pH 8.0, 50 mM NaCl, 1 mM DTT, 1 mM NAD^+) at 37˚C for 60 min (SIRT6 WT) or 90 min (SIRT6 G60A). For the deacetylation kinetics with 300 μM palmitic acid, 0.8 μM of SIRT6 WT or 4 μM of SIRT6 G60A was incubated with different concentrations of H3K9 acetyl peptides (5-160 μM) in 40 μL of reaction mixture (25 mM Tris-HCl pH 8.0, 50 mM NaCl, 1 mM DTT, 1 mM NAD^+) at 37˚C for 30 min (SIRT6 WT) or 90 min (SIRT6 G60A). To quench the reactions, 40 μL of cold acetonitrile was added into the reaction mixture. After centrifuging at 15,000 g for 15 min, the supernatant was collected and analyzed by HPLC using the same method described above. For all the reactions, the conversions of acyl H3K9 to H3K9 were < 10%.

***In vitro* histone deacetylation assay.** Chromatin was purified from HEK 293T cells. Briefly, the cells were collected at 500 g for 5 min and then lysed in Nonidet P-40

lysis buffer (25 mM Tris-HCl pH 7.4, 150 mM NaCl, 10% glycerol and 1 % Nonidet P-40) with protease inhibitor cocktail (1:100 dilution) at 4℃ for 5 min. After centrifuging at 15,000 g for 5 min, the pellets were collected and washed with the Nonidet P-40 lysis buffer. Then Nonidet P-40 lysis buffer with universal nuclease (1:1000 dilution) and protease inhibitor cocktail (1:100 dilution) were added to the pellets and incubated at 25 ℃ for 10 min. After centrifuging at 15,000 g for 15 min, the supernatant was collected as chromatin proteins. For the histone deacetylation assay, 1 μM of SIRT6 WT, S56Y, G60A, R65A or H133Y was incubated with 3 μg of chromatin proteins in 30 μL of reaction mixture (25 mM Tris-HCl pH 8.0, 50 mM NaCl, 1 mM DTT, 1 mM NAD^+) at 37℃ for 120 min. Then the SDS loading buffer was added. The whole reaction mixture was heated at 95 ˚C for 5 min and then used for western blot analysis.

***In vitro* mono-ADP-ribosylation assay.** *In vitro* mono-ADP-ribosylation assay was performed according to reported procedures[14]. Briefly, 2.5 μM of SIRT6 WT, S56Y, G60A, R65A or H133Y was incubated in 30 μL of reaction mixture (25 mM Tris-HCl pH 8.0, 50 mM NaCl, 1 mM DTT, 50 μM 6-alkyne-NAD) at 30 ℃ for 30 min. For negative control, 50 μM of NAD^+ was added to replace 6-alkyne-NAD. Then click chemistry was performed. BODIPY-N_3 (1 μL of 4.5 mM solution in DMF), Tris[(1-benzyl-1H-1,2,3-triazol-4-yl)methyl]amine (1.8 μL of 10 mM solution in DMF), CuSO4 (1.5 μL of 40 mM solution in H_2O) and Tris(2-carboxyethyl)phosphine (1.5 μL of 40 mM solution in H_2O) were added into the reaction mixture. The click chemistry reaction was allowed to proceed at room temperature for 30 min. Then SDS loading buffer was added and the mixture was heated at 95 ˚C for 5 min. The reaction mixture was resolved by 12% SDS-PAGE. Protein gel was incubated in destaining buffer (50% methanol, 40% water, 10% acetic acid) at room temperature for 2 h. BODIPY fluorescence signal was then recorded by Typhoon 9400 Variable Mode

Imager (GE Healthcare Life Sciences) with PMT 550 V and normal sensitivity. After recording the fluorescence, the gel was stained by Coomassie blue buffer (0.2% Coomassie brilliant blue R-250 dye, 50% methanol, 40% water, 10% acetic acid) to quantify the protein loading.

Stable overexpression of SIRT6 WT, S56Y, G60A, R65A or H133Y in *Sirt6* KO MEFs. Full-length human SIRT6 WT and mutants were inserted into lentiviral vector (pCDH-CMV-MCS-EF1-Puro) without tag. Lentivirus was generated by co-transfection of SIRT6, pCMV-dR8.2, and pMD2.G into HEK 293T cells. The medium was collected 48 h after transfection and was used to infect *Sirt6* KO MEFs. To obtain the SIRT6 stable overexpressed cells, the cells were treated by 1.5 mg/mL of puromycin 48 h after infection. Empty pCDH vector was used as the negative control.

Detection of lysine fatty-acylation on TNFα by in-gel fluorescence. Human full-length TNFα cDNA with N-terminal Flag tag was inserted into pCMV-Tag 4a vector. The TNFα plasmid was transfected into *Sirt6* KO MEFs and *Sirt6* KO MEFs expressing SIRT6 WT, S56Y, G60A, R65A, or H133Y by FuGene 6 transfection reagent. After 18 h, the cells were treated with 50 μM Alk14 and 4 μg/mL brefeldin A for another 6 h. The cells were collected at 500 g for 5 min and then lysed in Nonidet P-40 lysis buffer (25 mM Tris-HCl pH 7.4, 150 mM NaCl, 10% glycerol, and 1 % Nonidet P-40) with protease inhibitor cocktail (1:100 dilution) at 4℃ for 30 min. After centrifuging at 15,000 g for 15 min, the supernatant was collected and incubated with 20 μL of anti-Flag affinity gel at 4 ˚C for 2 h. The affinity gel was washed three times with washing buffer (25 mM Tris-HCl pH 7.4, 150 mM NaCl, 0.2% Nonidet P-40) and then re-suspended in 18 μL of washing buffer. BODIPY-N_3 (0.7 μL of 4.5 mM solution in DMF), Tris[(1-benzyl-1H-1,2,3-triazol-4-yl)methyl]amine (1.2 μL of 10 mM solution in DMF), CuSO4 (1 μL of 40 mM solution in H_2O) and Tris(2-carboxyethyl)phosphine (1 μL of 40 mM solution in H_2O) were added into the

reaction mixture. The click chemistry reaction was allowed to proceed at room temperature for 30 min. Then SDS loading buffer was added and heated at 95 ˚C for 10 min. After centrifugation at 15,000 g for 2 min, the supernatant was collected, treated with 400 mM hydroxylamine, and heated at 95 ˚C for 10 min. The samples were resolved by 12% SDS-PAGE. BODIPY fluorescence signal was recorded by Typhoon 9400 Variable Mode Imager (GE Healthcare Life Sciences) with PMT 550 V and normal sensitivity.

Generation of SIRT6 KO in HEK 293T cells by CRISPR/Cas9 technology. SIRT6 KO HEK 293T cells were generated according to reported procedures[24]. The guide RNAs were cloned into pLKO2 vector. The sequences of guide RNAs are:

SIRT6 Nickase pair 3_A: 5'- CACCGTCCATGGTCCAGACTCCGTG-3';

SIRT6 Nickase pair 3_A': 5'- AAACCACGGAGTCTGGACCATGGAC-3';

SIRT6 Nickase pair 3_B: 5'- CACCGACACCACCTTTGAGAGCGCG-3';

SIRT6 Nickase pair 3_B': 5'-AAACCGCGCTCTCAAAGGTGGTGTC-3'.

Western blot. Proteins were resolved by 12% or 15% SDS-PAGE and transferred to polyvinylidene fluoride (PVDF) membrane. The membrane was blocked with 5% BSA in TPBS (0.1% Tween-20 in PBS solution) at room temperature for 60 min. The antibody was diluted with fresh 5% BSA in TPBS (1:5000 dilution for Flag, β-Actin, GAPDH, HSP90, Ac-H3K9, Ac-H3K56 and histone H3, 1:1000 dilution for Na, K, ATPase, Lamin A/C, SIRT6, RanGAP1, Ran, Annexin A1, Tenascin, COL5A1, COL6A1, VCP, RPL17, RPS7 and CXCL1) and then incubated with membrane at room temperature for 1 h (Flag, β-Actin, GAPDH and histone H3) or at 4 ˚C for 12 h (Ac-H3K9, Ac-H3K56, SIRT6, RanGAP1, Ran, Annexin A1, Tenascin, COL5A1, COL6A1, VCP, RPL17,RPS7, CXCL1, Na, K, ATPase, Lamin A/C and HSP90). For histone H3, Ac-H3K9, Ac-H3K56, SIRT6, RanGAP1, Ran, Annexin A1, Tenascin, COL5A1, COL6A1, VCP, RPL17,RPS7, CXCL1, Na, K, ATPase, Lamin A/C and

HSP90 western blots, after washing the membrane three times by TPBS, the secondary antibody (1:3000 dilution in 5% BSA in TPBS) was added and then incubated at room temperature for 1 h. The chemiluminescence signal in membrane was recorded after developing in ECL plus western blotting detection reagents using Typhoon 9400 Variable Mode Imager (GE Healthcare Life Sciences).

ELISA analysis of TNFα secretion in MEFs. After transient transfection of TNFα into *Sirt6* WT MEFs, *Sirt6* KO MEFs and *Sirt6* KO MEFs expressing SIRT6 WT, G60A, or H133Y for 18 h, the medium was changed to fresh medium. The cells were incubated with the new medium for 12 h. Then the medium and the cells were collected separately. Human TNFα ELISA kit (eBioscience) was used for quantifying TNFα in the medium and the cells following the manufacturer's instructions. Percentage of secreted TNFα was calculated by the TNFα in the medium versus total TNFα in the medium and the cells.

Crystal violet assay. The cells were seeded onto 12-well plates at low density (3,000 cells/well). After 48 h, the medium was removed and glucose free DMEM medium with 10% heat inactivated FBS was added into each well for another 72 h. The cells were washed two times with cold PBS, and then fixed with cold methanol for 10 min. After removing the methanol, the crystal violet staining solution (0.2% in 2% ethanol solution) was added and incubated for 5 min. The cells were then washed with water until all excess dye was removed. Crystal violet dye that remained with the cells was solubilized by incubating with 0.5% SDS in 50% ethanol solution. The absorption of crystal violet was measured at 550 nm.

Collection of secreted protein in MEFs. The MEFs were cultured to 90% confluence. The medium was removed and the cells were washed 3 times with PBS and then 3 times with serum-free DMEM medium. Then the cells were cultured in serum free DMEM medium for 12 h. The medium was collected and first centrifuged

at 500 g for 5 min to pellet floating cells. Then a second centrifugation at 3,000 g for 10 min was carried out to remove cell debris. The supernatant containing total secreted proteins was transferred into Amicon Ultra-15 Centrifugal Filter Units with 10 kDa cutoff for concentration. The concentrated secreted proteins (100-150 times concentrated) were used for SDS-PAGE analysis and Stable Isotope Labeling by Amino acids in Cell culture (SILAC).

SILAC. *Sirt6* KO MEFs were cultured in DMEM with [$^{13}C_6$, $^{15}N_2$]-L-lysine and [$^{13}C_6$, $^{15}N_4$]-L-arginine for 5 generations. *Sirt6* WT MEFs, *Sirt6* KO MEFs expressing SIRT6 WT, G60A, or H133Y were cultured in normal DMEM for 5 generations. Then the secreted proteins were collected using the same method described above. After quantifying the concentration of total secreted proteins by Bradford assay, 40 μg of proteins of each pair of samples (heavy labeled and light labeled) was mixed. Disulfide reduction and protein denaturation were performed in 6 M urea, 10 mM DTT, 50 mM Tris-HCl pH 8.0 at room temperature for 1 h. Iodoacetamide was added (final concentration 40 mM) and incubated at room temperature for 1 h. DTT was then added and incubated at room temperature for 1 h to stop alkylation. After diluting the sample 7 times with 50 mM Tris-HCl pH 8.0 and 1 mM $CaCl_2$, trypsin digestion was performed at 37℃ for 18 h. Digestion was quenched with 0.1 % trifluoroacetic acid and the mixture was desalted using Sep-Pak C18 cartridge. The lyophilized peptides were used for LC-MS/MS analysis.

Nano LC-MS/MS analysis. The lyophilized peptides were dissolved in 2% acetonitrile with 0.5% formic acid for nano LC-ESI-MS/MS analysis, which was carried out on a LTQ-Orbitrap Elite mass spectrometer (Thermo Fisher Scientific, San Jose, CA). The Orbitrap was interfaced with Dionex UltiMate3000 MDLC system (Thermo Dionex, Sunnyvale, CA). Protein samples were injected onto a Acclaim PepMap nano Viper C18 trap column (5 μm, 100 μm × 2 cm, Thermo Dionex) at a

flow rate of 20 μL/min for on-line desalting and then separated on C18 RP nano column (5 μm, 75 μm × 50 cm, Magic C18, Bruker). The gradient for HPLC condition was 5-38% acetonitrile with 0.1% formic acid in 120 min. The flow rate was 0.3 μL/min. The Orbitrap Elite was operated in positive ion mode with spray voltage 1.6 kV and source temperature 275 ˚C. Data-dependent acquisition (DDA) mode was used by one precursor ions MS survey scan from m/z 300 to 1800 at resolution 60,000 using FT mass analyzer, followed by up to 10 MS/MS scans at resolution 15,000 on 10 most intensive peaks. All data were acquired in Xcalibur 2.2 operation software (Thermo Fisher Scientific).

RNA extraction, reverse transcription and PCR analysis of the mRNA levels of target genes. *Sirt6* WT MEFs, *Sirt6* KO MEFs, *Sirt6* KO MEFs expressing SIRT6 WT, G60A, or H133Y were collected and used for RNA extraction. Total RNAs were extracted using RNeasy Mini kit (QIAGEN). Reverse transcription were performed with SuperScript III First-Strand Synthesis kit (Invitrogen) following the manufacturer's instructions. For PCR amplication, Herculase II Fusion Enzyme with dNTPs Combo kit (Agilent) was used following the manufacturer's instructions. For real-time PCR analysis, iTaq Universal SYBR Green Supermix (Biorad) was used following the manufacturer's instructions. The reaction was monitored using LightCycle 480 II system (Roche).

SIRT6 localization by subcellular fractionation and confocal imaging. Subcellular fractionation and immunofluorescence were performed according to the reported procedures[25,26]. Confocal imaging was performed by Zeiss LSM880 confocal/multiphoton microscope.

Intrinsic tryptophan fluorescence of SIRT6 WT and mutants. Fluorescence emission was monitored by Cary Eclipse Fluorescence Spectrophotometer (Agilent). The excitation wavelength was set as 295 nm (slit 2.5 nm), and the emission spectra

were monitored from 320 to 390 nm (slit 5 nm). 3 μM SIRT6 WT, S56Y, G60A, R65A or H133Y in 25 mM Tris-HCl pH 7.4, 150 mM NaCl and 10% glycerol was used for measuring NAD^+ binding. Increasing concentrations of NAD^+ were added to 3 μM SIRT6 WT and mutants solution (0-100 μM NAD^+ for SIRT6 H133Y, 0-500 μM NAD^+ for SIRT6 WT and S56Y, and 0-5 mM NAD^+ for SIRT6 G60A and R65A), and the emission spectra were monitored. To measure SIRT6 WT and G60A binding to NAD^+ with saturated acetyl peptide, 1 mM Ac-H3K9 (without tryptophan) was mixed with 3 μM SIRT6 WT or G60A, then increasing concentrations of NAD^+ were added and the emission spectra were monitored. The peak maximum for each experiment was obtained. The following equation was used for calculating the fraction of NAD^+ bound (*NB*):

$$NB = \frac{F - F_0}{F_{sat} - F_0}$$

where F is the maximum fluorescence intensity at each NAD^+ concentration, F_0 is the maximum fluorescence intensity with 0 μM of NAD^+, and F_{sat} is the maximum fluorescence intensity with saturated NAD^+. The *NB* values were plotted against NAD^+ concentrations, and the curves were fitted to following equation (one-site binding) using GraphPad Prism:

$$NB = \frac{[E] + [NAD^+] + K_d - \sqrt{([E] + [NAD^+] + K_d)^2 - 4 \times [E] \times [NAD^+]}}{2 \times [E]}$$

where [E] is SIRT6 concentration (3 μM), [NAD^+] is NAD^+ concentration, and K_d is the dissociation constant.

To measure the emission spectra of SIRT6 WT and G60A with and without saturated Ac-H3K9 and Myr-H3K9, 3 μM SIRT6 WT or G60A was mixed with 1 mM Ac-H3K9 (without tryptophan) or 0.1 mM Myr-H3K9 (without tryptophan) and then the emission spectra were monitored. The emission spectra of blank buffer and 1 mM Ac-H3K9 or 0.1 mM Myr-H3K9 in blank buffer were also monitored as control.

HPLC analysis of SIRT6 binding to NAD^+. 10 μM of SIRT6 WT, G60A or H133Y was incubated with 10 μM NAD^+ in 50 μL of buffer (25 mM Tris-HCl pH 8.0, 50 mM NaCl) at room temperature for 30 min. Then 450 μL of buffer was added and all the 500 μL of buffer with SIRT6 and NAD^+ was transferred to Amicon Ultra-0.5 centrifugal filter unit with ultracel-10 membrane. After centrifuge at 15,000 g for 20 min, all filtrate (~400 μL) was collected and lyophilized. The lyophilized powder was dissolved in 50 μL water and used for HPLC analysis.

Thermal Shift Assay. 5 μM of SIRT6 WT or G60A was mixed with or without 1 mM H3K9 acetyl or 100 μM H3K9 myristoyl peptide in the reaction buffer (25 mM Tris-HCl pH 8.0, 50 mM NaCl). The temperature was set from 37 to 62 ˚C for 3 min in the PCR Thermocycler. Then the samples were centrifuged at 15,000 g for 20 min, the supernatant was analyzed by SDS-PAGE and proteins were visualized by Coomassie blue staining.

Isolation of microvesicles and exosomes. After two 150 mm dishes of the cells grow to 90% confluence, the medium was removed and the cells were washed 3 times with PBS and 3 times with serum-free DMEM medium. Then the culture medium was changed to serum-free medium and the cells were cultured for another 12 h. The medium was collected and subjected to two centrifuges: 500 g for 5 min (to pellet floating cells) and 3,000 g for 20 min (to pellet cell debris). The supernatant was subjected to 0.2 μm syringe filter with low flow rate (<1 drop/second), the vesicles retained on the filter (microvesicles) were washed once by PBS. The microvesicles were then lysed on the filter by Nonidet P-40 lysis buffer (25 mM Tris-HCl pH 7.4, 150 mM NaCl, 10% glycerol, and 1 % Nonidet P-40) with protease inhibitor cocktail (1:100 dilution). The filtrate was subjected to ultracentrifuge at 100,000 g for 2 h. The supernatant was vesicle free medium. The pellets were exosomes and were washed once by PBS and subjected to another ultracentrifuge at 100,000 g for 2 h. To get

proteins from the exosomes, the exosome pellets were lysed by Nonidet P-40 lysis buffer (25 mM Tris-HCl pH 7.4, 150 mM NaCl, 10% glycerol, and 1 % Nonidet P-40) with protease inhibitor cocktail (1:100 dilution). For cell proliferation experiment, the exosome pellets were suspended in serum-free DMEM. Exosome concentrations were determined by nanoparticle tracking analysis (NTA) according to the reported procedures[27].

Statistical Analysis. Data were expressed as mean ± s.d. (standard deviation, shown as error bars). Differences were examined by two-tailed Student's *t*-test between two groups; $*p < 0.05$, $**p < 0.01$, $***p < 0.005$.

REFERENCES

1 Mostoslavsky, R. *et al.* Genomic instability and aging-like phenotype in the absence of mammalian SIRT6. *Cell* **124**, 315-329, doi:10.1016/j.cell.2005.11.044 (2006).

2 Michishita, E. *et al.* SIRT6 is a histone H3 lysine 9 deacetylase that modulates telomeric chromatin. *Nature* **452**, 492-496, doi:10.1038/nature06736 (2008).

3 Kaidi, A., Weinert, B. T., Choudhary, C. & Jackson, S. P. Human SIRT6 promotes DNA end resection through CtIP deacetylation. *Science* **329**, 1348-1353, doi:10.1126/science.1192049 (2010).

4 Mao, Z. *et al.* SIRT6 promotes DNA repair under stress by activating PARP1. *Science* **332**, 1443-1446, doi:10.1126/science.1202723 (2011).

5 Sebastian, C. *et al.* The histone deacetylase SIRT6 is a tumor suppressor that controls cancer metabolism. *Cell* **151**, 1185-1199, doi:10.1016/j.cell.2012.10.047 (2012).

6 Zhong, L. *et al.* The histone deacetylase Sirt6 regulates glucose homeostasis via Hif1alpha. *Cell* **140**, 280-293, doi:10.1016/j.cell.2009.12.041 (2010).

7 Kawahara, T. L. *et al.* SIRT6 links histone H3 lysine 9 deacetylation to NF-kappaB-dependent gene expression and organismal life span. *Cell* **136**, 62-74, doi:10.1016/j.cell.2008.10.052 (2009).

8 Kanfi, Y. *et al.* The sirtuin SIRT6 regulates lifespan in male mice. *Nature* **483**, 218-221, doi:10.1038/nature10815 (2012).

9 Michishita, E. *et al.* Cell cycle-dependent deacetylation of telomeric histone H3 lysine K56 by human SIRT6. *Cell cycle* **8**, 2664-2666, doi:10.4161/cc.8.16.9367 (2009).

10 Feldman, J. L., Baeza, J. & Denu, J. M. Activation of the protein deacetylase SIRT6 by long-chain fatty acids and widespread deacylation by mammalian sirtuins. *The Journal of biological chemistry* **288**, 31350-31356,

doi:10.1074/jbc.C113.511261 (2013).
11 Jiang, H. *et al.* SIRT6 regulates TNF-alpha secretion through hydrolysis of long-chain fatty acyl lysine. *Nature* **496**, 110-113, doi:10.1038/nature12038 (2013).
12 Liszt, G., Ford, E., Kurtev, M. & Guarente, L. Mouse Sir2 homolog SIRT6 is a nuclear ADP-ribosyltransferase. *The Journal of biological chemistry* **280**, 21313-21320, doi:10.1074/jbc.M413296200 (2005).
13 Gil, R., Barth, S., Kanfi, Y. & Cohen, H. Y. SIRT6 exhibits nucleosome-dependent deacetylase activity. *Nucleic acids research* **41**, 8537-8545, doi:10.1093/nar/gkt642 (2013).
14 Du, J., Jiang, H. & Lin, H. Investigating the ADP-ribosyltransferase activity of sirtuins with NAD analogues and 32P-NAD. *Biochemistry* **48**, 2878-2890, doi:10.1021/bi802093g (2009).
15 Pan, P. W. *et al.* Structure and biochemical functions of SIRT6. *The Journal of biological chemistry* **286**, 14575-14587, doi:10.1074/jbc.M111.218990 (2011).
16 Tennen, R. I., Berber, E. & Chua, K. F. Functional dissection of SIRT6: identification of domains that regulate histone deacetylase activity and chromatin localization. *Mechanisms of ageing and development* **131**, 185-192, doi:10.1016/j.mad.2010.01.006 (2010).
17 Al-Nedawi, K., Meehan, B. & Rak, J. Microvesicles: messengers and mediators of tumor progression. *Cell cycle* **8**, 2014-2018 (2009).
18 Antonyak, M. A. *et al.* Cancer cell-derived microvesicles induce transformation by transferring tissue transglutaminase and fibronectin to recipient cells. *Proceedings of the National Academy of Sciences of the United States of America* **108**, 4852-4857, doi:10.1073/pnas.1017667108 (2011).
19 Costa-Silva, B. *et al.* Pancreatic cancer exosomes initiate pre-metastatic niche formation in the liver. *Nature cell biology* **17**, 816-826, doi:10.1038/ncb3169 (2015).
20 Ewald, C. Y., Landis, J. N., Porter Abate, J., Murphy, C. T. & Blackwell, T. K. Dauer-independent insulin/IGF-1-signalling implicates collagen remodelling in longevity. *Nature* **519**, 97-101, doi:10.1038/nature14021 (2015).
21 Zhu, A. Y. *et al.* Plasmodium falciparum Sir2A preferentially hydrolyzes medium and long chain fatty acyl lysine. *ACS chemical biology* **7**, 155-159, doi:10.1021/cb200230x (2012).
22 Charron, G. *et al.* Robust fluorescent detection of protein fatty-acylation with chemical reporters. *Journal of the American Chemical Society* **131**, 4967-4975, doi:10.1021/ja810122f (2009).
23 Jiang, H., Kim, J. H., Frizzell, K. M., Kraus, W. L. & Lin, H. Clickable NAD analogues for labeling substrate proteins of poly(ADP-ribose) polymerases. *Journal of the American Chemical Society* **132**, 9363-9372, doi:10.1021/ja101588r (2010).
24 Cong, L. *et al.* Multiplex genome engineering using CRISPR/Cas systems. *Science* **339**, 819-823, doi:10.1126/science.1231143 (2013).
25 Huang, Z. *et al.* Tumor suppressor Alpha B-crystallin (CRYAB) associates with the cadherin/catenin adherens junction and impairs NPC progression-

associated properties. *Oncogene* **31**, 3709-3720, doi:10.1038/onc.2011.529 (2012).
26 Jedrusik-Bode, M. *et al.* The sirtuin SIRT6 regulates stress granule formation in C. elegans and mammals. *Journal of cell science* **126**, 5166-5177, doi:10.1242/jcs.130708 (2013).
27 Soo, C. Y. *et al.* Nanoparticle tracking analysis monitors microvesicle and exosome secretion from immune cells. *Immunology* **136**, 192-197, doi:10.1111/j.1365-2567.2012.03569.x (2012).

CHAPTER 3

SIRT6 REGULATES RAS-RELATED PROTEIN R-RAS2 BY LYSINE DEFATTY-ACYLATION[a]

Abstract

The Ras family of GTPases are important in cell signaling and frequently mutated in human tumors. Understanding their regulation is thus important for studying biology and human diseases. Here we report that a novel posttranslational mechanism, reversible lysine fatty-acylation, regulates R-Ras2, a member of the Ras family. SIRT6, a sirtuin with established tumor suppressor function, regulates the lysine fatty-acylation of R-Ras2. In mouse embryonic fibroblasts (MEFs), *Sirt6* knockout (KO) increased R-Ras2 lysine fatty-acylation. Lysine fatty-acylation promotes the plasma membrane localization of R-Ras2 and its interaction with phosphatidylinositol 3-kinase PI3K, leading to activated Akt and increased cell proliferation. Our study establishes lysine fatty-acylation as a previously unknown mechanism that regulates the Ras family of GTPases and provides an important mechanism by which SIRT6 functions as a tumor suppressor.

[a] This is a revised version of our published paper: Zhang X, et al. SIRT6 regulates Ras-related protein R-Ras2 by lysine defatty-acylation. ***eLife***, 6 (2017) e25158

Introduction

SIRT6 (sirtuin 6) belongs to the Sir2 (silencing information regulator 2) family of nicotinamide adenine dinucleotide (NAD^+)-dependent protein lysine deacylases. It plays important roles in a variety of biological processes, including DNA damage and repair [1-3], glucose metabolism [4], and cell proliferation [5]. *Sirt6* knockout (KO) mice display multiple defects and die a few weeks after birth. Underlying its biological functions, SIRT6 has multiple enzymatic activities. It can deacetylate histone H3 lysine 9 (Ac-H3K9), lysine 18 (Ac-H3K18), and lysine 56 (Ac-H3K56) [6-9], to suppress target gene expression of several transcription factors, including NF-κB [10], HIF-1α [4], c-Jun [11], and c-Myc [5]. SIRT6 has also been reported to be an adenosine diphosphate (ADP)-ribosyltransferase [2,12]. We have recently identified SIRT6 as an efficient lysine defatty-acylase that regulates the secretion of tumor necrosis factor (TNFα) [13]. Mechanistically, lysine fatty-acylation promotes TNFα targeting to lysosome and thus decreases its secretion [14]. However, it remains unclear whether SIRT6 regulates other proteins by defatty-acylation.

The Ras family of proteins plays important roles in numerous biological pathways, including signal transduction, membrane trafficking, nuclear export/import, and cytoskeletal dynamics [15]. Five branches of the Ras superfamily (Ras, Rho, Rab, Arf and Ran) are classified according to sequence similarity. Ras proteins can exist in two conformational states: a GDP-bound inactive state and a GTP-bound active state. In the GTP-bound state, Ras proteins can recruit effector proteins and turn on specific signaling pathways [16,17]. Protein post-translational modifications (PTMs) play important roles in regulating the Ras family of proteins [18]. Ras and Rho families of GTPases are modified by prenylation (farnesylation or geranylgeranylation) on their C-terminal CaaX motif at the cysteine residue. Some proteins from Ras and Rho families, such as H-Ras and N-Ras, contain cysteine palmitoylation as a second

lipidation. Both prenylation and palmitoylation serve as important membrane targeting signals [19,20]. Other proteins from Ras and Rho families, such as K-Ras4B, do not have cysteine palmitoylation, and are thought to use a C-terminal polybasic sequence for membrane targeting [19,20].

Here we demonstrate that a Ras family protein, R-Ras2 (also called TC21 because it was cloned from a human teratocarcinoma cDNA library)[21], which is able to transform cells and is up-regulated in several human cancers [22-25], is regulated by a novel PTM, lysine fatty-acylation. Importantly, SIRT6 is identified as the defatty-acylase of R-Ras2. SIRT6 defatty-acylates R-Ras2 and attenuates its plasma membrane localization, therefore inhibits its ability to activate PI3K signaling pathway and cell proliferation.

Results and discussion

Defatty-acylation contributes to SIRT6's tumor-suppressor function

SIRT6 has been reported to be a tumor suppressor [5]. Decreased SIRT6 expression levels are found in several human cancers. Enhanced glycolysis is observed in SIRT6-deficient cells and tumors, which is thought to drive tumor formation *in vivo* [5]. Interestingly, the tumor formation promoted by the loss of SIRT6 is oncogene *HRAS*-independent. However, the exact role of SIRT6 in cancer is still not well understood. In particular, which enzymatic activity is important for the tumor suppression function is not clear.

We have recently identified a single point mutation (G60A) of SIRT6 that maintains the defatty-acylase activity but exhibits no detectable deacetylase activity in cells [26]. Utilizing this mutant, we first investigated whether the defatty-acylase activity of SIRT6 contributes to tumor suppression and aimed to identify the defatty-acylation substrate protein that is important for this function. We stably expressed SIRT6 wild

type (WT) (exhibits both deacetylase and defatty-acylase activities), G60A (exhibits only defatty-acylase activity in cells), or H133Y (exhibits neither activity in cells) into *Sirt6* KO mouse embryonic fibroblasts (MEFs) and tested their effects on cell proliferation. *Sirt6* KO MEFs expressing SIRT6 WT showed decreased cell proliferation compared to those without SIRT6 expression (**Figure 3.1a**), consistent with the reported role of SIRT6 in suppressing cell proliferation. In contrast, expressing the H133Y mutant had no significant effect on cell proliferation. Interestingly, expression of the G60A mutant, which only exhibits the defatty-acylase activity in cells, also decreased cell proliferation, similar to the expression of SIRT6 WT (**Figure 3.1a**). The suppression of cell proliferation by SIRT6 WT was only slightly better than that by the G60A mutant. This suggests that although both deacetylase and defatty-acylase activities of SIRT6 contribute, the defatty-acylase activity plays a major role in regulating cell proliferation.

Identification of SIRT6 defatty-acylation targets

To identify the lysine defatty-acylation targets of SIRT6 that contribute to its tumor suppressing function, we used a quantitative mass spectrometry method, stable isotope labeling with amino acids in cell culture (SILAC), to identify proteins with different lysine fatty-acylation levels in *Sirt6* WT and KO MEFs. We used fatty acid analogs to metabolically label fatty-acylated proteins and enriched these proteins by incorporating a biotin tag through the copper(I)-catalyzed alkyne-azide cycloaddition (typically called click chemistry) followed by streptavidin pull-down (**Figure 3.1b).** Two fatty acid analogs were used for cross comparison: Alk12 which better mimics myristic acid and Alk14 which better mimics palmitic acid[27]. When processing the samples, we used IpaJ, a cysteine protease from *Shigella flexneri* that has been reported to hydrolyze the peptide bond after *N*-myristoylated glycine [28], to reduce the

labeling background from *N*-myristoylation. We also used NH_2OH as nucleophile to remove fatty-acylation on cysteine residues.

There were 865 proteins identified in Alk12 SILAC and 1285 proteins identified in Alk14 SILAC. To narrow down the target lists, we filtered the data using 4 criteria (**Figure 3.1c**): 1) Protein score ≥ 10, and the number of unique peptide ≥ 2; 2) The target was present in both SILAC experiments, which could decrease the *N*-myristoylation background (proteins present only in Alk12 SILAC) and *S*-palmitoylation background (proteins present only in Alk14 SILAC); 3) Heavy/Light ratio ≥ 1.5, which allowed us to pick proteins that exhibited higher lysine fatty-acylation in *Sirt6* KO MEFs than in *Sirt6* WT MEFs; 4) The target had similar protein levels in *Sirt6* WT and KO MEFs by comparing the data from a total protein SILAC experiment, which was to make sure that proteins with higher Heavy/Light ratios in Alk12 and Alk14 SILAC were not due to increased protein levels. With these criteria, we narrowed down the target lists to 5 proteins (**Figure 3.1c**).

Interestingly, a Ras-related small GTPase, R-Ras2, was one of the possible defatty-acylation targets of SIRT6. R-Ras2, like its cousins (H-, N-, and K-Ras), is known to be highly relevant to cancer[24,29-31]. We thus hypothesized that the tumor suppressing function of SIRT6 could be through regulating R-Ras2. To test this hypothesis, we knocked down R-Ras2 in *Sirt6* WT and KO MEFs and examined the cell proliferation. Knockdown of R-Ras2 in both *Sirt6* WT and KO MEFs by two different shRNAs significantly decreased cell proliferation (**Figure 3.1d**), suggesting that R-Ras2 is important for cell proliferation in MEFs.

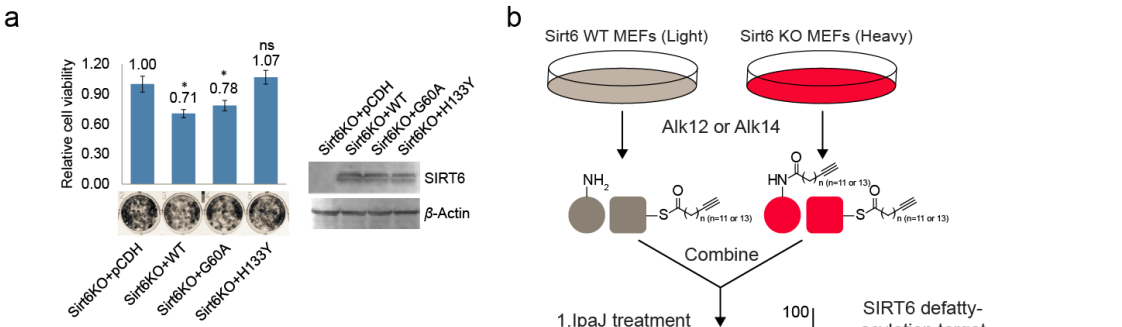

	Alk12 SILAC		Alk14 SILAC		Protein SILAC	
	Heavy/ Light	# Peptides	Heavy/ Light	# Peptides	Heavy/ Light	# Peptides
IMPDH2	2.39	6	2.24	4	1.04	11
PGK1	1.77	12	1.88	11	0.96	20
CAD	1.74	10	1.54	19	0.97	40
R-Ras2	1.70	3	1.61	2	0.93	3
GAPDH	1.66	14	1.84	12	1.08	15

Figure 3.1. Identification of defatty-acylation targets of SIRT6 that contribute to its function in cell proliferation. (a) Cell proliferation of *Sirt6* KO MEFs stably expressing pCDH empty vector, SIRT6 WT, G60A, or H133Y. Cell proliferation was assayed and quantified using crystal violet staining. Values with error bars indicate mean ± s.d. of three biological replicates. * indicates $p < 0.05$ and "ns" indicates no statistical significant when comparing to *Sirt6* KO MEFs with pCDH. (b) Schematic overview of the SILAC experiment to identify SIRT6 lysine defatty-acylation targets. (c) Data analysis and filter of SILAC results. (d) Effects of R-Ras2 knockdown on the proliferation of *Sirt6* WT and KO MEFs. Values with error bars indicate mean ± s.d. of three biological replicates. *** indicates $p < 0.005$ for comparing to *Sirt6* KO MEFs with ctrl shRNA.

R-Ras2 is SIRT6 defatty-acylation target

We then validated whether R-Ras2 has lysine fatty-acylation. We first examined R-Ras2 mRNA and proteins levels in *Sirt6* WT and KO MEFs. The results showed that SIRT6 did not affect the transcription and translation of R-Ras2 (**Figure 3.2a**). We then used the fatty acid analog Alk14 to metabolically label an overexpressed FLAG-tagged R-Ras2. After FLAG immunoprecipitation, we conjugated a fluorescent dye (520-BODIPY-azide) through click chemistry to allow visualization of fatty-acylated R-Ras2 by in-gel fluorescence (**Figure 3.2b**) . We used hydroxylamine (NH_2OH) to remove potential cysteine fatty-acylation. Thus, the in-gel fluorescence signal should be mainly attributed to fatty-acylation on lysine residues. R-Ras2 exhibited increased lysine (NH_2OH-resistant) fatty-acylation in *Sirt6* KO MEFs than in WT MEFs (**Figure 3.2c**). We also observed increased R-Ras2 lysine fatty-acylation in Human Embryonic Kidney (HEK) 293T cells after knocking down SIRT6 with two different Sirt6 shRNAs, but not with a control shRNA (**Figure 3.2d**).We then used an alternative method to detect lysine fatty-acylation on overexpressed FLAG-tagged R-Ras2. We treated the cells with Alk14, and then incorporated a biotin tag on fatty-acylated proteins (including R-Ras2) through click chemistry. We pulled down the fatty-acylated proteins using streptavidin beads and then removed *S*-palmitoylation from the streptavidin beads by NH_2OH treatment. The proteins on beads were then resolved by gel electrophoresis and the level of R-Ras2 was detected by FLAG western blot. This method also revealed more lysine fatty-acylation on overexpressed R-Ras2 in *Sirt6* KO MEFs than in *Sirt6* WT MEFs (**Figure 3.2e**).

Using a similar method, we set out to examine whether endogenous R-Ras2 was regulated by lysine fatty-acylation. Endogenous R-Ras2 labeled with Alk4 was conjugated to biotin and pulled down with streptavidin beads. More fatty-acylated endogenous R-Ras2 was pulled down from *Sirt6* KO MEFs than from WT MEFs (**Figure 3.2f**), suggesting that endogenous R-Ras2 contained more lysine fatty-

acylation in *Sirt6* KO MEFs.

To confirm that SIRT6 could defatty-acylate R-Ras2 directly, we overexpressed FLAG-tagged R-Ras2 in *Sirt6* KO MEFs, metabolically labeled with Alk14, and then purified R-Ras2 protein from total cell lysates. We then incubated R-Ras2 with SIRT6 in the presence of NAD^+ and subsequently performed click chemistry to detect R-Ras2 lysine fatty-acylation. In the presence of NAD^+, SIRT6 removed most of the lysine fatty-acylation signal from R-Ras2 (**Figure 3.2g**). We also used a previously established ^{32}P-NAD^+ assay, in which the newly generated fatty-acyl adenosine diphosphate ribose (ADPR) product could be easily detected on thin layer chromatography (TLC) plate, to detect lysine fatty-acylation on R-Ras2. SIRT6 WT, but not the catalytic mutant SIRT6 H133Y, generated the fatty-acyl ADPR spot in the presence of R-Ras2 isolated from *Sirt6* KO MEFs and NAD^+ (**Figure 3.2h**). These data suggested that R-Ras2 was fatty-acylated on lysine residues and SIRT6 could directly remove the fatty-acylation *in vitro*.

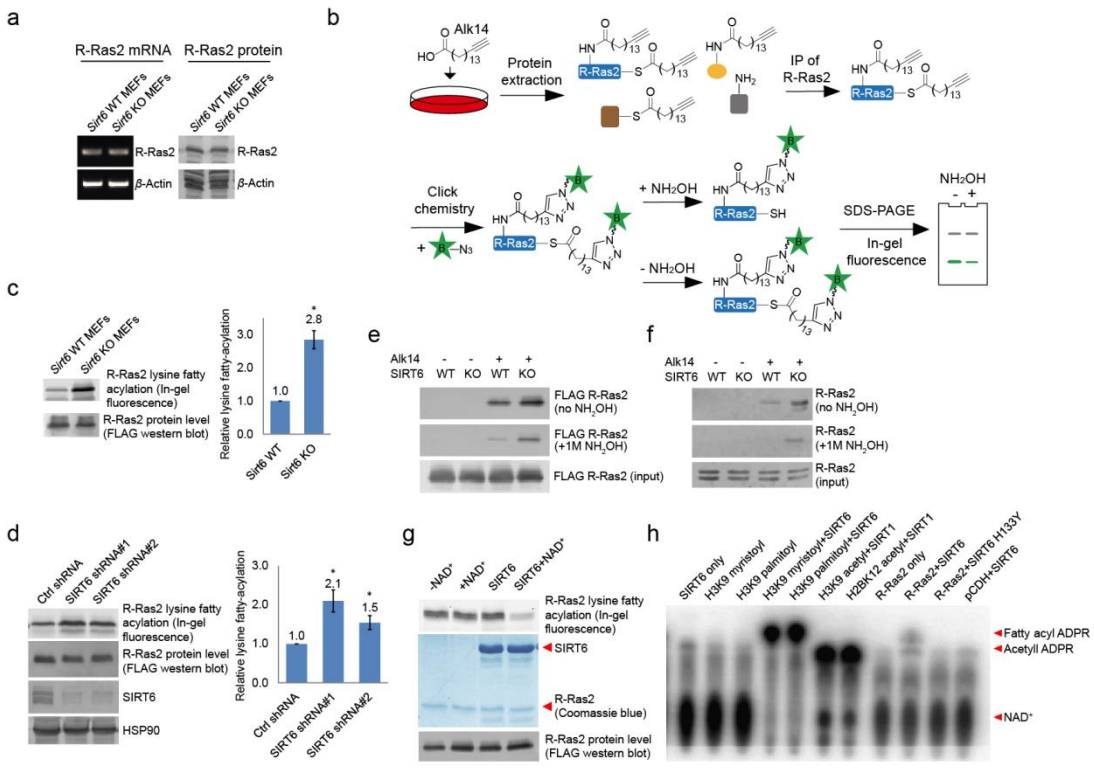

Figure 3.2. Validation of R-Ras2 as the defatty-acylation target of SIRT6. (a) mRNA and protein levels of R-Ras2 in *Sirt6* WT and KO MEFs. (b) Scheme showing the in-gel fluorescence method with Alk14 metabolic labeling to identify R-Ras2 as a lysine fatty-acylated protein. (c) In-gel fluorescence (with NH_2OH treatment) showing that R-Ras2 has higher lysine fatty-acylation level in *Sirt6* KO MEFs than in *Sirt6* WT MEFs. Right histogram shows the quantification of bands on the fluorescence gel. Values with error bars indicate mean ± s.d. of three biological replicates. * indicates $p < 0.05$. (d) Detection of R-Ras2 lysine fatty-acylation levels in control and SIRT6 knockown HEK 293T cells by in-gel fluorescence. Right histogram shows the quantification of bands on the fluorescence gel. Values with error bars indicate mean ± s.d. of three biological replicates. * indicates $p < 0.05$. (e) Lysine fatty-acylation levels of overexpressed R-Ras2 in *Sirt6* WT and KO MEFs. (f) Lysine fatty-acylation levels of endogenous R-Ras2 in *Sirt6* WT and KO MEFs. (g, h) SIRT6 defatty-acylated R-Ras2 in a NAD^+-dependent manner *in vitro*. In-gel fluorescence was used to detect R-

Ras2 lysine fatty-acylation (e). A ^{32}P-NAD^{+} assay was used to detect fatty-acyl ADPR product from defatty-acylation reaction. (f).

R-Ras2 is fatty-acylated on C-terminal lysine residues

Next, we set out to identify which lysine residues of R-Ras2 were fatty-acylated. We noticed that there are four lysine residues in the C-terminal hypervariable region (HVR) of R-Ras2: K192, K194, K196, and K197 (**Figure 3.3a**). This region is known as a C-terminal polybasic sequence and is generally believed to help anchor Ras proteins to the membrane through electrostatic interaction[18]. We suspected that some of these lysine residues might be fatty-acylated. We thus mutated these four lysine residues to arginine (the 4KR mutant), which should maintain the positive charge and thus, should not disrupt the membrane association provided by the positive charge. We examined the lysine fatty-acylation of R-Ras2 WT and 4KR in *Sirt6* KO MEFs and found that the 4KR mutant significantly decreased the lysine fatty-acylation signal (**Figure 3.3a**).

We then utilized mass spectrometry (MS) to directly identify the modification site using FLAG-tagged R-Ras2 purified from Alk14 treated *Sirt6* KO MEFs. A peptide (residue 193-197) carrying Alk14 modification on K194 was detected (**Figure 3.3b**). Interestingly, when we mutated each of these four lysine residues to arginine and detected their Alk14 labeling by in-gel fluorescence, the hydroxylamine-resistant labeling of all the single mutants was similar to that of WT (**Figure 3.3c**). This result suggested that K192, K194, K196, and K197 are likely to be fatty-acylated redundantly, although the MS result implied that K194 is preferentially fatty-acylated on WT R-Ras2 protein.

R-Ras2 is known to have palmitoylation on cysteine 199, which is close to the fatty-acylated lysine cluster. It is possible that lysine fatty-acylation occurs via acyl transfer

from the nearby acylated cysteine. To test this possibility, we mutated cysteine 199 to serine (the C199S mutant) and assayed its Alk14 labeling in HEK 293T cells. Alk14 labeling still occurred on R-Ras2 C199S mutant, which was NH_2OH resistant (**Figure 3.3d**), suggesting that cysteine fatty-acylation of R-Ras2 is not required for the occurrence of its lysine fatty-acylation.

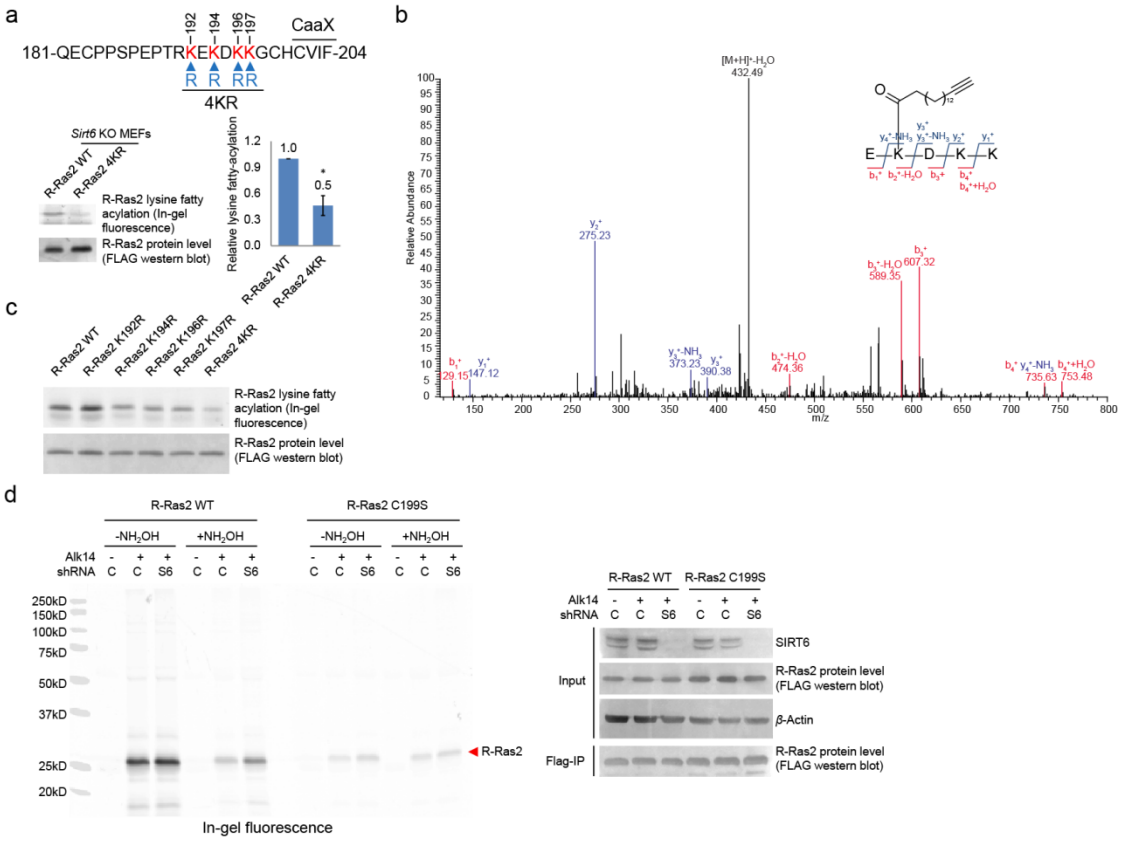

Figure 3.3. R-Ras2 is fatty-acylated on C-terminal lysine residues. (a) In-gel fluorescence (with NH_2OH treatment) showing that mutation of four lysine residues at the C-terminus of R-Ras2 significantly decreased lysine fatty-acylation in *Sirt6* KO MEFs. Right histogram shows the quantification of bands on the fluorescence gel. Values with error bars indicate mean ± s.d. of three biological replicates. * indicates $p < 0.05$. (b) Tandem mass (MS/MS) spectrum of doubly charged Alk14 modified (on K194) R-Ras2 peptide. The b- and y- ions are shown along with the peptide sequence.

(c) In-gel fluorescence (with NH_2OH treatment) showing that single mutation of four lysine residues at the C-terminus of R-Ras2 did not affect R-Ras2 lysine fatty-acylation. (d) In-gel fluorescence showing lysine fatty-acylation level of overexpressed R-Ras2 WT and C199S mutant in HEK 293T cells with SIRT6 knockdown. C, control shRNA. S6, SIRT6 shRNA#1.

Lysine fatty-acylation targets R-Ras2 to plasma membrane

To investigate the function of R-Ras2 lysine fatty-acylation, we first examined the subcellular localization of R-Ras2 WT and 4KR in both *Sirt6* WT and KO MEFs by confocal imaging. In *Sirt6* WT MEFs, both R-Ras2 WT and 4KR were localized in the plasma membrane and intracellular vesicles (**Figure 3.4a**). In contrast, in *Sirt6* KO MEFs, R-Ras2 WT was mainly localized in the plasma membrane, while R-Ras2 4KR was localized in both the plasma membrane and intracellular vesicles (**Figure 3.4a**). Considering that R-Ras2 WT in *Sirt6* KO MEFs has the highest lysine fatty-acylation level (**Figure 3.2c** and **3.3a**), this data suggests that lysine fatty-acylation helps targeting R-Ras2 to the plasma membrane.

In addition, we performed subcellular fractionation of HEK 293T cells overexpressing FLAG-tagged R-Ras2. Under normal conditions, SIRT6 was present and removed most fatty-acyl group from R-Ras2 lysine residues, and thus we did not observe obvious difference in plasma membrane and cytosol localizations between WT R-Ras2 and the 4KR mutant (**Figure 3.4b**). When we treated the cells with palmitic acid (to increase R-Ras2 lysine fatty-acylation) or SIRT6 inhibitor TM3 (to inhibit SIRT6 defatty-acylase activity)[32], we observed decreased cytosolic localization of WT R-Ras2, but not the 4KR mutant (**Figure 3.4b**). This data also supports that lysine fatty-acylation of R-Ras2 targets it to the plasma membrane.

To further confirm that SIRT6 regulates R-Ras2 by defatty-acylation and not

deacetylation, we expressed SIRT6 G60A, which exhibits no detectable deacetylase activity in cells, in *Sirt6* KO MEFs and examined the lysine fatty-acylation and subcellular localization of R-Ras2. Expressing the G60A mutant in *Sirt6* KO MEFs decreased R-Ras2 lysine fatty-acylation to the same level as expressing WT SIRT6 (**Figure 3.5a**). *In vitro*, the G60A mutant removed fatty-acylation from R-Ras2 similar to WT SIRT6 (**Figure 3.5b**). Confocal imaging results showed that in *Sirt6* KO MEFs, expression of the G60A mutant promoted R-Ras2 dissociation from the plasma membrane, similar to the expression of WT SIRT6 (**Figure 3.5c**). Subcellular fractionation of endogenous R-Ras2 showed that, similar to WT SIRT6, the G60A mutant decreased the plasma membrane-localized endogenous R-Ras2 and increased the cytosol-localized endogenous R-Ras2 (**Figure 3.5d**). These data collectively demonstrated that the defatty-acylase activity of SIRT6 is sufficient to regulate R-Ras2.

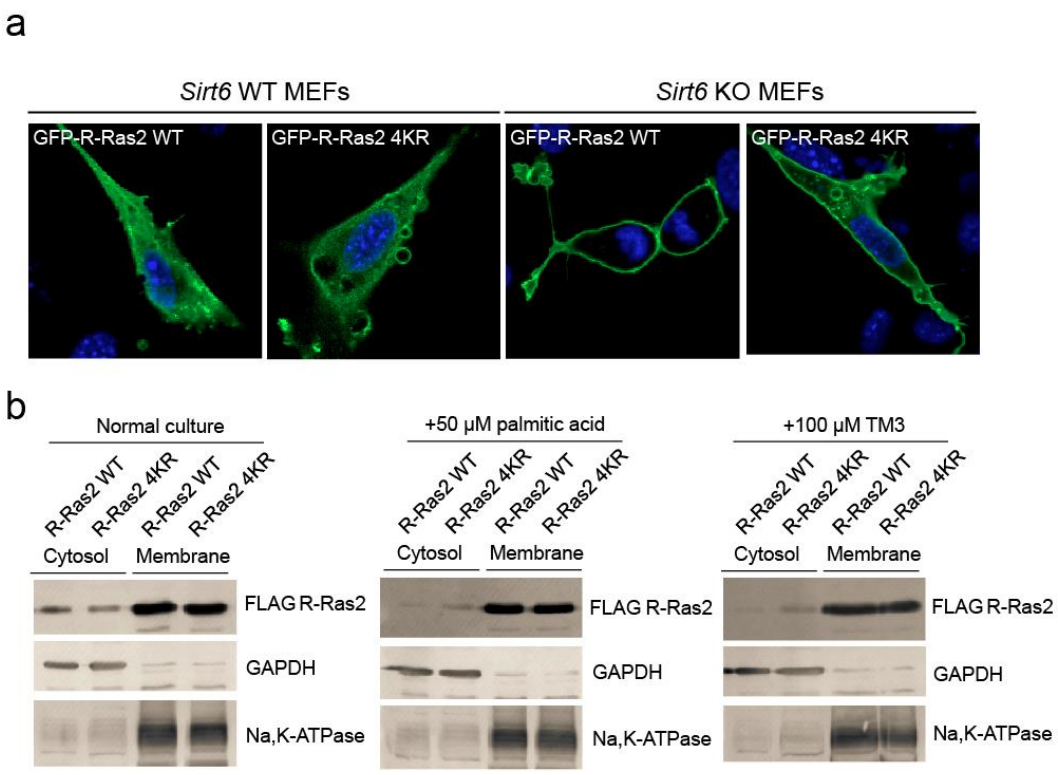

Figure 3.4. Lysine fatty-acylation targets R-Ras2 to plasma membrane. (a) Confocal imaging showed that R-Ras2 WT was mainly localized in the plasma membrane in *Sirt6* KO MEFs. R-Ras2 WT in *Sirt6* WT MEFs as well as R-Ras2 4KR in *Sirt6* WT and KO MEFs was localized in both the cytosol and plasma membrane (n = 5, 5, 5, 6 cells for each sample from left to right, respectively). (b) Subcellular fractionation of R-Ras2 WT and 4KR in HEK 293T cells with palmitic acid or TM3 treatment. GAPDH was used as the marker of cytosol fraction and Na,K-APTase was used as the marker of plasma membrane fraction.

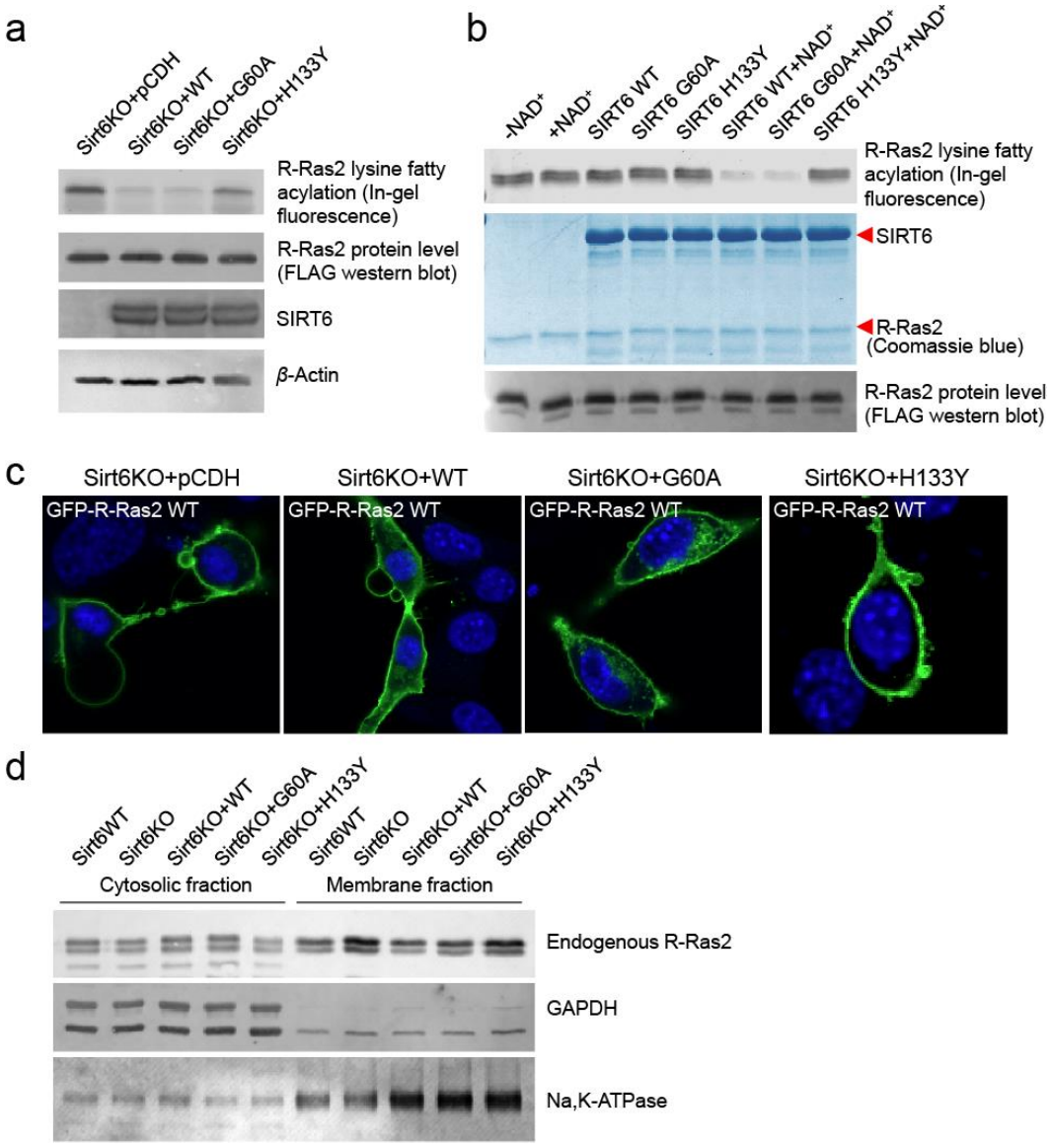

Figure 3.5. SIRT6 defatty-acylase activity is required for regulating R-Ras2 lysine fatty-acylation and subcellular localization. (a) Detection of R-Ras2 lysine fatty-acylation levels in *Sirt6* KO MEFs expressing pCDH empty vector, SIRT6 WT, G60A or H133Y by in-gel fluorescence. (b) In-gel fluorescence showed that SIRT6 WT and G60A defatty-acylated R-Ras2 in a NAD^+-dependent manner *in vitro*. (c) Confocal imaging showing the localization of R-Ras2 WT-GFP in *Sirt6* KO MEFs expressing pCDH empty vector, SIRT6 WT, G60A or H133Y (n = 5, 6, 5, 5 cells for each sample from left to right, respectively). (d) Subcellular fractionation showing the localization

of endogenous R-Ras2 in *Sirt6* WT MEF, *Sirt6* KO MEFs, and *Sirt6* KO MEFs expressing SIRT6 WT, G60A or H133Y.

Lysine fatty-acylation of R-Ras2 activates PI3K/Akt and promotes cell proliferation

We next investigated how lysine fatty-acylation of R-Ras2 affected its downstream signaling effect. There are two well-studied effector pathways of R-Ras2, the PI3K/Akt pathway [31,33] and the Raf/MAPK pathway [30]. We first examined whether R-Ras2 can activate the Raf/MAPK pathway in MEFs. We used Raf RBD-conjugated argarose beads to pull-down the active GTP-bound form of R-Ras2. The endogenous total Ras (H-Ras, N-Ras and K-Ras), but not the overexpressed or endogenous R-Ras2, was pulled down by Raf RBD (**Figure 3.6**), suggesting that in MEFs, R-Ras2 was unlikely to activate the Raf/MAPK pathway. We then examined the PI3K/Akt pathway by co-immunoprecipitation (co-IP). We overexpressed FLAG-tagged R-Ras2 WT and 4KR in *Sirt6* WT and KO MEFs, immunoprecipitated R-Ras2 and examined p110α, one isoform of the catalytic subunit of PI3K, which has been reported to interact with R-Ras2 [34]. WT R-Ras2 in *Sirt6* KO MEFs, which was shown to have the highest level of lysine fatty-acylation (**Figure 3.2c** and **3.3a**), had more p110α interaction than the WT R-Ras2 in *Sirt6* WT MEFs or the 4KR mutant in either *Sirt6* WT or KO MEFs (**Figure 3.7a**). This data suggested that lysine fatty-acylation of R-Ras2 promotes its interaction with p110α.

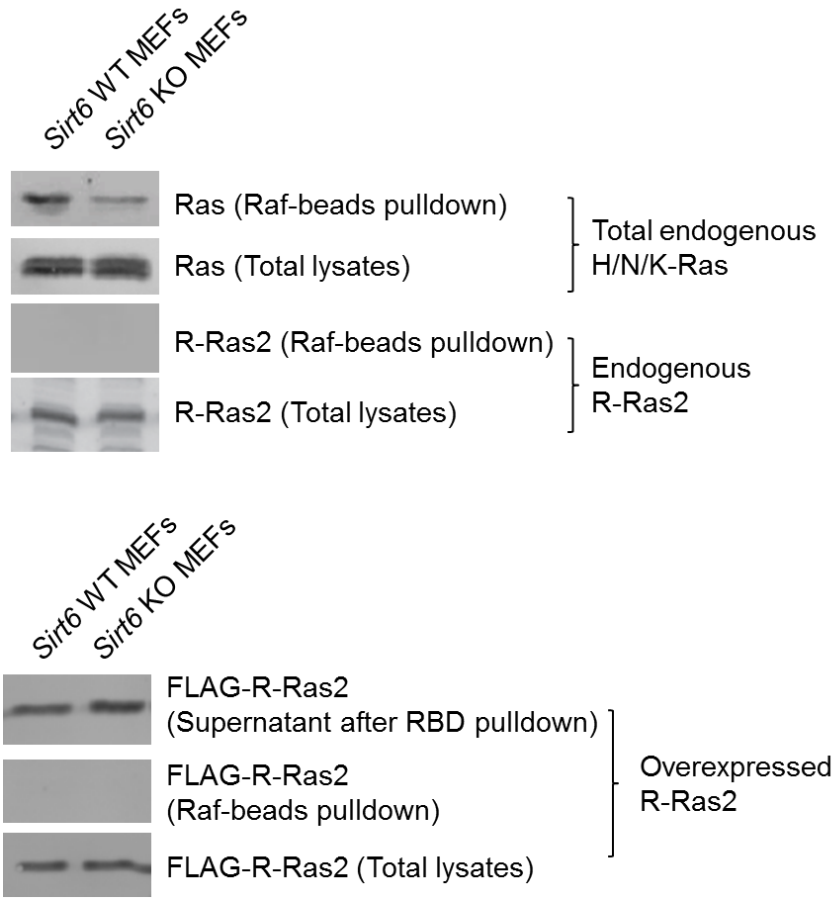

Figure 3.6. Raf-RBD binding assay showed that both overexpressed and endogenous R-Ras2 did not bind Raf RBD-conjugated argarose beads. Total endogenous Ras (H-Ras, N-Ras and K-Ras) was used as the positive control.

Then we examined whether the interaction of R-Ras2 with p110α could activate its downstream kinase Akt. *Sirt6* KO MEFs showed higher phosphorylated Akt on Thr308 (p-Akt Thr308), but not on Ser473 (p-Akt Ser473), when compared to *Sirt6* WT MEFs (**Figure 3.7b**). Knockdown of R-Ras2 in *Sirt6* WT MEFs did not affect p-Akt Thr308, while knockdown of R-Ras2 in *Sirt6* KO MEFs decreased p-Akt Thr308 to the same level as that in *Sirt6* WT MEFs (**Figure 3.7b**). We further found that expressing WT SIRT6 or the G60A mutant in *Sirt6* KO MEFs decreased p-Akt

Thr308 levels (**Figure 3.7c**), suggesting that the defatty-acylation activity of SIRT6 is important for regulating p-Akt Thr308. All the data combined suggested that SIRT6 defatty-acylates R-Ras2 and attenuates its interaction with p110α, resulting in decreased Akt phosphorylation on Thr308.

Finally, to confirm that lysine fatty-acylation of R-Ras2 is important for its role in promoting cell proliferation, we overexpressed R-Ras2 WT and 4KR in *Sirt6* WT and KO MEFs and measured the cell proliferation. Expression of R-Ras2 WT in *Sirt6* KO MEFs significantly increased cell proliferation compared with vector control (**Figure 3.7d**), while expressing R-Ras2 4KR in *Sirt6* KO MEFs did not increase cell proliferation (**Figure 3.7d**). In *Sirt6* WT MEFs, neither overexpressing WT R-Ras2 nor the 4KR mutant increased cell proliferation compared with vector control (**Figure 3.7d**). These data suggested that lysine fatty-acylation of R-Ras2 is important for promoting MEFs cell proliferation.

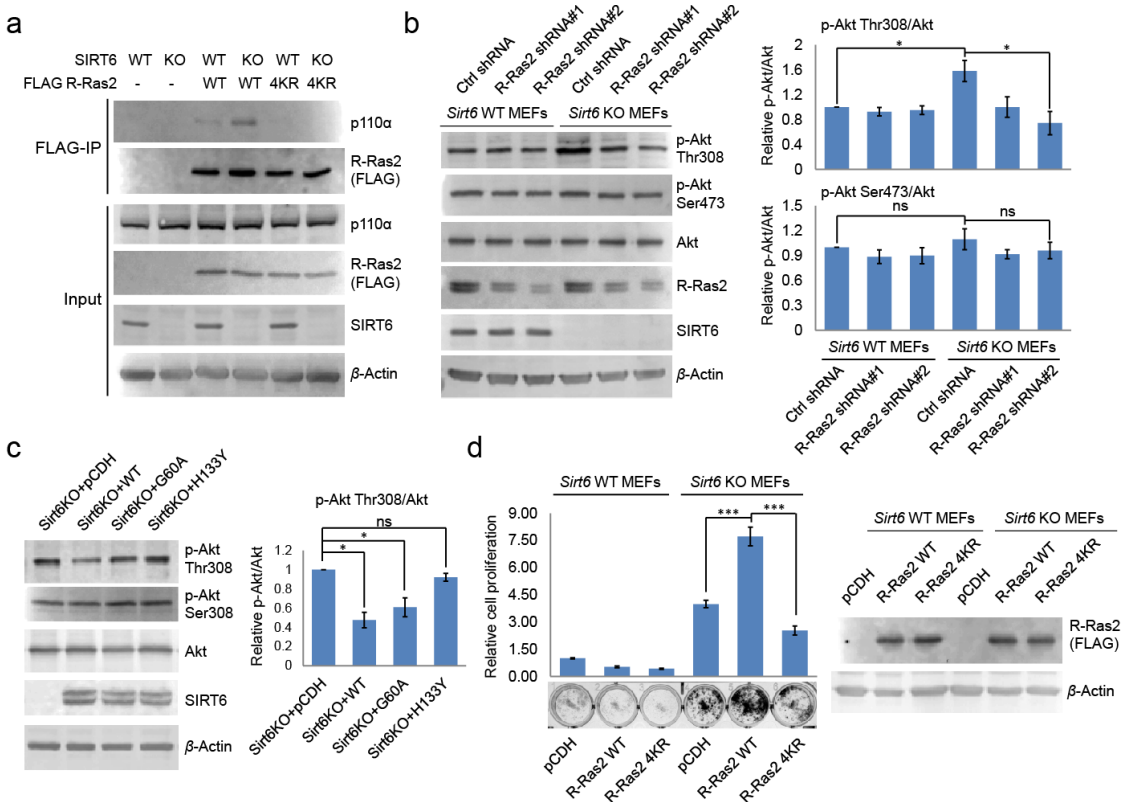

Figure 3.7. Lysine fatty-acylation of R-Ras2 activates PI3K-Akt pathway and promotes cell proliferation in MEFs. (a) Co-IP experiment showed that R-Ras2 WT in *Sirt6* KO MEFs had more p110α interaction than R-Ras2 WT in *Sirt6* WT MEFs and R-Ras2 4KR in *Sirt6* WT or KO MEFs. (b) Knockdown of R-Ras2 in *Sirt6* KO MEFs decreased p-Akt Thr308, but not p-Akt Ser473, to a level similar to that in *Sirt6* WT MEFs. Right histogram shows the quantification of bands on the western blot membrane. Values with error bars indicate mean ± s.d. of three biological replicates. * indicates $p < 0.05$. (c) Expressing SIRT6 WT or SIRT6 G60A in *Sirt6* KO MEFs decreased p-Akt Thr308, but not p-Akt Ser473. Right histogram shows the quantification of bands on the western blot membrane. Values with error bars indicate mean ± s.d. of three biological replicates. * indicates $p < 0.05$. (d) R-Ras2 WT but not R-Ras2 4KR promoted cell proliferation in *Sirt6* KO MEFs. Values with error bars indicate mean ± s.d. of three biological replicates. *** indicates $p < 0.005$.

In this study, we found that the defatty-acylase activity of SIRT6 is important for regulating cell proliferation. Using a proteomics approach, we identified a small GTPase, R-Ras2, as a defatty-acylation target of SIRT6. R-Ras2 has a higher lysine fatty-acylation level in *Sirt6* KO MEFs than that in *Sirt6* WT MEFs. Lysine fatty-acylation targets R-Ras2 to the plasma membrane, facilitates its interaction with p110α, and activates the Akt signaling pathway. This is important for the proliferative phenotype of *Sirt6* KO MEFs because when we knocked down R-Ras2 or decreased its lysine fatty-acylation in *Sirt6* KO MEFs, the p-Akt Thr308 level and cell proliferation became similar to those in *Sirt6* WT MEFs.

Previously, the function of SIRT6 was mainly explained through transcriptional regulation, which typically occurs at the end of signal transduction pathways. Now we showed that SIRT6 can also function at the top of the signal transduction pathway by regulating a GTPase in the Ras family. SIRT6 is known to be a tumor suppressor and down-regulated in many different human cancers[5]. Our study suggests that *Sirt6* KO increases lysine fatty-acylation of R-Ras2 and activates the PI3K-Akt pathway, leading to higher cell proliferation. Thus, the defatty-acylation and suppression of R-Ras2 is a major contributor to the tumor suppressor role of SIRT6.

For the Ras proteins that do not have palmitoylated cysteine (such as K-Ras4B), they are thought to use polybasic sequences for membrane targeting [16,35]. Interestingly, in addition to palmitoylation on Cys199 and farnesylation on Cys201, R-Ras2 contains several lysine residues at the C-terminus (Lys192, 194, 196, 197). One question is, if these lysine residues also help to target R-Ras2 to membranes via electrostatics, why cells use lysine instead of arginine? Our study has shed lights onto this question and identified a novel regulatory mechanism for this family of proteins, which may help to develop new strategies to pharmacologically target R-Ras2 to treat human diseases. In

a recent paper, the lysine residues at the C-terminal of K-Ras4B have been shown to play important roles for phospholipid binding and K-Ras4B signal output[36]. The lysine to arginine mutant had distinct lipid binding capacity, suggesting that simple electrostatic interaction may not be the mechanism how polybasic sequences target to the membrane. It is possible that the lysine residues at the C-terminal of K-Ras4B are similarly regulated by fatty-acylation, which could explain the distinct lipid binding capacity of the lysine-to-arginine mutant. However, we could not completely rule out that the lysine residues at the C-terminal of R-Ras2 may also function in phospholipid binding and thus affect its signaling output, in addition to being regulated by lysine fatty-acylation and SIRT6.

Many Ras family of small GTPases contain polybasic sequences at the C-termini. It is possible that lysine fatty-acylation also occur on these GTPases and regulate their localization and activities. If so, study how these GTPases are regulated by lysine fatty-acylation and whether sirtuins also serve as deacylases for these proteins is an ongoing direction in our laboratory.

Our study also expands the biological significance of protein lysine fatty-acylation. Protein lysine fatty-acylation was first reported in 1992[37]. Since then, only a few proteins were known to have this modification and whether this PTM has important biological function or not was not known. We previously identified that lysine fatty ayclation regulates protein secretion (e.g. TNFα and ribosomal proteins)[13,26]. The finding that lysine fatty-acylation regulates the Ras family of proteins suggest that this PTM may have very broad and important biological functions.

Methods

Reagents. Anti-FLAG affinity gel (#A2220, RRID: AB_10063035) and anti-FLAG antibody conjugated with horseradish peroxidase (#A8592, RRID: AB_439702) were

purchased from Sigma. Human/mouse SIRT6 (#12486), p110α (#4249, RRID: AB_2165248), p-Akt Thr308 (#13038, RRID: AB_2629447), p-Akt Ser473 (#4060, RRID: AB_2315049), Akt (#4691, RRID: AB_915783), HSP90 (#4877, RRID: AB_2121214) and Na,K-ATPase (#3010, RRID: AB_2060983) antibodies were purchased from Cell Signaling Technology. β-Actin (sc-4777) and GAPDH (sc-20357, RRID:AB_641107) antibodies were purchased from Santa Cruz Biotechnology. R-Ras2 antibody (#H00022800-M01, RRID:AB_547895) was purchased from Novus Biologicals. ^{32}P-NAD^{+} was purchased from PerkinElmer. 3X FLAG peptide, Azide-PEG3-biotin, Tris[(1-benzyl-1H-1,2,3-triazol-4-yl)methyl]amine (TBTA), Tris(2-carboxyethyl)phosphine (TCEP), hydroxylamine, NAD^{+}, and protease inhibitor cocktail were purchased from Sigma. Sequencing grade modified trypsin and FuGene 6 transfection reagent were purchased from Promega. ECL plus western blotting detection reagent and Streptavidin agarose beads were purchased from Thermo Scientific Pierce. Sep-Pak C18 cartridge and polyester-backed silica plate were purchased from Waters. 520-BODIPY azide was purchased from Active Motif. Ras assay kit (Raf-1 RBD, agarose) was purchased from EMD Millipore. R-Ras2 and SIRT6 shRNA lentiviral plasmids (pLKO.1-puro vector) were purchased from Sigma, the sequence of shRNA was: R-Ras2 shRNA#1: TRCN0000306170 (ccggtaagagtcccttgaggtttagctcgagctaaacctcaagggactcttatttttg); R-Ras2 shRNA#2: TRCN0000077748 (ccggcgctagatattgactgttatactcgagtataacagtcaatatctagcgtttttg); SIRT6 shRNA#1: TRCN0000378253 (ccggcagtacgtccgagacacagtcctcgaggactgtgctcggacgtactgtttttg); SIRT6 shRNA#2: TRCN0000232528 (ccgggaagaatgtgccaagtgtaagctcgagcttacacttggcacattcttctttttg). Alk12 and Alk14 were synthesized according to reported procedures[27]. Plasmid of IpaJ in pET2-8b vector was a kind gift from Prof. Neal M. Alto at Department of Microbiology, University of

Texas Southwestern Medical Center. IpaJ was purified according to reported procedures[28].

Cell Culture. *Sirt6* wild type (WT) and knockout (KO) MEFs were kindly provided by Prof. Raul Mostoslavsky at Massachusetts General Hospital Cancer Center, Harvard Medical School, which were prepared and authenticated by the authors as described previously[5]. Human Embryonic Kidney (HEK) 293T cells were purchased from ATCC (RRID: CVCL_0063). All the cell lines have been tested for mycoplasma contamination by PCR-based mycoplasma detection kit (Sigma, MP0025) and showed no contamination. *Sirt6* WT, *Sirt6* KO MEFs and *Sirt6* KO MEFs expressing SIRT6 WT, G60A or H133Y were cultured in Dulbecco's Modified Eagle Medium (DMEM) with 10% fetal bovine serum (FBS). HEK 293T cells were cultured in DMEM medium with 10% FBS.

Cloning, expression and purification of SIRT6 WT, G60A and H133Y from *Escherichia coli* (*E. coli*). Human SIRT6 was inserted into pET-28a vector. SIRT6 G60A and H133Y mutants were made by QuikChange. The plasmids of SIRT6 WT and mutants were transformed into *E. coli* BL21 (DE3) cells. The proteins were purified according to reported procedures[13].

Cloning, expression and purification of R-Ras2 WT and 4KR from *Sirt6* KO MEFs and HEK 293T cells. Human R-Ras2 was inserted into lentiviral vector (pCDH-CMV-MCS-EF1-Puro) with N-FLAG tag. R-Ras2 4KR mutant was made by QuikChange. R-Ras2 lentivirus was generated by co-transfection of R-Ras2, pCMV-dR8.2, and pMD2.G into HEK 293T cells. After transfection for 48 h, the medium was collected and used for infecting *Sirt6* KO MEFs or HEK 293T cells. To obtain the R-Ras2 stable overexpressed cells, the cells were treated by 1.5 mg/mL of puromycin 48 h after infection and cultured for 1 week while passing cells every 2-3 days. To purify R-Ras2 from *Sirt6* KO MEFs or HEK 293T cells, the cells were collected at 500 g for

5 min and then lysed in Nonidet P-40 lysis buffer (25 mM Tris-HCl pH 7.4, 150 mM NaCl, 10% glycerol and 1 % Nonidet P-40) with protease inhibitor cocktail (1:100 dilution). Anti-FLAG affinity gel was used to enrich the R-Ras2 protein from total cell lysates. Then R-Ras2 was eluted and purified by 3X FLAG peptide following the manual.

Stable overexpression of SIRT6 WT, G60A or H133Y in *Sirt6* KO MEFs. Human SIRT6 WT was inserted into pCDH-CMV-MCS-EF1-Puro vector without tag. SIRT6 G60A and H133Y mutants were made by QuikChange. SIRT6 lentivirus was generated by co-transfection of SIRT6, pCMV-dR8.2, and pMD2.G into HEK 293T cells. After transfection for 48 h, the medium was collected and used for infecting *Sirt6* KO MEFs. *Sirt6* KO MEFs with stable expressed SIRT6 WT, G60A or H133Y was selected by 1.5 mg/mL of puromycin. Empty pCDH vector was used as the negative control.

Labeling of R-Ras2 in MEFs with Alk14 and detection of lysine fatty-acylation on R-Ras2 by in-gel fluorescence. R-Ras2 WT or 4KR was transfected into MEFs or HEK 293T cells by FuGene 6 transfection reagent. After 24 h, the cells were treated with 50 μM of Alk14 for 6 h. The cells were collected at 500 g for 5 min and then lysed in Nonidet P-40 lysis buffer (25 mM Tris-HCl pH 7.4, 150 mM NaCl, 10% glycerol, and 1 % Nonidet P-40) with protease inhibitor cocktail. The total lysate was incubated with anti-FLAG affinity gel at 4 ˚C for 1 h. The affinity gel was then washed three times by immunoprecipitation (IP) washing buffer (25 mM Tris-HCl pH 7.4, 150 mM NaCl and 0.2% Nonidet P-40) and then re-suspended in 18 μL of IP washing buffer. The click chemistry reaction was performed by adding the following reagents: 520-BODIPY azide (0.8 μL of 1.5 mM solution in DMF), TBTA (1.2 μL of 10 mM solution in DMF), $CuSO_4$ (1 μL of 40 mM solution in H_2O) and TCEP (1 μL of 40 mM solution in H_2O). The reaction was allowed to proceed at room temperature

for 45 min. Then the SDS loading buffer was added and heated at 95 ˚C for 10 min. After centrifugation at 15,000 g for 2 min, the supernatant was collected and treated with 300 mM hydroxylamine at 95 ˚C for 7 min. The samples were resolved by 12% SDS-PAGE. In-gel fluorescence signal was recorded by Typhoon 9400 Variable Mode Imager (GE Healthcare Life Sciences).

Detection of lysine fatty-acylation of endogenous R-Ras2 in MEFs. *Sirt6* WT and KO MEFs were treated with 50 μM Alk14 for 6 h. Cells were collected and lysed by Nonidet P-40 lysis buffer using the same method descried above. The total lysates were subjected to click chemistry reaction by adding the following reagents: Azide-PEG3-biotin (final concentration was 100 μM), TBTA (final concentration was 0.5 mM), $CuSO_4$ (final concentration was 1 mM) and TCEP (final concentration was 1 mM). The reaction was allowed to proceed at room temperature for 45 min, and then the total proteins were precipitated by methanol/chloroform (2.5/1) and washed by ice-cold methanol. The protein pellets were re-solubilized in 1.5% SDS, 1% Brij97, 100 mM NaCl and 50 mM triethanolamine. Streptavidin agarose beads were added and incubated at room temperature for 1 h. After washing the beads three times by 0.2% SDS in PBS buffer, the beads were treated with 1 M hydroxylamine (pH 7.4) at room temperature for 1 h. Then the beads were washed three times with 0.2% SDS in PBS buffer. The SDS loading buffer was added to the beads, heated at 95 ˚C for 10 min, and then used for western blot.

Defatty-acylation of R-Ras2 by SIRT6 *in vitro*. R-Ras2 WT was transfected into *Sirt6* KO MEFs treated with 50 μM Alk14 for 6 h and purified using the method described above. The *in vitro* assay was proceeded in the assay buffer (50 mM Tris-HCl pH 8.0, 100 mM NaCl, 2 mM $MgCl_2$, 1 mM DTT, 1 mM NAD^+) with 15 μM of SIRT6 and incubated at 37 °C for 2 h. Proteins were precipitated by methanol/chloroform (2.5/1) and washed by ice-cold methanol. The protein pellets

were re-solubilized in 4% SDS, 150 mM NaCl and 50 mM triethanolamine. Then click chemistry reaction and in-gel fluorescence were carried out as described above.

^{32}P-NAD^{+} assay. R-Ras2 WT was transfected into *Sirt6* KO MEFs and purified by FLAG affinity gel. Purified R-Ras2 on the FLAG affinity gel was used for ^{32}P-NAD^{+} assay. 10 μL of reaction buffer containing 50 mM Tris pH 8.0, 150 mM NaCl, 1 mM DTT, 5 μM SIRT6 WT or H133Y, and 0.1 μCi of ^{32}P-NAD was mixed with R-Ras2 protein. The reaction was allowed to proceed at 37 ˚C for 2 h. 2 μL of the reaction mixture was spotted onto the polyester-backed silica plate. The plate was developed in 30:70 (v/v) 1 M ammonium bicarbonate/95% ethanol. Then the plate was exposed in the phosphor imaging screen (GE Healthcare) for 4 h. The signal was detected using Typhoon 9400 Variable Mode Imager. H3K9 myristoyl and H3K9 palmitoyl peptides were incubated with SIRT6 in the same reaction buffer as positive control for fatty-acyl ADPR. H2BK12 acetyl peptide was incubated with SIRT1 in the same reaction buffer as positive control for acetyl ADPR. All the peptides were synthesized according to the reported procedures[38].

Western blot. The proteins were resolved by 12% SDS-PAGE and transferred to polyvinylidene fluoride (PVDF) membrane. The membrane was incubated with 5% bovine serum albumin (BSA) in TPBS buffer (0.1% Tween-20 in PBS solution) at room temperature for 60 min. Then the antibody was diluted with fresh 5% BSA in TPBS buffer and incubated with the membrane for different time points according to the manual. After washing three times by TPBS buffer, the secondary antibody was diluted with fresh 5% BSA in TPBS buffer and then incubated with the membrane at room temperature for 1 h. The chemiluminescence signal in membrane was recorded after developing in ECL plus western blotting detection reagents using Typhoon 9400 Variable Mode Imager.

Crystal violet cell proliferation assay. Cells were seeded in 12-well plates (5,000

cells/well) or 24-well plates (2,500 cells/well), and then maintained in DMEM medium with 10% FBS for 5 days. After washing twice with ice-cold PBS, cells were fixed by ice-cold methanol for 10 min. Then methanol was removed and crystal violet (0.2% in 2% ethanol solution) was added and incubated for 5 min. Cells were then washed with water until all excess dye was removed. Crystal violet dye that remained with the cells was solubilized by 0.5% SDS in 50% ethanol solution. The absorption of crystal violet was measured at 550 nm.

SILAC. *Sirt6* KO MEFs were cultured in DMEM medium with [$^{13}C_6$, $^{15}N_2$]-L-lysine and [$^{13}C_6$, $^{15}N_4$]-L-arginine for 5 generations. *Sirt6* WT MEFs were cultured in normal DMEM medium for 5 generations. The cells were treated with 50 μM Alk12 or Alk14 for 6 h. After quantifying the concentration of total proteins by Bradford assay, 2.5 mg of total proteins from each sample were mixed. IpaJ was added (final concentration was 150 μg/mL) and incubated with the total lysate at 30 ˚C for 1 h. The click chemistry reaction was then performed by adding the following reagents: Azide-PEG3-biotin (final concentration was 100 μM), TBTA (final concentration was 0.5 mM), $CuSO_4$ (final concentration was 1 mM) and TCEP (final concentration was 1 mM). The reaction was allowed to proceed at room temperature for 45 min, and then the total proteins were precipitated by methanol/chloroform (2.5/1) and washed by ice-cold methanol. After re-solubilize the protein pellets in 1.5% SDS, 1% Brij97, 100 mM NaCl and 50 mM triethanolamine, streptavidin agarose beads were added and incubated with the lysates at room temperature for 1 h. After washing the beads three times by 0.2% SDS in PBS buffer, the beads were treated with 0.5 M hydroxylamine (pH 7.4) at room temperature for 1 h. Then the beads were washed three times with 0.2% SDS in PBS buffer. The beads were incubated with 6 M urea and 10 mM TCEP in PBS at 37 ˚C for 30 min, then 400 mM iodoacetamide was added and incubated with the beads at 37 ˚C for 30 min. After washing the beads with 2 M urea in PBS, the

beads were incubated with 2 μg trypsin in 2 M urea in PBS at 37 ˚C for 8 h. The digestion reaction was quenched with 0.1% trifluoroacetic acid and the mixture was desalted using a Sep-Pak C18 cartridge. The lyophilized peptides were used for nano LC-MS/MS analysis. LC-MS/MS analysis was performed using LTQ-Orbitrap Elite mass spectrometer. The lyophilized peptides were dissolved in 2% acetonitrile containing 0.5% formic acid. The Orbitrap was interfaced with a Dionex UltiMate3000 MDLC system. The peptide samples were injected onto C18 RP nano column (5 μm, 75 μm×50 cm, Magic C18, Bruker) at a flow rate of 0.3 μL/min. The gradient for HPLC condition was 5-38% acetonitrile containing 0.1% formic acid in 120 min. The Orbitrap Elite was operated in positive ion mode with spray voltage 1.6 kV and source temperature 275 ˚C. Data-dependent acquisition (DDA) mode was used by one precursor ions MS survey scan from m/z 300 to 1800 at resolution 60,000 using FT mass analyzer, followed by up to 10 MS/MS scans at resolution 15,000 on 10 most intensive peaks. All data were acquired in Xcalibur 2.2 operation software.

Detection of lysine fatty-acylation on R-Ras2 by mass spectrometry. *Sirt6* KO MEFs stably expressing FLAG R-Ras2 were used for detecting lysine fatty-acylation on R-Ras2. Cells were treated with 50 μM Alk14 for 6 h, collected and lysed by Nonidet P-40 lysis buffer using the same method described above. 40 mg of total protein lysates were used for FLAG IP. After washing the FLAG resin three times with IP washing buffer, R-Ras2 protein was eluted by heating at 95 ℃ for 10 min in buffer containing 1% SDS and 50 mM Tris-HCl pH 8.0. The supernatant was treated with 300 mM NH_2OH pH 7.4 at 95 ℃ for 10 min. R-Ras2 protein was then precipitated by methanol/chloroform and processed for disulfide reduction, denaturing, alkylation and neutralization using the same method described above. The processed R-Ras2 protein was digested with 1.5 μg of trypsin in a glass vial at 37˚C for 2 h, and then desalted using Sep-Pak C18 cartridge. For the LC-MS/MS analysis of

lysine fatty-acylated peptides, the same settings as SILAC experiment was applied except the LC gradient, which was 5-95% ACN with 0.1% trifluoroacetic acid from 0-140 min. All data were acquired in Xcalibur 2.2 operation software.

RNA extraction, reverse transcription and PCR analysis of mRNA levels. Total RNAs were extracted using RNeasy Mini kit (QIAGEN). Reverse transcription was performed using SuperScript III First-Strand Synthesis kit (Invitrogen). PCR amplification was performed using Herculase II Fusion Enzyme with dNTPs Combo kit (Agilent).

R-Ras2 localization by subcellular fractionation and confocal imaging. Subcellular fractionation and confocal imaging were performed according to reported procedures[39]. Confocal imaging was performed on a Zeiss LSM880 confocal/multiphoton microscope.

Statistical Analysis. Data were expressed as mean ± s.d. (standard deviation, shown as error bars). Differences were examined by two-tailed Student's *t*-test between two groups; $*p < 0.05$, $**p < 0.01$, $***p < 0.005$.

REFERENCES

1 Kaidi, A., Weinert, B. T., Choudhary, C. & Jackson, S. P. Human SIRT6 promotes DNA end resection through CtIP deacetylation. *Science* **329**, 1348-1353, doi:10.1126/science.1192049 (2010).

2 Mao, Z. *et al.* SIRT6 promotes DNA repair under stress by activating PARP1. *Science* **332**, 1443-1446, doi:10.1126/science.1202723 (2011).

3 Toiber, D. *et al.* SIRT6 recruits SNF2H to DNA break sites, preventing genomic instability through chromatin remodeling. *Molecular cell* **51**, 454-468, doi:10.1016/j.molcel.2013.06.018 (2013).

4 Zhong, L. *et al.* The histone deacetylase Sirt6 regulates glucose homeostasis via Hif1alpha. *Cell* **140**, 280-293, doi:10.1016/j.cell.2009.12.041 (2010).

5 Sebastian, C. *et al.* The histone deacetylase SIRT6 is a tumor suppressor that controls cancer metabolism. *Cell* **151**, 1185-1199, doi:10.1016/j.cell.2012.10.047 (2012).

6 Michishita, E. *et al.* SIRT6 is a histone H3 lysine 9 deacetylase that modulates telomeric chromatin. *Nature* **452**, 492-496, doi:10.1038/nature06736 (2008).

7 Yang, B., Zwaans, B. M., Eckersdorff, M. & Lombard, D. B. The sirtuin

SIRT6 deacetylates H3 K56Ac in vivo to promote genomic stability. *Cell cycle* **8**, 2662-2663, doi:10.4161/cc.8.16.9329 (2009).
8 Michishita, E. *et al.* Cell cycle-dependent deacetylation of telomeric histone H3 lysine K56 by human SIRT6. *Cell cycle* **8**, 2664-2666 (2009).
9 Tasselli, L. *et al.* SIRT6 deacetylates H3K18ac at pericentric chromatin to prevent mitotic errors and cellular senescence. *Nature structural & molecular biology* **23**, 434-440, doi:10.1038/nsmb.3202 (2016).
10 Kawahara, T. L. *et al.* SIRT6 links histone H3 lysine 9 deacetylation to NF-kappaB-dependent gene expression and organismal life span. *Cell* **136**, 62-74, doi:10.1016/j.cell.2008.10.052 (2009).
11 Sundaresan, N. R. *et al.* The sirtuin SIRT6 blocks IGF-Akt signaling and development of cardiac hypertrophy by targeting c-Jun. *Nat Med* **18**, 1643-1650, doi:10.1038/nm.2961 (2012).
12 Liszt, G., Ford, E., Kurtev, M. & Guarente, L. Mouse Sir2 homolog SIRT6 is a nuclear ADP-ribosyltransferase. *The Journal of biological chemistry* **280**, 21313-21320, doi:10.1074/jbc.M413296200 (2005).
13 Jiang, H. *et al.* SIRT6 regulates TNF-alpha secretion through hydrolysis of long-chain fatty acyl lysine. *Nature* **496**, 110-113, doi:10.1038/nature12038 (2013).
14 Jiang, H., Zhang, X. & Lin, H. Lysine fatty acylation promotes lysosomal targeting of TNF-alpha. *Scientific reports* **6**, 24371, doi:10.1038/srep24371 (2016).
15 Wennerberg, K., Rossman, K. L. & Der, C. J. The Ras superfamily at a glance. *Journal of cell science* **118**, 843-846, doi:10.1242/jcs.01660 (2005).
16 Hancock, J. F. Ras proteins: different signals from different locations. *Nature reviews. Molecular cell biology* **4**, 373-384, doi:10.1038/nrm1105 (2003).
17 Karnoub, A. E. & Weinberg, R. A. Ras oncogenes: split personalities. *Nature reviews. Molecular cell biology* **9**, 517-531, doi:10.1038/nrm2438 (2008).
18 Ahearn, I. M., Haigis, K., Bar-Sagi, D. & Philips, M. R. Regulating the regulator: post-translational modification of RAS. *Nature reviews. Molecular cell biology* **13**, 39-51, doi:10.1038/nrm3255 (2011).
19 Ahearn, I. M., Haigis, K., Bar-Sagi, D. & Philips, M. R. Regulating the regulator: post-translational modification of RAS. *Nature reviews. Molecular cell biology* **13**, 39-51, doi:10.1038/nrm3255 (2012).
20 Linder, M. E. & Deschenes, R. J. Palmitoylation: policing protein stability and traffic. *Nature reviews. Molecular cell biology* **8**, 74-84, doi:10.1038/nrm2084 (2007).
21 Drivas, G. T., Shih, A., Coutavas, E., Rush, M. G. & D'Eustachio, P. Characterization of four novel ras-like genes expressed in a human teratocarcinoma cell line. *Molecular and cellular biology* **10**, 1793-1798 (1990).
22 Lee, J. H. *et al.* Greater expression of TC21/R-ras2 in highly aggressive malignant skin cancer. *International journal of dermatology* **50**, 956-960, doi:10.1111/j.1365-4632.2010.04846.x (2011).
23 Gutierrez-Erlandsson, S. *et al.* R-RAS2 overexpression in tumors of the human

central nervous system. *Molecular cancer* **12**, 127, doi:10.1186/1476-4598-12-127 (2013).
24 Erdogan, M., Pozzi, A., Bhowmick, N., Moses, H. L. & Zent, R. Signaling pathways regulating TC21-induced tumorigenesis. *The Journal of biological chemistry* **282**, 27713-27720, doi:10.1074/jbc.M703037200 (2007).
25 Murphy, G. A. *et al.* Involvement of phosphatidylinositol 3-kinase, but not RalGDS, in TC21/R-Ras2-mediated transformation. *The Journal of biological chemistry* **277**, 9966-9975, doi:10.1074/jbc.M109059200 (2002).
26 Zhang, X. *et al.* Identifying the functional contribution of the defatty-acylase activity of SIRT6. *Nature chemical biology* **12**, 614-620, doi:10.1038/nchembio.2106 (2016).
27 Charron, G. *et al.* Robust fluorescent detection of protein fatty-acylation with chemical reporters. *Journal of the American Chemical Society* **131**, 4967-4975, doi:10.1021/ja810122f (2009).
28 Burnaevskiy, N. *et al.* Proteolytic elimination of N-myristoyl modifications by the Shigella virulence factor IpaJ. *Nature* **496**, 106-109, doi:10.1038/nature12004 (2013).
29 Clark, G. J., Kinch, M. S., Gilmer, T. M., Burridge, K. & Der, C. J. Overexpression of the Ras-related TC21/R-Ras2 protein may contribute to the development of human breast cancers. *Oncogene* **12**, 169-176 (1996).
30 Rosario, M., Paterson, H. F. & Marshall, C. J. Activation of the Raf/MAP kinase cascade by the Ras-related protein TC21 is required for the TC21-mediated transformation of NIH 3T3 cells. *The EMBO journal* **18**, 1270-1279, doi:10.1093/emboj/18.5.1270 (1999).
31 Rong, R., He, Q., Liu, Y., Sheikh, M. S. & Huang, Y. TC21 mediates transformation and cell survival via activation of phosphatidylinositol 3-kinase/Akt and NF-kappaB signaling pathway. *Oncogene* **21**, 1062-1070, doi:10.1038/sj.onc.1205154 (2002).
32 He, B., Hu, J., Zhang, X. & Lin, H. Thiomyristoyl peptides as cell-permeable Sirt6 inhibitors. *Organic & biomolecular chemistry* **12**, 7498-7502, doi:10.1039/c4ob00860j (2014).
33 Rosario, M., Paterson, H. F. & Marshall, C. J. Activation of the Ral and phosphatidylinositol 3' kinase signaling pathways by the ras-related protein TC21. *Molecular and cellular biology* **21**, 3750-3762, doi:10.1128/MCB.21.11.3750-3762.2001 (2001).
34 Rodriguez-Viciana, P., Sabatier, C. & McCormick, F. Signaling specificity by Ras family GTPases is determined by the full spectrum of effectors they regulate. *Molecular and cellular biology* **24**, 4943-4954, doi:10.1128/MCB.24.11.4943-4954.2004 (2004).
35 Cox, A. D., Fesik, S. W., Kimmelman, A. C., Luo, J. & Der, C. J. Drugging the undruggable RAS: Mission possible? *Nature reviews. Drug discovery* **13**, 828-851, doi:10.1038/nrd4389 (2014).
36 Zhou, Y. *et al.* Lipid-Sorting Specificity Encoded in K-Ras Membrane Anchor Regulates Signal Output. *Cell* **168**, 239-251 e216, doi:10.1016/j.cell.2016.11.059 (2017).

37 Stevenson, F. T., Bursten, S. L., Locksley, R. M. & Lovett, D. H. Myristyl acylation of the tumor necrosis factor alpha precursor on specific lysine residues. *The Journal of experimental medicine* **176**, 1053-1062 (1992).
38 Zhu, A. Y. *et al.* Plasmodium falciparum Sir2A preferentially hydrolyzes medium and long chain fatty acyl lysine. *ACS chemical biology* **7**, 155-159, doi:10.1021/cb200230x (2012).
39 Huang, Z. *et al.* Tumor suppressor Alpha B-crystallin (CRYAB) associates with the cadherin/catenin adherens junction and impairs NPC progression-associated properties. *Oncogene* **31**, 3709-3720, doi:10.1038/onc.2011.529 (2012).

CHAPTER 4

GLOBAL MAP OF KRAS4A AND KRAS4B INTERACTING PROTEINS

Abstract

Ras proteins are tumor drivers and play pivotal roles in numerous biological processes. KRAS mutant is the most prevalent mutant oncogene in different types of cancer. It has two alternatively spliced gene products which are translated into two proteins, KRas4a and KRas4b. Currently, the shared and unique signaling pathways and biological functions of the two KRas proteins are poorly understood. Here we report the nucleotide-dependent interaction map of KRas4a and KRas4b to understand the signaling pathways regulated by KRas4a and KRas4b. In addition to known interacting proteins, we identified many previously unknown KRas4a and KRas4b interacting proteins that belong to diverse functional classes. We found that some proteins interact with both isoforms while others prefer one of the two isoforms. For example, v-ATPase a2 and eIF2Bδ interact with only KRas4b. Biochemical studies suggested that KRas4b C-terminal hypervariable region (HVR) determines the binding specificity. By comparing WT and G12D mutant of KRas, we were also able to examine the difference in the effector proteins of the two KRas isoforms. Interestingly, we found that KRas4a has a stronger RAF1 interaction than KRas4b. Correspondingly, KRas4a can better promote ERK phosphorylation and anchorage-independent cell growth of NIH 3T3 cells than KRas4b. In addition, we identified mTOR as a novel KRas4a/b interacting protein. KRas4a/b forms a new mTOR complex without raptor and rictor in cells. The KRas4a and KRas4b interactome data from this study thus represents a useful resource to understand the functional differences between KRas4a and KRas4b and to discover the new biological functions

for them. As the Ras superfamily of small GTPases contain more than 150 members that function similarly to KRas, the interactome approach described here represents a powerful method that can be used to understand the functions of these small GTPases and to discover previously unknown functions of these GTPases.

Introduction

The Ras superfamily of small GTPases consists of more than 150 members and plays important roles in numerous biological processes such as signal transduction, membrane trafficking, nuclear export/import, and cytoskeletal dynamics[1]. Among all these members, four Ras proteins (HRas, NRas, KRas4a, and KRas4b) encoded by three RAS genes (HRAS, NRAS, and KRAS) attract attention because their deregulation is frequently found in various human cancers[2]. It is well established that mutant Ras proteins are cancer drivers[3]. Ras proteins are active in GTP-bound state and inactive in GDP-bound state. Guanine nucleotide exchange factors (GEFs) and GTPase-activating proteins (GAPs) are two types of proteins that regulate the GTP and GDP exchange on Ras proteins[4]. GEFs facilitate the formation of GTP-bound Ras, while GAPs activate Ras intrinsic GTP hydrolysis and promote the formation of GDP-bound Ras. GTP loading on Ras protein induces a conformational change in switch I region, which allows the recruitment of effector proteins, therefor turning on Ras signaling[5]. Four Ras proteins share high sequence identities in their conserved domain (residues 1-165), which include nucleotide and effector binding regions. Ras proteins also have C-terminal hypervariable region (HVR), which have low sequence identities. The C-terminal HVR plays important roles in membrane targeting, protein-protein interaction, as well as signal transduction[6]. Different Ras proteins share many effector proteins, such as RAF1, RalGDS, PI3K, and PLCε[5], and were originally thought to have similar biological functions. However, accumulating evidence has

shown that different Ras proteins exhibit different signaling and biological functions. For example, HRas, NRas, and KRas exhibit different leukemogenic potentials in mice[7]. KRas but not HRas can translocate from the plasma membrane (PM) to the Golgi complex and early/recycling endosomes in a Ca^{2+}/calmodulin dependent manner[8]. The different functions of Ras proteins suggest that they may recruit different proteins that determine the signaling outputs, or bind to the same effector protein with different affinities which could also lead to different signaling outputs. Even KRas4a and KRas4b, two alternatively spliced products from KRAS gene, were shown to have different subcellular localizations and biological functions[9,10]. However, the molecular basis for the different signaling functions of different Ras proteins, especially the two KRas isoforms, is poorly understood.

mTOR is a central energy regulator in mammals, which forms functional complex in cells. Currently, there are two well established mTOR complexes: mTOR complex 1 (mTORC1) and mTOR complex 2 (mTORC2), depending on whether mTOR interacts with raptor (to form mTORC1) or rictor (to form mTORC2)[11]. Both mTOR complexes interact with another essential component mLST8 (also known as GβL)[11]. Recently, ubiquitination of mLST8 has been show to regulate the balance between mTORC1 and mTORC2[12]. Crystal (PDB: 4JSN) and cryo-EM (PDB: 5FLC) structures of mTOR provide molecular basis of how mTOR interacts with raptor and mLST8 in mTORC1[13,14]. mTORC1 and mTORC2 activate different signalings and therefore regulate different cellular functions. mTORC1 senses amino acids and functions in translation, autophagy, and transcription regulation[11]. Localization to the lysosome is essential for mTORC1 activation[15]. The GTPases RagA/C heterodimer has been shown to regulate the lysosome localization of mTORC1[15]. Recent studies identified CASTOR as the arginine sensor[16] and Sestrin2 as the leucine sensor[17] that integrate cellular arginine and leucine status to GATOR1, the GAP of RagA/C[18], therefore

regulating mTORC1-mediated amino acids sensing. Active mTORC1 phosphorylates two key proteins S6K and 4E-BP1, and promotes global protein synthesis[19,20]. Another important substrate of mTORC1 is ULK1, mTOR prevents autophagy by phosphorylating ULK1[21]. Rapamycin is a frequently used mTORC1 inhibitor. It binds to FKBP12, then the rapamycin-FKBP12 complex serves as an allosteric inhibitor to disrupt mTORC1 assembly[14]. mTORC2 is mainly regulated by growth factors and is not affected by rapamycin (rapamycin-FKBP12 does not bind to mTORC2). Compared with mTORC1, mTORC2 is less studied, especially how it is regulated in cells. The currently identified mTORC2 substrates include Akt[22], PKC[23] and SGK[24].

The interactome of a protein of interest can provide important functional clues for that protein, thereby facilitating the discoveries of new functions for the protein. This is especially important for proteins whose functions mainly rely on recruiting other proteins, such as the Ras proteins. Currently, the most well established protein interactome database is BioPlex 2.0, which includes interactome data for almost half of the human proteome[25]. However, for each single protein, only the most abundant and high-confident interacting proteins are present in the database. For example, we searched KRas interacting proteins in BioPlex 2.0 and only found RIN1 and BRAF (http://bioplex.hms.harvard.edu), two known Ras interacting proteins[26,27]. No additional information is available for KRas in the interactome database, and the number of KRas interacting proteins is far fewer than the number of known KRas interacting proteins. Moreover, a lot of protein-protein interactions are protein state dependent. For example, Ras-effector interaction is dependent on the nucleotide binding state. Knowing the state-dependent interactome is thus important for understanding protein functions. Such state-dependent protein-protein interaction information is not available in the reported interactome database. In this study, we report the state-dependent interaction map of the two KRas isoforms, KRas4a and

KRas4b, acquired using stable isotope labeling with amino acids in cell culture (SILAC) and affinity-purification mass spectrometry (AP-MS). These interactions not only can explain some of the functional differences between KRas4a and KRas4b, but can also facilitate the discovery of new signaling functions of the two KRas isoforms.

Results and discussion

Identify KRas4a and 4b interacting proteins in HEK293T cells by SILAC and AP-MS

We utilized SILAC and AP-MS to construct the interactome network of FLAG-tagged wild-type (WT) and constitutively active Gly12Asp mutant (G12D) of KRas4a and 4b. It has been shown that most WT KRas is in the GDP-bound state in cells (~93%)[28]. In contrast, mutation of KRas Gly12 to any other amino acids except proline blocks GAP arginine finger assisted GTP hydrolysis, leading to most mutant KRas bound to GTP[29]. It has been shown that different Gly12 mutants have different GTP-loading percentages. We chose G12D mutant for the interactome study because KRas G12D has been found as the most abundant mutation in many types of cancer, such as pancreatic ductal adenocarcinoma (PDAC) and colon and rectal carcinoma (CRC)[2]. Comparing the interactome of KRas4a/b WT and G12D mutant may reveal KRas4a/b GTP- or GDP-bound state dependent interacting proteins. The usage of SILAC will help rule out the unspecific interacting proteins and efficiently reduce the false positives, which is a common problem for AP-MS based interactome studies. We transiently transfected tag-free KRas4a/b WT or G12D into 'light' HEK293T cells, and FLAG-tagged KRas4a/b WT or G12D into 'heavy' HEK293T cells (**Figure 4.1a**). Each FLAG-tagged protein had similar expression level, which was reflected by similar peptide number (KRas4a WT: 21, KRas4a G12D: 21, KRas4b WT: 22, KRas4b G12D: 24) and sequence coverage (KRas4a WT: 75%, KRas4a G12D: 75%,

KRas4b WT: 83%, KRas4b G12D: 83%) in MS. To enhance the data reliability and reduce false positive hits, we performed reverse SILAC in parallel, in which the 'heavy' and 'light' samples were swapped. We plotted KRas4a/b interacting proteins (with ≥2 unique peptides identified) against their heavy/light ratios in both forward and reverse SILAC to get the overall interacting proteins (**Figure 4.1b**). We set heavy/light >1.5 in forward SILAC and heavy/light <0.67 in reverse SILAC as the filter criteria (50% more proteins enriched in FLAG-tagged protein than tag-free protein) to obtain a list of confident KRas4a/b WT and G12D interacting proteins. Over 85% of proteins from original mass spectrometry result list were ruled out, leaving comparable numbers of interacting proteins for each KRas protein (KRas4a WT: 103 proteins, KRas4a G12D: 96 proteins, KRas4b WT: 94 proteins, KRas4b G12D: 110 proteins, **Figure 4.1c, d**). By comparing with previously published proteomics data of global protein expression levels in HEK293T cells[30], our data suggested that KRas4a/b interacting proteins spanned a broad range in abundance across the HEK293T proteome (**Figure 4.1e**). Many known KRas4a/b interacting proteins were identified (**Figure 4.1f**), suggesting the reliability of the dataset. Some proteins are present in only one but not the other SILAC (either forward or reverse), or have low peptide number, which might be due to low protein expression levels. They may still be KRas4a/b interacting proteins. Therefore, we also considered these proteins as potential KRas4a/b interacting proteins and subjected them for biochemical validation if they have interesting functional implications.

For each KRas isoform, comparison of WT and G12D indicated that more than half of interacting proteins were shared (**Figure 4.1g**), suggesting that GTP/GDP exchange on KRas affected some but not the majority of interacting protein profile. Among interacting proteins that were not shared between WT and G12D, we found many known KRas4a/b effector proteins that only interacted with G12D, such as ARAF and

BRAF (**Figure 4.1f**). This indicated that by comparing WT and G12D interactome, we may identify new KRas4a/b effector proteins. Comparison of different KRas isoforms (KRas4a versus KRas4b, or KRas4a G12D versus KRas4b G12D) suggested that more than half of interacting proteins were isoform specific (**Figure 4.1g**). We combined WT and G12D interactome for each KRas isoform and analyzed their biological processes. We found many shared biological processes such as nucleotide-binding and alternative splicing (**Figure 4.1h**). Some biological processes showed KRas isoform specificity. For example, KRas4a is involved in mitosis, DNA damage, and ion transport, while KRas4b is involved in neurodegeneration, mRNA transport, lipid metabolism, and protein biosynthesis (**Figure 4.1h**).

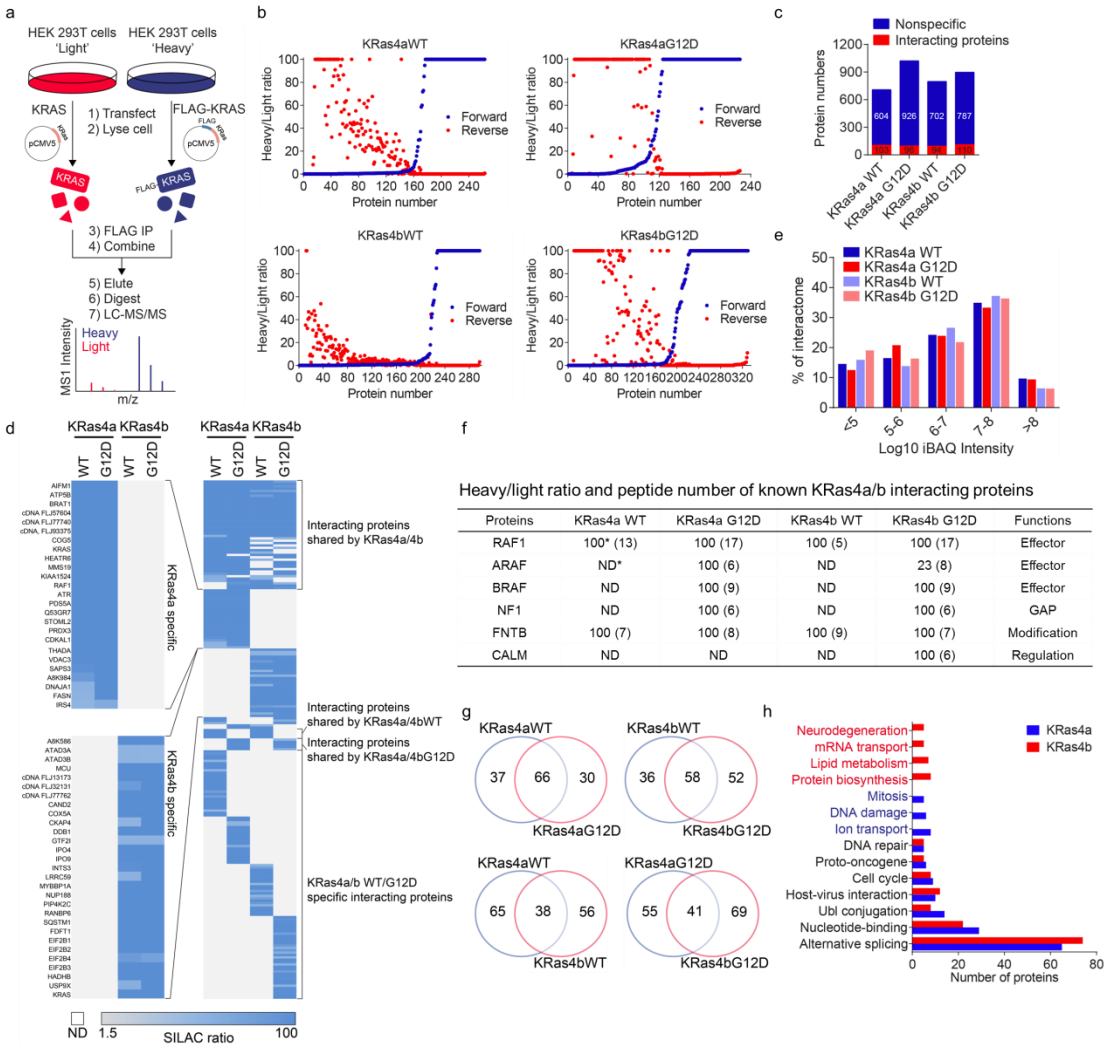

Proteins	KRas4a WT	KRas4a G12D	KRas4b WT	KRas4b G12D	Functions
RAF1	100* (13)	100 (17)	100 (5)	100 (17)	Effector
ARAF	ND*	100 (6)	ND	23 (8)	Effector
BRAF	ND	100 (9)	ND	100 (9)	Effector
NF1	ND	100 (6)	ND	100 (6)	GAP
FNTB	100 (7)	100 (8)	100 (9)	100 (7)	Modification
CALM	ND	ND	ND	100 (6)	Regulation

Figure 4.1. Identify KRas4a and 4b interacting proteins in HEK293T cells by SILAC and AP-MS. (a) Scheme showing identification of KRas4a/b interacting proteins in HEK293T cells by SILAC and AP-MS. (b) Plotting KRas4a/b interacting proteins (with ≥2 peptides) against their heavy/light ratios. (c) Nonspecific versus confident interacting proteins of KRas4a/b WT/G12D in HEK293T cells. (d) Heatmap showing the heavy/light ratios of KRas4a/b WT/G12D interacting proteins in HEK293T cells. (e) iBAQ values (from HEK293T cells) showing the abundance distribution of KRas4a/b WT/G12D interacting proteins. (f) Heavy/light ratio and peptide number (within brackets) of known KRas4a/b interacting proteins. (g) Venn diagram showing

the numbers of shared and unique interacting proteins of KRas4a/b WT/G12D in HEK293T cells. (h) Biological process analysis of KRas4a and KRas4b interacting proteins. Categories were assigned based on DAVID analysis UP_KEYWORDS.

We noticed that some proteins only interacted with one KRas isoform. KRas4a and 4b are alternatively spliced isoforms, their conserved domains are 99% identical (residues 1-150 are 100% identical), but their C-terminal HVR are highly diverse. Hence, we hypothesized that for any proteins that show KRas4a/b interaction specificity, the C-terminal HVR should contribute to the interaction. We chose two proteins for validation. The first protein is v-ATPase a2, which only interacted with KRas4b but not KRas4a (**Figure 4.2a**). We transfected FLAG-tagged KRas4a and 4b into HEK293T cells. Immunoprecipitation of FLAG-tagged KRas4b, but not KRas4a, pulled out endogenous v-ATPase a2 (**Figure 4.2b**). We also found that FLAG-tagged HRas did not interact with endogenous v-ATPase a2 (**Figure 4.2c**). To confirm whether KRas4b C-terminal HVR contributed to the interaction, we made FLAG-tagged HRas-KRas4a/b chimeric protein constructs by adding KRas4a/b C-terminal HVR (residues 165-189 on KRas4a and residues 165-188 on KRas4b) after the HRas conserved domain (residues 1-164) (**Figure 4.2c**). We transfected FLAG-tagged HRas (1-164)-KRas4a (165-189) and HRas (1-164)-KRas4b (165-188) into HEK293T cells. Immunoprecipitation of FLAG-tagged HRas (1-164)-KRas4b (165-188), but not FLAG-tagged HRas (1-164)-KRas4a (165-189), pulled out endogenous v-ATPase a2 to the similar level as FLAG-tagged KRas4b did (**Figure 4.2c**), suggesting that KRas4b C-terminal HVR accounted for specific binding to v-ATPase a2. The unique KRas4b-v-ATPase a2 interaction suggested that v-ATPase a2 is unlikely a KRas4b effector protein. We then confirmed this by examining the interactions between v-ATPase a2 and KRas4a G12D (constitutively active, always binds to effector protein)

or S17N (dominant negative, cannot bind to effector protein)[31]. KRas4b G12D and S17N showed comparable v-ATPase a2 interactions (**Figure 4.2d**), suggesting that v-ATPase a2 is not the effector protein of KRas4b. The other protein we chose for validation is eukaryotic initiation factor 2B subunit δ (eIF2Bδ), which only interacted with KRas4b but not KRas4a (**Figure 4.2e**). Co-immunoprecipitation (Co-IP) confirmed that endogenous eIF2Bδ interacted with FLAG-tagged KRas4b but not KRas4a in HEK293T cells (**Figure 4.2f**). Furthermore, immunoprecipitation of FLAG-tagged HRas (1-164)-KRas4b (165-188), but not FLAG-tagged HRas (1-164)-KRas4a (165-189), pulled out endogenous eIF2Bδ to the similar level as FLAG-tagged KRas4b did (**Figure 4.2g**), suggesting that KRas4b C-terminal HVR contributed to the interaction with eIF2Bδ. Similar as v-ATPase a2, the eIF2Bδ-KRas4b interaction was not dependent on KRas4b nucleotide binding state because in HEK293T cells, both KRas4b G12D and S17N showed comparable eIF2Bδ interactions (**Figure 4.2h**).

These previously unknown KRas4a/b interacting proteins uncovered by our interactome data may facilitate the discovery of new KRas4a/b functions. For example, v-ATPase is known to localize on the surface of lysosome membrane[32]. The interaction between KRas4b and v-ATPase indicated that KRas4b may also localize on the lysosome. Although KRas4b is reported to mainly localize on the plasma membrane, our study suggested that KRas4b may localize on the lysosome and participate in v-ATPase related functions. eIF2B is the GEF of eIF2α and plays pivotal roles in translation initiation[33]. It consists of five subunits (eIF2Bα, eIF2Bβ, eIF2Bγ, eIF2Bδ, and eIF2Bε)[34]. Indeed, all the other four eIF2B subunits were identified as KRas4b specific interacting proteins (**Figure 4.2i**), suggesting that KRas4b may regulate translation initiation by interacting with eIF2B.

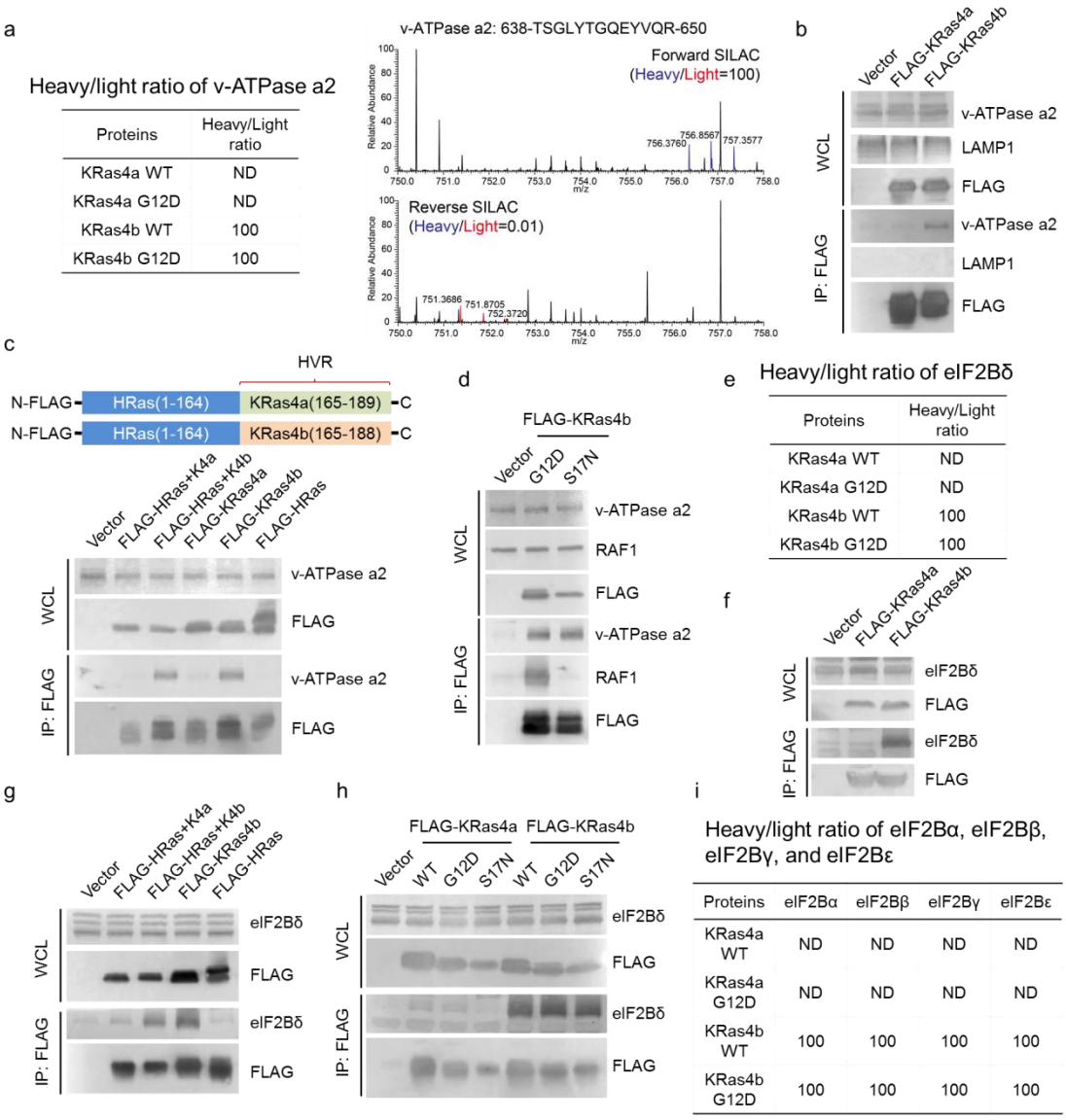

Figure 4.2. KRas4b interacts with v-ATPase a2 and eIF2Bδ through its C-terminal HVR. (a) Heavy/light ratio of v-ATPase a2 in KRas4a/b SILAC and primary mass spectra of one v-ATPase a2 peptide (residues 638-650) in forward and reverse SILAC. (b) Immunoprecipitation of FLAG-tagged KRas4b, but not KRas4a, pulled out endogenous v-ATPase a2 in HEK293T cells. LAMP1 was used as a negative control. (c) Immunoprecipitation of FLAG-tagged HRas (1-164)+KRas4b (165-188), but not FLAG-tagged HRas (1-164)+KRas4a (165-189), pulled out endogenous v-ATPase a2 as FLAG-tagged KRas4b did. (d) Immunoprecipitation of both FLAG-tagged KRas4b

G12D and S17N pulled out similar levels of endogenous v-ATPase a2. RAF1 was used as a positive control, which only interacted with KRas4b G12D but not S17N. (e) Heavy/light ratio of eIF2Bδ in KRas4a/b SILAC. (f) Immunoprecipitation of FLAG-tagged KRas4b, but not KRas4a, pulled out endogenous eIF2Bδ in HEK293T cells. (g) Immunoprecipitation of FLAG-tagged HRas (1-164)+KRas4b (165-188), but not HRas (1-164)+KRas4a (165-189), pulled out endogenous eIF2Bδ as FLAG-tagged KRas4b did. (h) Immunoprecipitation of FLAG-tagged KRas4b WT, G12D and S17N pulled out similar levels of endogenous eIF2Bδ. (i) Heavy/light ratios of eIF2Bα, eIF2Bβ, eIF2Bγ and eIF2Bε in KRas4a/b SILAC.

KRas4a has more RAF1 interaction than KRas4b in cells

We next asked whether we could identify the KRas4a/b interacting proteins that contribute to the different biological functions of KRas4a and 4b. We found that RAF1, a well characterized Ras effector protein, had more peptide number and higher protein score in the KRas4a WT interactome than in the KRas4b WT interactome (**Figure 4.1f**, peptide number: 13 vs. 5, protein score: 42.7 vs. 16.6), suggesting that KRas4a had more RAF1 interaction than KRas4b. Moreover, RAF1 was identified in KRas4a WT reverse SILAC but not in KRas4b WT reverse SILAC, which was likely due to the low interaction abundance in the KRas4b WT sample. Although both KRas4a G12D and KRas4b G12D pulled out similar levels of RAF1 (**Figure 4.1f**), we reasoned that the high percentage of GTP-loading on overexpress KRas4a/b G12D may saturate RAF1 binding and obscure the difference in binding. We first validated KRas4a/b and RAF1 interaction in HEK293T cells. Immunoprecipitation of FLAG-tagged KRas4a WT pulled out more endogenous RAF1 than FLAG-tagged KRas4b WT did (**Figure 4.3a**). We also included FLAG-tagged HRas and NRas in our co-IP experiment and found that KRas4a had the highest RAF1 interaction among four Ras

proteins (**Figure 4.3a**). Immunoprecipitation of FLAG-tagged KRas4a G12D and KRas4b G12D had comparable RAF1 interactions (**Figure 4.3a**), which is consistent with the SILAC result. To reduce the effect of saturated RAF1 binding on KRas4a/b G12D, we lowered KRas4a/b G12D expression levels by stably expressing them in NIH 3T3 cells. NIH 3T3 cells were also a better cell model and wildely used for studying Ras related cancer biology than HEK293T cells[35]. We selected the cells that expressed similar levels of endogenous and overexpressed Ras proteins (**Figure 4.3b**), to reduce the artifact caused by too much protein overexpression. We first examined KRas4a/b G12D and RAF1 interactions in NIH 3T3 cells. Immunoprecipitation of KRas4a G12D pulled out more RAF1 than KRas4b G12D and HRas G12D did (**Figure 4.3c**). The other two members of RAF family, ARAF and BRAF, showed comparable interactions with KRas4a G12D and KRas4b G12D (**Figure 4.3c**), suggesting that the increased RAF-KRas4a interaction was specific to RAF1. These different RAF1 interactions might be attributed to KRas4a and 4b C-terminal HVRs. To test this, we transfected FLAG-tagged HRas (1-164)-KRas4a (165-189) and HRas (1-164)-KRas4b (165-188) into HEK293T cells. Immunoprecipitation of FLAG-tagged HRas (1-164)-KRas4a (165-189) pulled out more endogenous RAF1 than FLAG-tagged HRas (1-164)-KRas4b (165-188) did (**Figure 4.3d**). ARAF was included as a control and it showed similar bindings for these chimeric proteins (**Figure 4.3d**). This result suggested that besides switch I region, KRas4a C-terminal HVR also contributed to RAF1 binding, which led to increased KRas4a-RAF1 interaction. In addition, we found that in KRas4a G12D expressed cells, ERK, a well-established RAF kinase downstream protein[36], had higher phosphorylation than that in KRas4b G12D or HRas G12D expressed cells (**Figure 4.3e**), suggesting that the increased KRas4a-RAF1 interaction also led to increased RAF-MEK-ERK signaling as expected.

Next, we set out to look for different KRas4a and 4b related phenotypes that may potentially be attributed to different KRas4a/b-RAF1 bindings. As a tumor driver and the most common mutated gene in human cancer, KRAS plays crucial roles in tumorigenesis and tumor growth[37]. However, which KRas isoform plays more important roles remains a matter of debate[9]. Therefore, we employed two classical and widely used assays, anchorage-independent growth and anchorage-dependent growth, to evaluate the tumorigenesis and growth of KRas4a and 4b transformed cells. Both anchorage-independent and anchorage-dependent growths are integrated phenotypes that are attributed by different molecular signaling events but they are generally thought to be mainly regulated by RAF-MEK-ERK and PI3K-Akt-mTOR pathways[38]. Anchorage-dependent cell proliferation assay showed that KRas4a G12D and KRas4b G12D increased NIH 3T3 cell proliferation to similar extents (**Figure 4.3f**), suggesting that the differential KRas4a/b-RAF1 interaction was unlikely to contribute to the anchorage-dependent cell growth in this context. Indeed, we examined PI3K-Akt-mTOR pathway which was also known as Ras effector pathway[39], and found that HRas, KRas4a, and KRas4b activated this pathway similarly. All three Ras proteins increased p-Akt (Thr308), p-Akt (Ser473), p-S6K (Thr389) and p-4E-BP1 (Thr37,46) to similar extents (**Figure 4.3g**), suggesting that PI3K-Akt-mTOR pathway likely played more important role in anchorage-dependent cell growth in KRas4a/b transformed NIH 3T3 cells. On the other hand, anchorage-independent soft agar assay showed that KRas4a G12D expressed NIH 3T3 cells had significantly higher colony numbers than KRas4b G12D or HRas G12D expressed cells (**Figure 4.3h**). This result suggested that in KRas4a/b transformed NIH 3T3 cells, the differential KRas4a/b-RAF1 interaction may contribute to differential anchorage-independent growth, and increased KRas4a-RAF1 may lead to improved tumorigenic capability (**Figure 4.3i**).

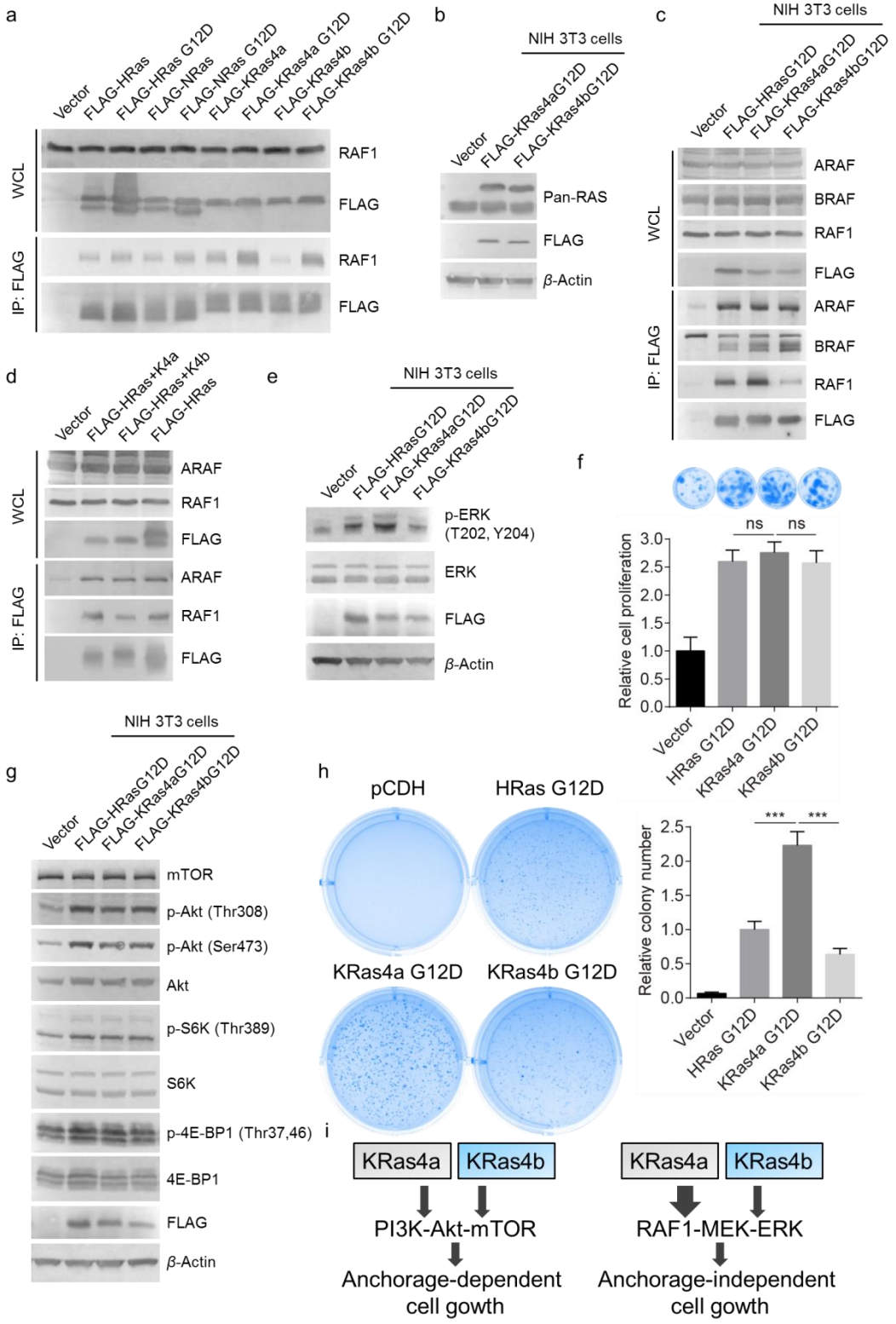

Figure 4.3. KRas4a has more RAF1 interaction than KRas4b in cells. (a) Detection of

interactions between endogenous RAF1 and FLAG-tagged WT and G12D HRas, NRas, KRas4a and KRas4b in HEK293T cells. (b) FLAG-tagged KRas4a/b G12D and endogenous Ras expression levels in NIH 3T3 cells. FLAG-tagged KRas4a/b had higher molecular weight and therefore produced band shift. (c) Immunoprecipitation of FLAG-tagged KRas4a G12D pulled out more endogenous RAF1, but not ARAF and BRAF, than FLAG-tagged HRas G12D and KRas4b G12D did in NIH 3T3 cells. (d) Immunoprecipitation of FLAG-tagged HRas(1-164)+KRas4a(165-189) pulled out more endogenous RAF1 than FLAG-tagged HRas(1-164)+KRas4b(165-188) did in HEK293T cells. (e) p-ERK (Thr202, Tyr204) and ERK levels in NIH 3T3 cells expressing pCDH vector, FLAG-tagged HRas G12D, KRas4a G12D, or KRas4b G12D. (f) Anchorage-dependent cell proliferation of NIH 3T3 cells expressing pCDH vector, FLAG-tagged HRas G12D, KRas4a G12D, or KRas4b G12D. (g) FLAG-tagged HRas G12D, KRas4a G12D and KRas4b G12D increased several key players (p-Akt Thr308, p-Akt Ser473, p-S6K Thr389 and p-4E-BP1 Thr37,46) in PI3K-Akt-mTOR pathway similarly in NIH 3T3 cells. (h) Anchorage-independent soft agar assay showing KRas4a G12D expressed NIH 3T3 cells had higher colony number than HRas G12D or KRas4b G12D expressed NIH 3T3 cells. (i) In NIH 3T3 cells, increased KRas4a-RAF1 interaction may contribute to increased anchorage-independent cell growth.

mTOR interacts with KRas4a and 4b

We noticed that a serine/threonine-protein kinase mTOR was identified as a KRas4a and 4b interacting protein (**Figure 4.4a**) and decided to investigate this interaction further. mTOR is an essential energy regulator. Although KRas4a/b is known to activate mTOR through PI3K-Akt-mTOR and MAPK pathways[11,40], currently no studies have shown a direct connection between KRas4a/b and mTOR.

We first set out to validate the KRas4a/b-mTOR interaction by transiently transfecting FLAG-tagged HRas, NRas, or KRas4a/b into HEK293T cells followed by FLAG immnuprecipitation. Immunoprecipitation of both FLAG-tagged KRas4a and 4b pulled out endogenous mTOR (**Figure 4.4b**). In contrast, HRas showed little mTOR interaction (**Figure 4.4b**). NRas had slightly increased mTOR interaction compared with HRas but the interaction was still much lower than KRas4a/b (**Figure 4.4b**), suggesting that mTOR interacts with KRas4a/b better than with HRas and NRas. We also transfected FLAG-tagged KRas4a/b in mouse cells (NIH 3T3 cells) and observed interactions between FLAG-tagged KRas4a/b and endogenous mouse mTOR (**Figure 4.4c**). Alternatively, immunoprecipitation of endogenous mTOR pulled out FLAG-tagged KRas4b in HEK293T cells (**Figure 4.4d**). We next examined if this interaction occurred on endogenous KRas4a/b and mTOR. We used HCT116 and HT29 cell lines since both cells express relatively high levels of KRas[9]. We tested several commercial KRas antibodies for immunoprecipitation but none of them efficiently pulled out endogenous KRas4a/b from the proteome, therefore we used a pan-Ras antibody (Y13-259) that had been shown to work well for endogenous KRas immnoprecipitation in many studies[41,42]. In both HCT116 and HT29 cells, immnoprecipitation of endogenous Ras pulled out endogenous mTOR (**Figure 4.4e**), suggesting that this interaction also occurred for endogenous KRas and mTOR. We then performed a KRas4a/b and mTOR *in vitro* binding assay. We transfected FLAG-tagged KRas4a/b into HEK293T cells and purified KRas4a/b protein using anti-FLAG beads. Endogenous mTOR was purified by immunoprecipitating FLAG-tagged Raptor in 0.3% CHAPS lysis buffer followed by 1% NP40 lysis buffer elution (see **Figure 4.10** in Methods). Incubation of the purified mTOR with FLAG-tagged KRas4a/b on FLAG beads led to pull down of mTOR on FLAG beads (**Figure 4.4f**).

Next we examined whether KRas4a/b and mTOR interaction depended on KRas4a/b

GTP or GDP bound state. Immunoprecipitation of WT, G12D, and S17N FLAG-tagged KRas4a/b showed comparable mTOR interactions (**Figure 4.4g**), suggesting that the nucleotide binding state did not affect KRas4a/b-mTOR interaction. This result also suggested that the mTOR binding region of KRas4a/b was likely located away from switch I, which is the Ras effector binding region[43]. To further understand how KRas4a/b interacts with mTOR, we examined which domain of mTOR was important for the interaction. We transfected FLAG-tagged KRas4a/b and full-length or truncated (residues 1-1482, 1271-2008, or 1750-2549) Myc-tagged mTOR into HEK293T cells. Immunoprecipitation of full-length mTOR pulled out FLAG-tagged KRas4a/b, while truncated mTOR pulled out little KRas4a/b (**Figure 4.4h**), suggesting that the KRas4a/b-mTOR interaction requires the full length mTOR.

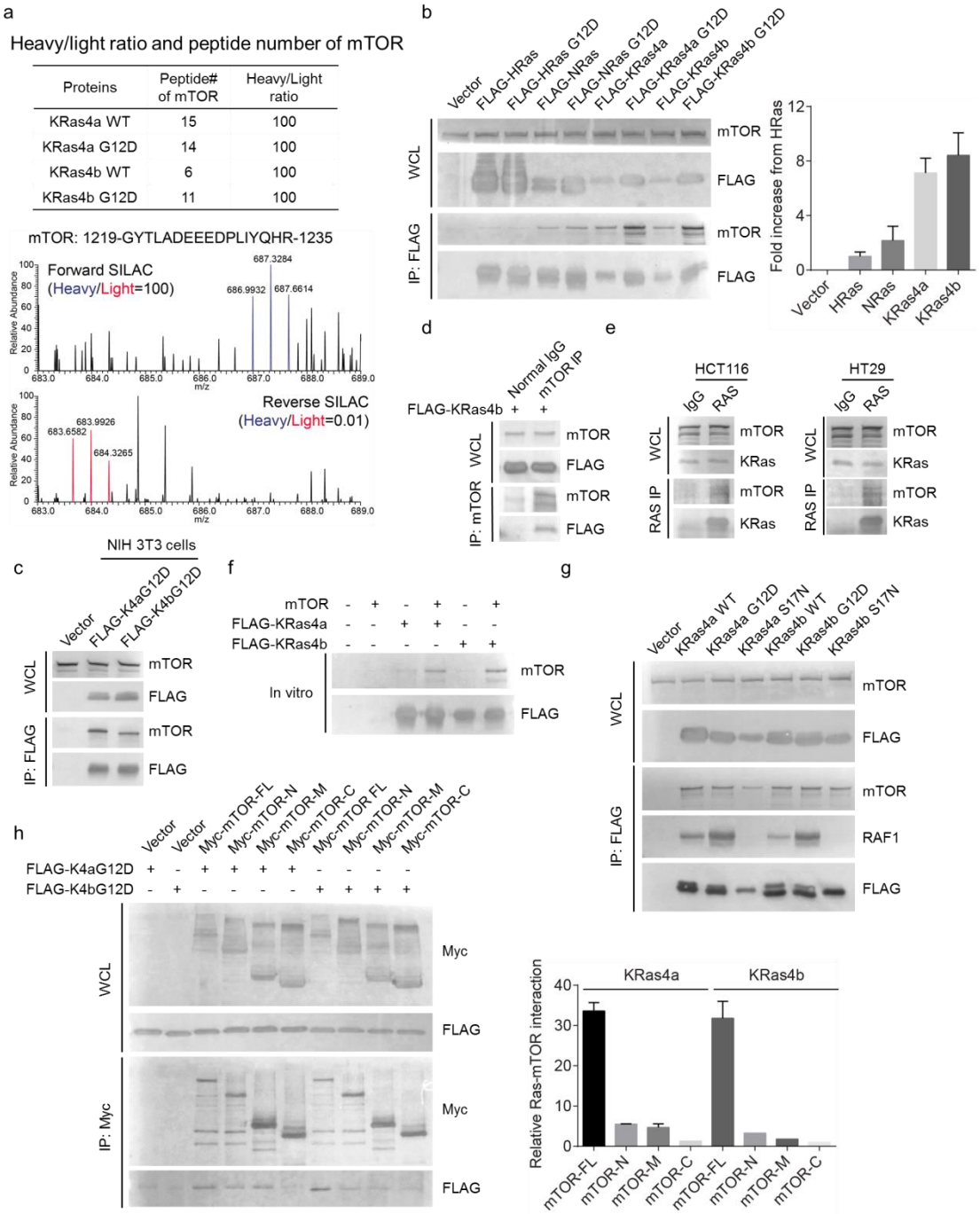

Figure 4.4. mTOR interacts with KRas4a and 4b. (a) Heavy/light ratio and peptide number of mTOR in KRas4a/b SILAC and primary mass spectra of one mTOR peptide (residues 1219-1235) in forward and reverse KRas4a WT SILAC. (b) Immunoprecipitation of FLAG-tagged KRas4a and 4b pulled out endogenous mTOR

in HEK293T cells. Right histogram shows the quantification of bands in western blot. Values with error bars indicate mean ± s.d. of three biological replicates. (c) Immunoprecipitation of FLAG-tagged KRas4a and 4b pulled out endogenous mTOR in NIH 3T3 cells. (d) Immunoprecipitation of endogenous mTOR pulled out overexpressed FLAG-tagged KRas4b in HEK293T cells. (e) Immunoprecipitation of endogenous RAS pulled out endogenous mTOR in both HCT116 and HT29 cells. (f) FLAG-tagged KRas4a and 4b interacts with mTOR *in vitro*. (g) Immunoprecipitation of WT, G12D and S17N of FLAG-tagged KRas4a and 4b pulled out similar levels of endogenous mTOR in HEK293T cells. RAF1 was used as a positive control, which only showed interaction with G12D KRas4a and 4b but not S17N KRas4a and 4b. (h) Immunoprecipitation of Myc-tagged full-length mTOR pulled out more FLAG-tagged KRas4a and 4b than Myc-mTOR-N (1-1482), Myc-mTOR-M (1271-2008), and Myc-mTOR-C (1750-2549) did.

To map the KRas4a/b and mTOR binding region, we used disuccinimidyl sulfoxide (DSSO) crosslinker combined with mass spectrometry to identify the crosslinked peptides from purified FLAG-tagged KRas4b G12D and mTOR protein. DSSO has been used to study protein-protein interaction because its C-S bonds can be cleaved during collision-induced dissociation (CID) or higher-energy collisional dissociation (HCD) (**Figure 4.5a**), generating signature ions from crosslinked peptide[44,45]. We identified one intermolecular crosslinked peptide with high confidence ($mTOR_{2218-2224}$ and $KRas4b_{124-135}$) (**Figure 4.5a**). The identification of crosslinked peptide further supported that KRas4a/b interacts with mTOR directly. We noticed that near the crosslinked KRas4b lysine residue (Lys128), there were five amino acids that were not conserved between KRas4a/b and HRas (**Figure 4.5b**). Since HRas had little mTOR interaction (**Figure 4.4b**), we wondered if these five amino acids contributed to

KRas4a/b and mTOR interaction. We mutated these five amino acids on KRas4b to HRas sequence (M1: P121A+S122A, M2: E126D+S127T+R128K, M3: M1+M2, **Figure 4.5c**) and examined their interactions with mTOR. However, we did not observe abolished mTOR interaction (**Figure 4.5c**). Similar result was observed when we examined KRas4a M3 mutant-mTOR interaction (**Figure 4.5c**). We also mutated the five amino acids on HRas to KRas4a/b sequence (M3': A121P, A122S, D126E, T127S and K128R) but this again did not rescue the interaction with mTOR (**Figure 4.5d**). These results suggested that although KRas4a/b Lys128 was close to mTOR Lys2218 upon binding (the distance is likely around 10 Å because the fully expanded DSSO spacer length is ~10 Å), they may not be indispensable for the interaction. Other regions on KRas4a/b may also be important for binding to mTOR, especially the C-terminal HVR whose sequence information was missing in cross-linking experiment due to its polylysine clusters (generating either multiple DSSO crosslinks on the same peptide or short single DSSO crosslinked peptide). We then examined if KRas4a/b C-terminal HVR was important for binding to mTOR. We transfected FLAG-tagged HRas (1-164)-KRas4a (165-189), HRas (1-164)-KRas4b (165-189), HRas, KRas4a, and KRas4b into HEK293T cells. Immunoprecipitation of FLAG-tagged HRas (1-164)-KRas4a (165-189) and HRas (1-164)-KRas4b (165-189) pulled out similar amount of endogenous mTOR as FLAG-tagged KRas4a/b did (**Figure 4.5e**), suggesting that KRas4a/b C-terminal HVR was important for binding to mTOR.

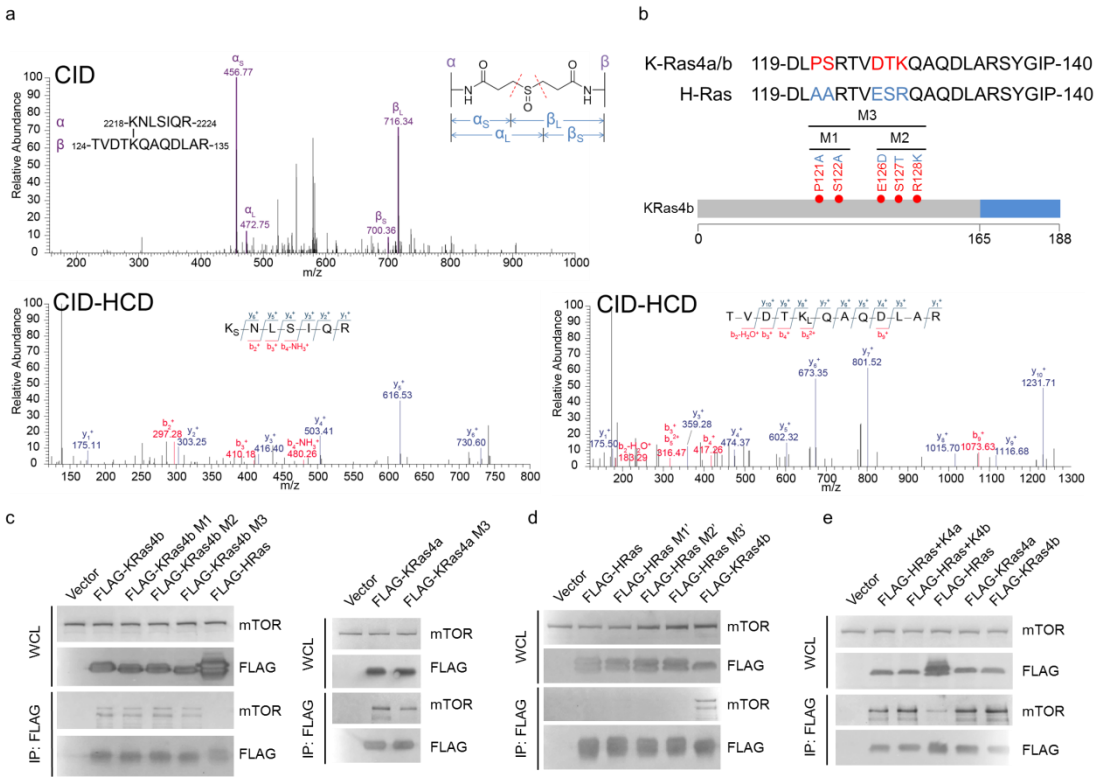

Figure 4.5. Identify KRas and mTOR binding region by DSSO crosslinker. (a) Specific fragmentation pattern of DSSO crosslinked interpeptide under CID. The signature MS precursor ion was then subjected to CID-HCD fragmentation for identifying the sequence from crosslinked interpeptide. (b) Sequence alignment between KRas4a/b (residues 119-140) and HRas (residues 119-140). (c) Immunoprecipitation of FLAG-tagged KRas4a/b WT, M1 (P121A,S122A), M2 (E126D, S127T, R128K) and M3 (M1+M2) pulled out similar amounts of endogenous mTOR in HEK293T cells. (d) Immunoprecipitation of FLAG-tagged HRas4b WT, M1' (A121P,S122S), M2' (D126E, T127S, K128R) and M3' (M1'+M2') did not pull out endogenous mTOR in HEK293T cells. (e) Immunoprecipitation of FLAG-tagged HRas (1-164)+KRas4a (165-189) and HRas (1-164)+KRas4b (165-188) pulled out similar levels of endogenous mTOR as FLAG-tagged KRas4a/b did.

KRas forms a new mTOR complex in the absence of raptor and rictor

The next question we asked was whether KRas4a/b was present in mTORC1 or mTORC2. We first examined the proteomics data and found that mLST8, an essential component of both mTORC1 and mTORC2, was identified as KRas4a/b interacting protein (**Figure 4.6a**). We validated KRas4a/b and mLST8 interaction by co-IP. In both HEK293T and NIH 3T3 cells, immunoprecipitation of FLAG-tagged KRas4a/b pulled out endogenous mLST8 (**Figure 4.6b** and **4.7a**). We further found that HRas did not interact with mLST8 (**Figure 4.6c**), and replacing the HVR of HRas with that of KRas4a/b fully rescued its interaction with mLST8 (**Figure 4.6c**), suggesting that mLST8 and mTOR had similar interaction patterns with KRas4a/b (see discussion in **Figure 4.8**).

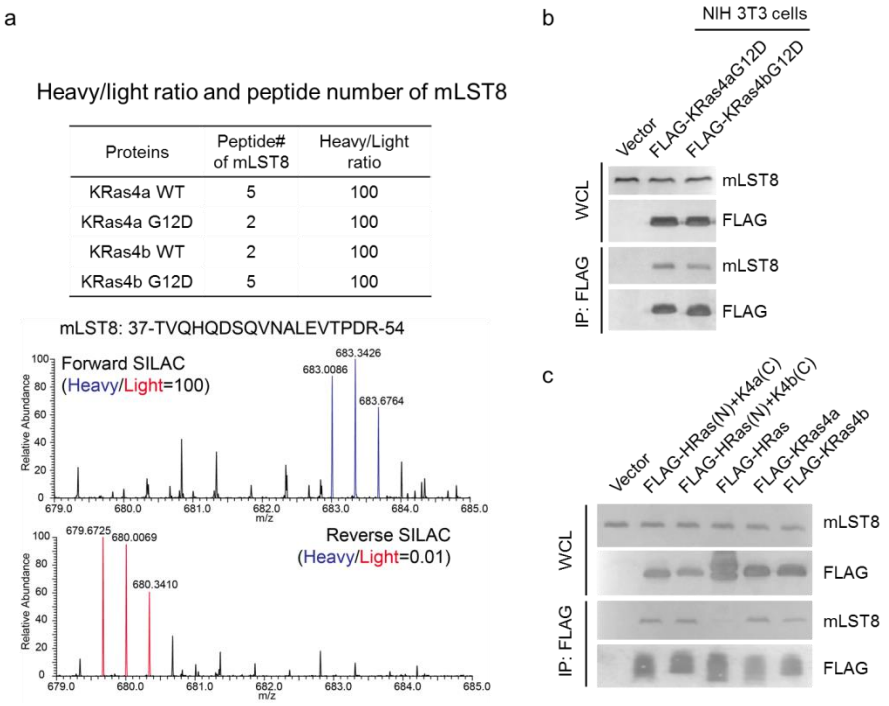

Figure 4.6. KRas4a/b interact with mLST8. (a) Heavy/light ratio and peptide number of mLST8 in KRas4a/b SILAC and primary mass spectra of one mLST8 peptide (residues 37-54) in forward and reverse SILAC. (b) Immunoprecipitation of FLAG-tagged KRas4a and 4b pulled out endogenous mLST8 in NIH 3T3 cells. (c) Immunoprecipitation of FLAG-tagged HRas (1-164)+KRas4a (165-189) and HRas (1-

164)+KRas4b (165-188) pulled out endogenous mLST8, similar to FLAG-tagged KRas4a and 4b. FLAG-tagged HRas did not pull out endogenous mLST8.

We did not find raptor and rictor in our proteomics data. It is known that mTOR-raptor and mTOR-rictor interactions are sensitive to detergents such as NP40 and Triton X100[46,47]. When performing SILAC experiment, we used 1% NP40 buffer to lyse the cells, suggesting the absence of raptor and rictor could be due to the lysis method we used. We then used 0.3% CHAPS lysis buffer, which had been shown to maintain mTOR complexes[46,47], to lyse the cells. To our surprise, neither raptor nor rictor was pulled out by FLAG-tagged KRas4a/b immunoprecipitation (**Figure 4.7a**). Alternatively, we transfected FLAG-tagged KRas4b into HEK293T cells. Immunoprecipitation of endogenous raptor or rictor pulled out endogenous mTOR but not FLAG-tagged KRas4b (**Figure 4.7b**). In contrast, endogenous mTOR immunoprecipitation pulled out endogenous raptor, rictor, and FLAG-tagged KRas4b (**Figure 4.7b**). This result suggested that KRas may form an mTOR complex without raptor or rictor. We noticed that the Western blot signals of endogenous raptor and rictor were not strong. The absence of KRas4a/b-raptor and KRas4a/b-rictor interactions may be due to low protein expression or low antibody sensitivity. To test this, we co-transfected FLAG-tagged raptor and tag-free KRas4a/b in HEK293T cells to obtain high protein expressions for both raptor and KRas4a/b (**Figure 4.7c**). Immunoprecipitation of raptor efficiently pulled out mTOR and mLST8, but not KRas4a/b (**Figure 4.7c**), again suggesting that KRas4a/b did not form complex with mTORC1. Similarly, co-transfection of Myc-tagged rictor and tag-free KRas4a/b followed by Myc-tag immunoprecipitation pulled out mTOR and mLST8, but not KRas4a/b (**Figure 4.7d**), suggesting that KRas4a/b did not interact with mTORC2. We also examined whether KRas4a/b and mTOR interaction was sensitive to

rapamycin, an allosteric mTORC1 inhibitor. The result suggested that rapamycin treatment did not affect KRas4a/b binding to mTOR (**Figure 4.7e**). The next question we asked was whether KRas4a/b changed mTOR kinase activity through this interaction. We purified mTOR protein in the absence of raptor and rictor (see **Figure 4.10** in Methods) and performed *in vitro* kinase activity assay using HA-tagged S6K as a substrate. Neither KRas4a nor 4b changed mTOR activity *in vitro* (**Figure 4.7f**), suggesting that KRas4a/b may not directly alter mTOR kinase activity.

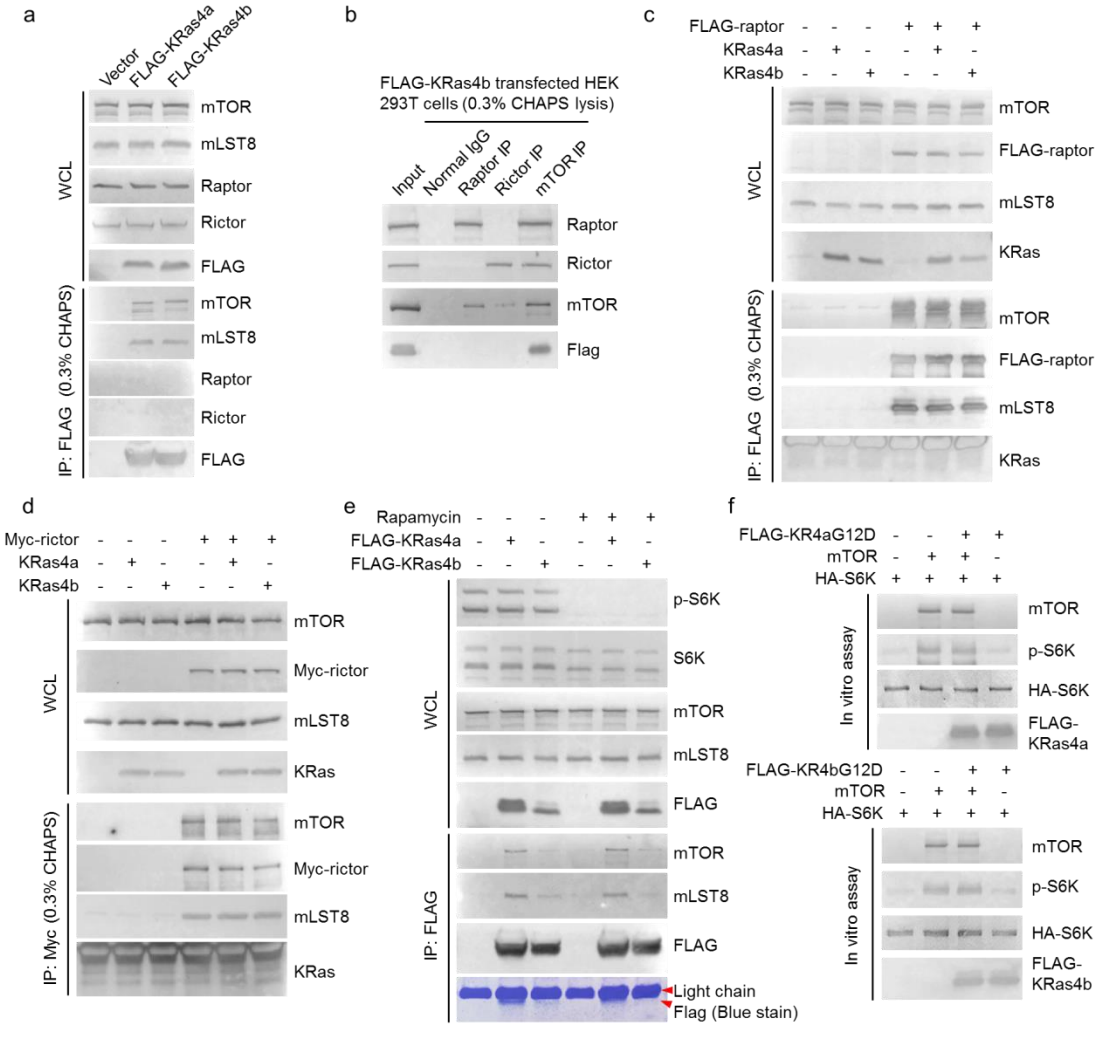

Figure 4.7. KRas4a/b and mTOR form a complex without of raptor and rictor. (a) Immunoprecipitation of FLAG-tagged KRas4a and 4b pulled out endogenous mTOR

and mLST8 but not raptor and rictor in HEK293T cells. (b) Immunoprecipitation of endogenous raptor and rictor did not pull out FLAG-tagged KRas4b in HEK293T cells. Immunoprecipitation of endogenous mTOR pulled out FLAG-tagged KRas, raptor and rictor. (c) Immunoprecipitation of FLAG-tagged raptor pulled out mTOR and mLST8, but not KRas4a and 4b in HEK293T cells. (d) Immunoprecipitation of Myc-tagged rictor pulled out mTOR and mLST8, but not KRas4a and 4b in HEK293T cells. (e) Rapamycin treatment did not affect KRas4a/b-mTOR interaction in HEK293T cells. The weaker KRas4b-mTOR interaction compared to the KRas4a-mTOR interaction was likely due to lower KRas4b expression level (indicated by coomassie blue stain membrane). (f) mTOR *in vitro* kinase activity assay with or without KRas4a/b. Purified HA-tagged S6K was used as an mTOR substrate.

We then proposed a KRas4a/b-mTOR interaction model using published cryo-EM structure of mTORC1 (PDB: 5FLC) and full-length crystal structure of KRas4b (PDB: 5TAR). First, the cross-linking result suggested that the crosslinked KRas4b peptide (residues 124-135) was from its α4 helix, which is on the back side of KRas4b effector and nucleotide binding regions (P-loop, switch I and II). Given that KRas4a/b-mTOR interaction was nucleotide binding state-independent (**Figure 4.4g**), the KRas4b effector and nucleotide binding region may not participate in mTOR interaction and likely point away from the mTOR binding surface. Secondly, the crosslinked mTOR peptide (residues 2218-2224) was located away from mTOR catalytic loop (residues 2335-2344) and activation loop (residues 2357-2380), suggesting that KRas4a/b-mTOR interaction is unlikely to affect mTOR activation and catalysis, which was supported by mTOR *in vitro* kinase activity assay (**Figure 4.7f**). Our study suggested that the KRas4a/b-mTOR interaction was insensitive to rapamycin. Rapamycin is known to interact with FKBP12, and the rapamycin-FKBP12 complex binds to mTOR

FKBP-rapamycin-binding (FRB) domain, which is located near the mTOR active cleft[14]. This data further supported the model that that KRas4a/b may bind to a region on mTOR that is not involved in mTOR kinase activity. Based on above information, we docked KRas4b (PDB: 5TAR) onto mTOR (PDB: 5FLC). A large groove on mTOR serves as the binding pocket for KRas4b α4 helix (**Figure 4.8**), with KRas4b switch I and II exposed. The absence of raptor and rictor in KRas4a/b-mTOR complex suggested that KRas4a/b binding to mTOR may affect mTOR-raptor and mTOR-rictor interaction. It is known that raptor and rictor interact with mTOR HEAT repeats domain[11]. In mTOR-raptor cryo-EM structure, the raptor binding site is > 60 Å away from mTOR-KRas4b crosslinked lysine residue (Lys2218), which is longer than the diameter of correctly folded KRas4b conserved region (residues 1-165, < 40 Å). Since KRas4a/b C-terminal HVR is a flexible domain, which can extend ~ 33 Å from KRas4a/b conserved region, the full-length KRas4a/b may reach raptor binding region on mTOR through its C-terminal tail. Therefore, KRas4b C-terminal HVR likely pointed towards raptor binding site on mTOR (**Figure 4.8**). Our data suggested that KRas4a/b interacted with mLST8 through its C-terminal HVR (**Figure 4.6c**). Since mLST8 interacts with mTOR near the active cleft, mLST8 is likely an indirect interacting protein of KRas4a/b that is mediated by mTOR (**Figure 4.8**). Overall, the HEAT repeats domain and the rest of mTOR formed a clam-like structure that held KRas4b protein by interacting with both KRas4b C-terminal HVR and α4 helix. Our data suggested that none of mTOR truncates (1-1482, 1271-2008, and 1750-2549) showed comparable KRas4a/b interactions to full-length mTOR, which further confirmed the importance of whole mTOR structure. Mutation of several amino acids on or near the α4 helix of KRas4a/b did not abolish KRas4a/b-mTOR interaction (**Figure 4.5c**), but fusing KRas4a/b C-terminal HVR (165-188/9) on HRas conserved domain (1-164) gained the ability to interact with mTOR (**Figure 4.5e**). We reasoned

that KRas4a/b C-terminal HVR may form stronger mTOR interaction than α4 helix. One possibility was that KRas4a/b contained more charged residues in C-terminal HVR than HRas and NRas (HRas: 5, NRas: 5, KRas4a: 10, KRas4b: 13), these charged residues may form strong electrostatic interactions with mTOR on its HEAT repeats.

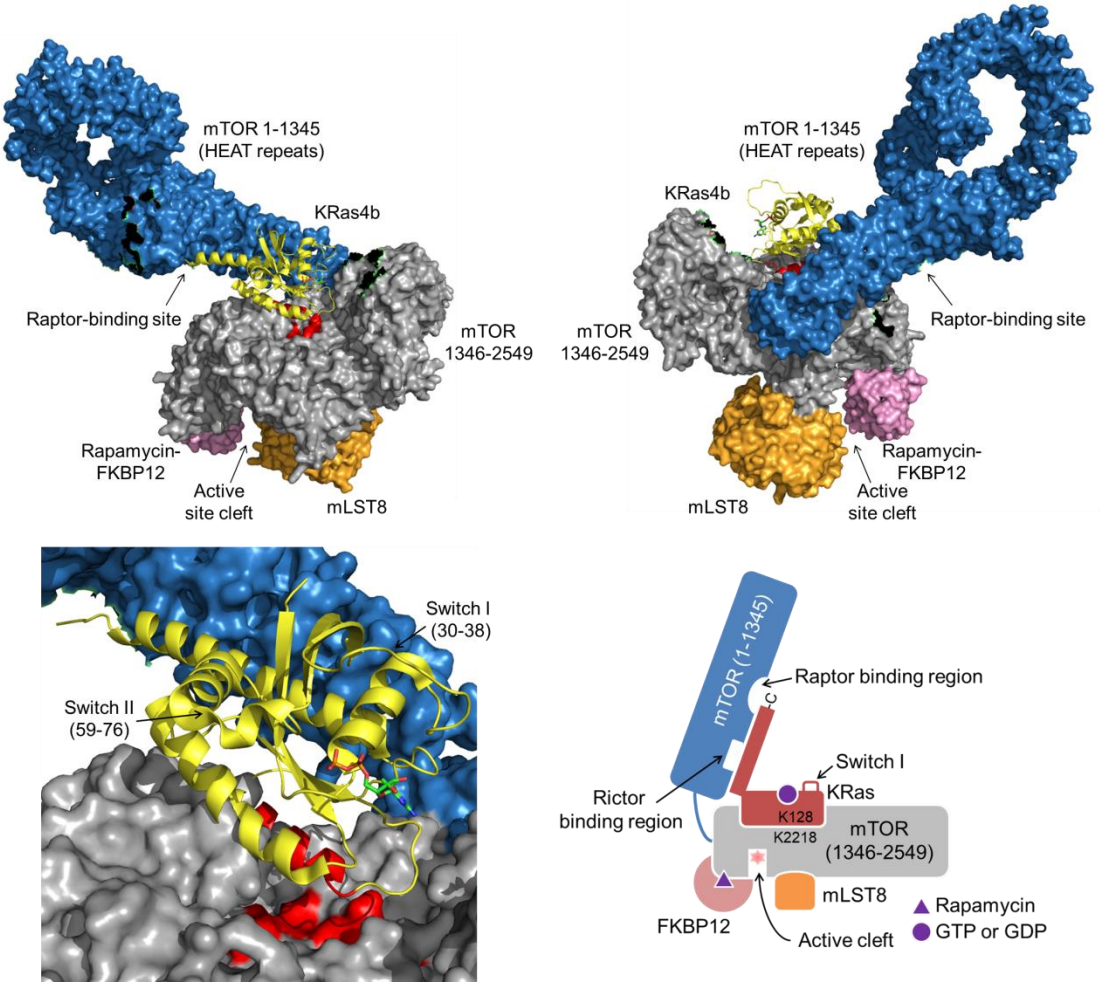

Figure 4.8. A proposed KRas4b-mTOR interaction model. Full-length KRas4b (PDB: 5TAR) was docked onto mTOR (PDB: 5FLC) in PyMOL. Red color indicated the crosslinked peptides from KRas4b and mTOR.

In this study, we performed state-dependent KRas4a and KRas4b interactome study

and identified many previously unknown KRas4a and KRas4b interacting proteins. Comparison of KRas4a and KRas4b interactome also revealed many proteins that showed isoform selectivity, which may help understand the signaling and functional differences of KRas4a and KRas4b. Interestingly, KRas4a had higher RAF1 interaction than KRas4b, which led to increased RAF1-MEK-ERK signaling cascade. This could contribute to more colonies formed in KRas4a transformed cells than in KRas4b transformed cell. Moreover, KRas4a and KRas4b interactome revealed mTOR as a KRas4a/b interacting protein. Interestingly, KRas4a/b forms an mTOR complex without raptor or rictor, indicating that KRas4a/b-mTOR complex may regulate a new pathway differently from mTORC1 and mTORC2. Indeed, we examined the effect of KRas4a/b on some well-studied mTORC1 and mTORC2 substrates in NIH 3T3 cells and HEK293T cells, including S6K, 4E-BP1, ULK1, and Akt (**Figure 4.9**). Although overexpression of KRas4a and KRas4b increased the phosphorylations of S6K, 4E-BP1 and Akt, overexpression of HRas had the similar effect. Since HRas has negligible mTOR interaction compared with KRas4a/b (**Figure 4.4b, 4.5c** and **4.5d**), it is likely the increased phorphorylation by KRas4a/b is due to other signaling pathways shared by HRas. Therefore, the KRas4a/b-mTOR complex identified in this study may have a completely different signaling cascade from mTORC1 and mTORC2.

We noticed that the KRas4a/b-mTOR interaction does not depend on KRas4a/b nucleotide-binding state (**Figure 4.4g**), suggesting that mTOR is unlikely a KRas4a/b effector protein. This also means the exposed KRas4a/b switch I is able to recruit another effector protein in KRas4a/b-mTOR complex. Identification of this effector protein may help uncover the function of KRas4a/b-mTOR complex. On the other hand, our data showed that KRas4a/b-mTOR binding site is away from mTOR active cleft (**Figure 4.7e** and **4.7f**). This suggests that the purpose of KRas4a/b-mTOR

interaction is not to change mTOR activity directly. Instead, KRas4a/b in KRas4a/b-mTOR complex is more likely an anchor protein to recruit mTOR to a specific region in cells, where mTOR phosphorylates its substrate. This is similar as mTORC1-RagA/C-the role of RagA/C is to recruit mTORC1 to the lysosome but not change mTORC1 kinase activity. Investigation of where KRas4a/b-mTOR interaction occurs may help identify the substrate of KRas4a/b-mTOR complex and therefore illustrate its functional outputs.

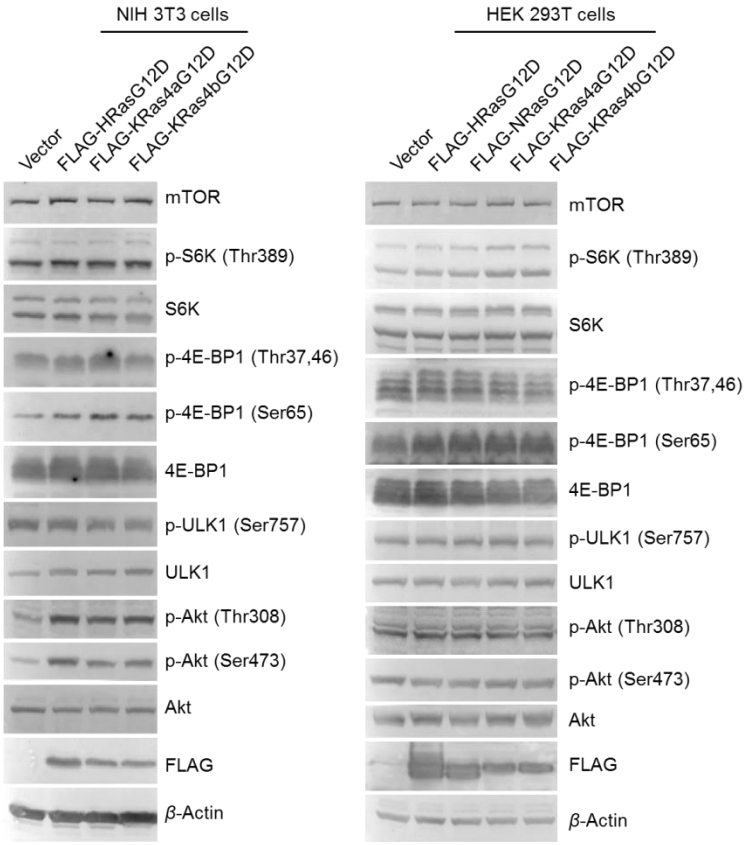

Figure 4.9. HRas, KRas4a and KRas4b increase the phosphorylation of some well-studied mTORC1 and mTORC2 substrates to the similar extents.

Methods

Antibodies. LAMP1 (#9091), ERK (#4696), p-ERK Thr202,Tyr204 (#4370), Akt

(#4691), p-Akt Thr308 (#13038), p-Akr Ser473 (#4060), S6K (#9202), p-S6K Thr389 (#9234), 4E-BP1 (#9644), p-4E-BP1 Thr37,46 (#2855), mTOR (#2983 for western blot, #2972 for immunoprecipitation), mLST8 (#3274), raptor (#2280), rictor (#2114 for western blot, #5379 for immunoprecipitation), Myc-tag (#2278), HA-tag (#3724) antibodies were purchased from Cell Signaling Technology. ARAF (sc-408), BRAF (sc-166), RAF1 (sc-227), KRas (sc-30), β-Actin (sc-4777) antibodies were purchased Santa Cruz Biotechnology. eIF2Bδ (11332-1-AP) antibody was purchased from Proteintech. v-ATPase a2 (GTX111275) antibody was purchased from GeneTex. pan-RAS (OP01) antibody was purchased from EMD Millipore. Anti-c-Myc agarose (#20168) and anti-HA agarose (26181) were purchased from ThermoFisher. Anti-FLAG affinity gels (#A2220) and FLAG antibody (#A8592) were purchased from Sigma.

Reagents. DSSO crosslinker was synthesized as described previously[45]. HA peptide, 3X FLAG peptide, protease inhibitor cocktail, puromycin, crystal violet, [$^{13}C_6$, $^{15}N_2$]-L-lysine, [$^{13}C_6$, $^{15}N_4$]-L-arginine, L-lysine, L-arginine were purchased from Sigma. Rapamycin was purchased from Cell Signaling Technology. FuGENE 6 transfection reagent and sequencing grade modified trypsin and were purchased from Promega. MEM non-essential amino acids and ECL plus western blotting detection reagent were purchased from ThermoFisher. Sep-Pak C18 cartridge was purchased from Waters.

Cell culture. Human Embryonic Kidney (HEK) 293T cells were cultured in Dulbecco's Modified Eagle Medium (DMEM) medium (ThermoFisher) with 10% heat inactivated FBS (ThermoFisher). Mouse embryonic fibroblast NIH 3T3 cells were cultured in DMEM medium with 15% heat inactivated FBS and MEM non-essential amino acids. HCT116 cells and HT29 cells were cultured McCoy's 5A medium (ThermoFisher) with 10% heat inactivated FBS. All the cell lines have been tested for mycoplasma contamination and showed no mycoplasma contamination.

Cloning, transfection and transduction. Human HRAS, NRAS, KRAS4A and KRAS4B were inserted into pCMV5 and pCDH-CMV-MCS-EF1-Puro vectors with N-terminal FLAG tag. All mutants were generated by QuikChange site-directed mutagenesis. All transient transfections were performed using FuGENE 6 transfection reagent according to manufacturer's protocol. HRas G12D, KRas4a G12D and KRas4b G12D lentivirus were generated by co-transfection of HRas/KRas4a/KRas4b G12D, pCMV-dR8.2, and pMD2.G into HEK293T cells. To obtain the HRas/KRas4a/KRas4b G12D stably overexpressed NIH 3T3 cells, cells were treated with 2 mg/mL of puromycin 48 h after lentivirus infection.

Co-immunoprecipitation. Cells were collected and lysed in 1% NP40 lysis buffer (1% NP40, 25 mM Tris-HCl pH 7.4, 150 mM NaCl and 10% glycerol) or 0.3% CHAPS lysis buffer (0.3% CHAPS, 40 mM HEPES pH 7.4, 150 mM NaCl and 2 mM EDTA) with protease inhibitor cocktail (1:100 dilution) on ice for 30 min. After centrifuging at 15,000 g for 10 min, supernatant (total lysates) was collected for FLAG, Myc, HA or endogenous protein immunoprecipitation following manufacturer's protocol. The affinity gel was washed three times with NP40 washing buffer (0.2% NP40, 25 mM Tris-HCl pH 7.4 and 150 mM NaCl) or 0.3% CHAPS lysis buffer. To detect the interacting proteins, the affinity gel was heated at 95 °C for 10 min in 2X protein loading buffer, followed by western blot analysis. For SILAC, the affinity gel was heated at 95 °C for 10 min in 1% SDS elution buffer (1% SDS, 25 mM Tris-HCl pH 7.4 and 150 mM NaCl), followed by methanol/chloroform protein precipitation.

Western blot. Western blot analysis was performed according to previously published paper[48]. The proteins of interest were detected and visualized using the Typhoon FLA 7000 (GE Healthcare).

SILAC and nano LC-MS/MS analysis. 'Heavy' HEK293T cells were cultured in

DMEM with [$^{13}C_6$, $^{15}N_2$]-L-lysine, [$^{13}C_6$, $^{15}N_4$]-L-arginine and 10% dialysed FBS for 5 generations. 'Light' HEK293T cells were cultured in DMEM with normal L-lysine, L-arginine and 10% dialysed FBS for 5 generations. After transient transfection of desired plasmids, 'heavy' and 'light' cells were lysed in 1% NP40 lysis buffer separately according to the protocol described above separately. 8 mg input of each 'heavy' and 'light' total lysate was subjected for FLAG immunoprecipitation. After washing the affinity gel three times with NP40 washing buffer, 'heavy' and 'light' samples were mixed and washed two more times with NP40 washing buffer. To elute FLAG-tagged protein with its interacting proteins, the affinity gel was heated at 95 °C for 10 min in 1% SDS elution buffer (1% SDS, 25 mM Tris-HCl pH 7.4 and 150 mM NaCl), followed by methanol/chloroform protein precipitation. The protein pellets were denatured in 6 M urea, 10 mM DTT and 50 mM Tris-HCl pH 8.0 at room temperature for 1 h. The proteins were alkylated by incubating with 40 mM iodoacetamide at room temperature for 1 h. DTT was then added to stop alkylation at room temperature for 1 h. After diluting protein sample 7 times with 50 mM Tris-HCl pH 8.0 and 1 mM $CaCl_2$, 1 μg of trypsin was added and incubated with the protein at 37 ℃ for 18 h. 0.1 % trifluoroacetic acid was added to quench the trypsin digestion, followed by desalting using Sep-Pak C18 cartridge. The lyophilized peptide powders were collected for LC-MS/MS analysis (LTQ-Orbitrap Elite mass spectrometer coupled with nanoLC). The lyophilized peptide powders were dissolved in 2% acetonitrile (ACN) with 0.5% formic acid (FA). The reconstituted peptides were injected into Acclaim PepMap nano Viper C18 trap column (5 μm, 100 μm × 2 cm, Thermo Dionex) and separated in C18 RP nano column (5 μm, 75 μm × 50 cm, Magic C18, Bruker). The flow rate was set as 0.3 μL/min. The gradient was set as following: 5-38% ACN with 0.1% FA (0-120 min), 38-95% ACN with 0.1% FA (120-127 min), 95% ACN with 0.1% FA (127-135 min). Positive ion mode was used in LTQ-Orbitrap

Elite mass spectrometer (spray voltage 1.6 kV, source temperature 275 ˚C). The precursor ions scan from m/z 375 to 1800 at resolution 120,000 using FT mass analyzer. Collision-induced dissociation (CID) was used for MS/MS scan at resolution 15,000 on 10 most intensive peaks, isolation width was set as 2.0 m/z and normalized collision energy was set as 35%. Xcalibur 2.2 operation software was used for collecting the data. The MS data was further processed using Sequest HT in Proteome Discoverer 1.4.1.14 (PD 1.4, Thermo Scientific).

Purification of endogenous mTOR. HEK293T cells stably expressing FLAG-tagged raptor were lysed in 0.3% CHAPS lysis buffer with protease inhibitor cocktail. FLAG-tagged raptor was immunoprecipitated and washed as described above. The affinity gel was incubated three times with 1% NP40 lysis buffer to elute endogenous mTOR from the affinity gel.

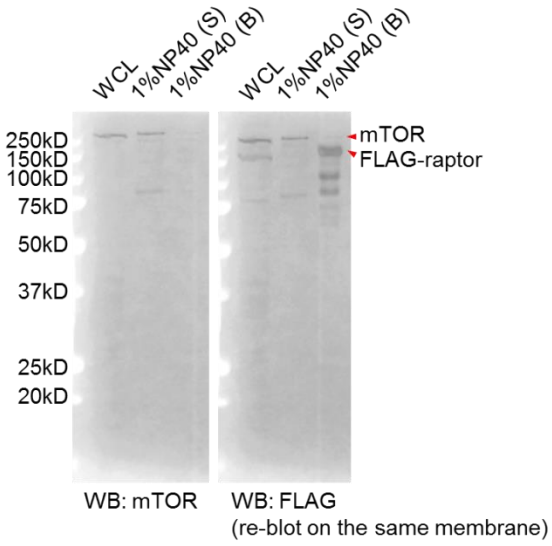

Figure 4.10. Purification of endogenous mTOR from HEK 293T cells. WCL, whole cell lysates. S, supernatant. B, FLAG beads.

Purification of FLAG-tagged KRas4a/b. HEK293T cells transiently expressing FLAG-tagged KRas4a/b were lysed in 1% NP40 lysis buffer with protease inhibitor

cocktail. FLAG-tagged KRas4a/b was immunoprecipiated and washed as described above. FLAG-tagged KRas4a/b was eluted by 3X FLAG peptide following manufacturer's protocol.

Purification of HA-tagged S6K. HEK293T cells transiently expressing HA-tagged S6K were lysed in 1% NP40 lysis buffer with protease inhibitor cocktail. HA-tagged S6K was immunoprecipitated and washed as described above. HA-tagged S6K was eluted by HA peptide following manufacturer's protocol.

Anchorage-dependent cell proliferation assay. NIH 3T3 cells stably expressing pCDH, HRas G12D, KRas4a G12D or KRas4b G12D were seeded into 12-well plate (200 cells/well). The medium was changed every 48 h. After 9 days of culture, the cells were washed with PBS and fixed with ice-cold methanol for 10 min. After removing the methanol, the cells were stained with crystal violet staining solution (0.2% in 2% ethanol) for 5 min. Then the cells were rinsed with water to remove extra crystal violet. The absorption of crystal violet was measured at 550 nm after solubilizing the stained cells with 0.5% SDS in 50% ethanol.

Anchorage-independent soft agar assay. 1.5 mL of 0.6% base low-melting point agarose was added into 6-well plate. After the agarose was solidified, 5.0×10^3 of NIH 3T3 cells stably expressing pCDH, HRas G12D, KRas4a G12D or KRas4b G12D were mixed with 0.3% low-melting point agarose and plated into 6-well plate on top of the 0.6% base agarose layer. 150 μL of normal culture medium was added on top of the 0.3% low-melting point agarose. The medium was changed every 48 h. After 14 days of culture, colonies were stained with crystal violet staining solution (0.1% in 25% methanol) for 30 min. Then the cells were rinsed with 50% methanol to remove extra crystal violet.

mTOR and KRas4a/b *in vitro* binding assay. Purified endogenouso mTOR was incubated with purified FLAG-tagged KRas4a/b (on-beads) at room temperature for

30min. The affinity gel was washed three times with NP40 washing buffer and another three times with high salt NP40 washing buffer (0.2% NP40, 25 mM Tris-HCl pH 7.4 and 500 mM NaCl). The affinity gel was then heated at 95 °C for 10 min in 2X protein loading buffer, followed by western blot analysis.

DSSO crosslinking. Purified FLAG-tagged KRas4b and endogenous mTOR were subjected for buffer exchange in PBS until the final concentration of Tris was lower than 20 μM. DSSO crosslinking reaction was performed by mixing mTOR, KRas4b and 2mM DSSO at room temperature for 1h. 25 mM Tris was added to quench the reaction. The crosslinked protein was precipitated by methanol/chloroform. The protein pellets were denatured, alkylated, neutralized, trypsinized, and then analyzed by LC-MS/MS according to the protocol described above.

***In vitro* mTOR kinase activity assay.** FLAG-tagged KRas4a/b and endogenous mTOR were purified as described above. *In vitro* mTOR kinase activity assay was performed as described previously[46].

Statistical analysis. Quantitative data were expressed as mean ± SD (standard deviation, represent by error bar). Differences were examined by two-tailed Student's t-test; *$p < 0.05$, **$p < 0.01$, ***$p < 0.005$.

REFERENCES

1 Wennerberg, K., Rossman, K. L. & Der, C. J. The Ras superfamily at a glance. *Journal of cell science* **118**, 843-846, doi:10.1242/jcs.01660 (2005).

2 Cox, A. D., Fesik, S. W., Kimmelman, A. C., Luo, J. & Der, C. J. Drugging the undruggable RAS: Mission possible? *Nature reviews. Drug discovery* **13**, 828-851, doi:10.1038/nrd4389 (2014).

3 Karnoub, A. E. & Weinberg, R. A. Ras oncogenes: split personalities. *Nature reviews. Molecular cell biology* **9**, 517-531, doi:10.1038/nrm2438 (2008).

4 Vigil, D., Cherfils, J., Rossman, K. L. & Der, C. J. Ras superfamily GEFs and GAPs: validated and tractable targets for cancer therapy? *Nature reviews. Cancer* **10**, 842-857, doi:10.1038/nrc2960 (2010).

5 Lu, S. *et al.* Ras Conformational Ensembles, Allostery, and Signaling. *Chemical reviews* **116**, 6607-6665, doi:10.1021/acs.chemrev.5b00542 (2016).

6 Ahearn, I. M., Haigis, K., Bar-Sagi, D. & Philips, M. R. Regulating the regulator: post-translational modification of RAS. *Nature reviews. Molecular cell biology* **13**, 39-51, doi:10.1038/nrm3255 (2011).
7 Parikh, C., Subrahmanyam, R. & Ren, R. Oncogenic NRAS, KRAS, and HRAS exhibit different leukemogenic potentials in mice. *Cancer research* **67**, 7139-7146, doi:10.1158/0008-5472.CAN-07-0778 (2007).
8 Fivaz, M. & Meyer, T. Reversible intracellular translocation of KRas but not HRas in hippocampal neurons regulated by Ca2+/calmodulin. *The Journal of cell biology* **170**, 429-441, doi:10.1083/jcb.200409157 (2005).
9 Tsai, F. D. *et al.* K-Ras4A splice variant is widely expressed in cancer and uses a hybrid membrane-targeting motif. *Proc Natl Acad Sci U S A* **112**, 779-784, doi:10.1073/pnas.1412811112 (2015).
10 Villalonga, P. *et al.* Calmodulin binds to K-Ras, but not to H- or N-Ras, and modulates its downstream signaling. *Molecular and cellular biology* **21**, 7345-7354, doi:10.1128/MCB.21.21.7345-7354.2001 (2001).
11 Saxton, R. A. & Sabatini, D. M. mTOR Signaling in Growth, Metabolism, and Disease. *Cell* **169**, 361-371, doi:10.1016/j.cell.2017.03.035 (2017).
12 Wang, B. *et al.* TRAF2 and OTUD7B govern a ubiquitin-dependent switch that regulates mTORC2 signalling. *Nature* **545**, 365-369, doi:10.1038/nature22344 (2017).
13 Yang, H. *et al.* mTOR kinase structure, mechanism and regulation. *Nature* **497**, 217-223, doi:10.1038/nature12122 (2013).
14 Aylett, C. H. *et al.* Architecture of human mTOR complex 1. *Science* **351**, 48-52, doi:10.1126/science.aaa3870 (2016).
15 Sancak, Y. *et al.* Ragulator-Rag complex targets mTORC1 to the lysosomal surface and is necessary for its activation by amino acids. *Cell* **141**, 290-303, doi:10.1016/j.cell.2010.02.024 (2010).
16 Chantranupong, L. *et al.* The CASTOR Proteins Are Arginine Sensors for the mTORC1 Pathway. *Cell* **165**, 153-164, doi:10.1016/j.cell.2016.02.035 (2016).
17 Wolfson, R. L. *et al.* Sestrin2 is a leucine sensor for the mTORC1 pathway. *Science* **351**, 43-48, doi:10.1126/science.aab2674 (2016).
18 Bar-Peled, L. *et al.* A Tumor suppressor complex with GAP activity for the Rag GTPases that signal amino acid sufficiency to mTORC1. *Science* **340**, 1100-1106, doi:10.1126/science.1232044 (2013).
19 Brunn, G. J. *et al.* Phosphorylation of the translational repressor PHAS-I by the mammalian target of rapamycin. *Science* **277**, 99-101 (1997).
20 Holz, M. K., Ballif, B. A., Gygi, S. P. & Blenis, J. mTOR and S6K1 mediate assembly of the translation preinitiation complex through dynamic protein interchange and ordered phosphorylation events. *Cell* **123**, 569-580, doi:10.1016/j.cell.2005.10.024 (2005).
21 Kim, J., Kundu, M., Viollet, B. & Guan, K. L. AMPK and mTOR regulate autophagy through direct phosphorylation of Ulk1. *Nature cell biology* **13**, 132-141, doi:10.1038/ncb2152 (2011).
22 Sarbassov, D. D., Guertin, D. A., Ali, S. M. & Sabatini, D. M. Phosphorylation and regulation of Akt/PKB by the rictor-mTOR complex. *Science* **307**, 1098-

1101, doi:10.1126/science.1106148 (2005).
23 Jacinto, E. *et al.* Mammalian TOR complex 2 controls the actin cytoskeleton and is rapamycin insensitive. *Nature cell biology* **6**, 1122-1128, doi:10.1038/ncb1183 (2004).
24 Garcia-Martinez, J. M. & Alessi, D. R. mTOR complex 2 (mTORC2) controls hydrophobic motif phosphorylation and activation of serum- and glucocorticoid-induced protein kinase 1 (SGK1). *The Biochemical journal* **416**, 375-385, doi:10.1042/BJ20081668 (2008).
25 Huttlin, E. L. *et al.* Architecture of the human interactome defines protein communities and disease networks. *Nature* **545**, 505-509, doi:10.1038/nature22366 (2017).
26 Hu, H., Bliss, J. M., Wang, Y. & Colicelli, J. RIN1 is an ABL tyrosine kinase activator and a regulator of epithelial-cell adhesion and migration. *Current biology : CB* **15**, 815-823, doi:10.1016/j.cub.2005.03.049 (2005).
27 Weber, C. K., Slupsky, J. R., Kalmes, H. A. & Rapp, U. R. Active Ras induces heterodimerization of cRaf and BRaf. *Cancer research* **61**, 3595-3598 (2001).
28 Bollag, G. *et al.* Biochemical characterization of a novel KRAS insertion mutation from a human leukemia. *The Journal of biological chemistry* **271**, 32491-32494 (1996).
29 Bos, J. L., Rehmann, H. & Wittinghofer, A. GEFs and GAPs: critical elements in the control of small G proteins. *Cell* **129**, 865-877, doi:10.1016/j.cell.2007.05.018 (2007).
30 Geiger, T., Wehner, A., Schaab, C., Cox, J. & Mann, M. Comparative proteomic analysis of eleven common cell lines reveals ubiquitous but varying expression of most proteins. *Molecular & cellular proteomics : MCP* **11**, M111 014050, doi:10.1074/mcp.M111.014050 (2012).
31 Nassar, N., Singh, K. & Garcia-Diaz, M. Structure of the dominant negative S17N mutant of Ras. *Biochemistry* **49**, 1970-1974, doi:10.1021/bi9020742 (2010).
32 Zoncu, R. *et al.* mTORC1 senses lysosomal amino acids through an inside-out mechanism that requires the vacuolar H(+)-ATPase. *Science* **334**, 678-683, doi:10.1126/science.1207056 (2011).
33 Jackson, R. J., Hellen, C. U. & Pestova, T. V. The mechanism of eukaryotic translation initiation and principles of its regulation. *Nature reviews. Molecular cell biology* **11**, 113-127, doi:10.1038/nrm2838 (2010).
34 Kashiwagi, K. *et al.* Crystal structure of eukaryotic translation initiation factor 2B. *Nature* **531**, 122-125, doi:10.1038/nature16991 (2016).
35 Stacey, D. W. & Kung, H. F. Transformation of NIH 3T3 cells by microinjection of Ha-ras p21 protein. *Nature* **310**, 508-511 (1984).
36 Lavoie, H. & Therrien, M. Regulation of RAF protein kinases in ERK signalling. *Nature reviews. Molecular cell biology* **16**, 281-298, doi:10.1038/nrm3979 (2015).
37 Ostrem, J. M. & Shokat, K. M. Direct small-molecule inhibitors of KRAS: from structural insights to mechanism-based design. *Nature reviews. Drug discovery* **15**, 771-785, doi:10.1038/nrd.2016.139 (2016).

38 Dohn, M. R., Brown, M. V. & Reynolds, A. B. An essential role for p120-catenin in Src- and Rac1-mediated anchorage-independent cell growth. *The Journal of cell biology* **184**, 437-450, doi:10.1083/jcb.200807096 (2009).
39 Rubio, I., Rodriguez-Viciana, P., Downward, J. & Wetzker, R. Interaction of Ras with phosphoinositide 3-kinase gamma. *The Biochemical journal* **326 (Pt 3)**, 891-895 (1997).
40 Mendoza, M. C., Er, E. E. & Blenis, J. The Ras-ERK and PI3K-mTOR pathways: cross-talk and compensation. *Trends in biochemical sciences* **36**, 320-328, doi:10.1016/j.tibs.2011.03.006 (2011).
41 Trahey, M. & McCormick, F. A cytoplasmic protein stimulates normal N-ras p21 GTPase, but does not affect oncogenic mutants. *Science* **238**, 542-545 (1987).
42 Whyte, D. B. *et al.* K- and N-Ras are geranylgeranylated in cells treated with farnesyl protein transferase inhibitors. *The Journal of biological chemistry* **272**, 14459-14464 (1997).
43 Spoerner, M., Herrmann, C., Vetter, I. R., Kalbitzer, H. R. & Wittinghofer, A. Dynamic properties of the Ras switch I region and its importance for binding to effectors. *Proc Natl Acad Sci U S A* **98**, 4944-4949, doi:10.1073/pnas.081441398 (2001).
44 Liu, F., Rijkers, D. T., Post, H. & Heck, A. J. Proteome-wide profiling of protein assemblies by cross-linking mass spectrometry. *Nature methods* **12**, 1179-1184, doi:10.1038/nmeth.3603 (2015).
45 Kao, A. *et al.* Development of a novel cross-linking strategy for fast and accurate identification of cross-linked peptides of protein complexes. *Molecular & cellular proteomics : MCP* **10**, M110 002212, doi:10.1074/mcp.M110.002212 (2011).
46 Kim, D. H. *et al.* mTOR interacts with raptor to form a nutrient-sensitive complex that signals to the cell growth machinery. *Cell* **110**, 163-175 (2002).
47 Sarbassov, D. D. *et al.* Rictor, a novel binding partner of mTOR, defines a rapamycin-insensitive and raptor-independent pathway that regulates the cytoskeleton. *Current biology : CB* **14**, 1296-1302, doi:10.1016/j.cub.2004.06.054 (2004).
48 Zhang, X. *et al.* Identifying the functional contribution of the defatty-acylase activity of SIRT6. *Nature chemical biology* **12**, 614-620, doi:10.1038/nchembio.2106 (2016).

CONCLUSIONS AND FUTURE DIRECTIONS

In my thesis work, I first investigated the functional contributions of different SIRT6 enzymatic activities, especially the newly discovered lysine defatty-acylase activity. I found that SIRT6 defatty-acylase activity regulates protein secretion, protein sorting into the exosomes, and cell proliferation. Proteomics studies led to the identification of R-Ras2 as a SIRT6 defatty-acylation target that contributes to SIRT6's role as a tumor suppressor. I also investigated the novel signaling and biological functions of KRas4a and KRas4b by proteomics. This study led to the identification of many previously unknown KRas4a and KRas4b interacting proteins that could not only explain the functional differences between KRas4a and KRas4b, but also help to uncover new signaling functions of the two KRas isoforms.

In Chapter 2, I described the discovery of the SIRT6 Gly60Ala mutant, which abolishes lysine deacetylase activity and maintains lysine defatty-acylase activity. This mutant could be used to differentiate the functional contributions of different SIRT6 deacylase activities. Using this mutant, I found that SIRT6 defatty-acylase activity regulates the secretion of numerous proteins and the sorting of ribosomal proteins into the exosomes. However, the SIRT6 defatty-acylation target(s) that mediate these functions remain unclear. I initially hypothesized that SIRT6 may directly defatty-acylate these secreted proteins and regulate their secretions, similar to the regulation of TNFα secretion[1]. However, I chose several proteins for validation and did not observe lysine fatty-acylation on these proteins, suggesting that this hypothesis is not true. Identification of SIRT6 defatty-acylation targets that contribute to these functions will uncover the missing molecular mechanisms. To do this, one approach is to directly identify SIRT6 defatty-acylation target(s) by proteomics as described in Chapter 3. However, none of the proteins from the high confident SIRT6 defatty-acylation targets

list has been implicated in protein secretion or vesicle trafficking (**Figure 3.1c**). One possibility is that the regulation of protein secretion is a novel function for these high confidence proteins. Another possibility is that the target(s) has low abundance and was not identified with high confidence. In any case, selection of proteins from the lysine fatty-acylation proteomics list for validation could be a useful direction to figure out the missing mechanisms. An alternative approach to address this question is conducting phenotypic screening (**Figure 6.1**). For example, I showed that the ribosomal proteins were sorted into the exosomes more efficiently in Sirt6 KO MEFs than in Sirt6 WT MEFs. To identify the proteins that cause this phenotype, one can conjugate a molecular barcode (eg. GFP) to a certain ribosomal protein. The GFP signal from the culture medium could be used as the readout to indicate the secretion status of this ribosomal protein. Then siRNA screening could be performed to identify which gene/protein is essential for this phenotype in Sirt6 KO MEFs but not in Sirt6 WT MEFs. The identified genes/proteins could help establish the novel signaling cascade that regulates the sorting of ribosomal proteins into the exosomes and also uncover the potential SIRT6 defatty-acylation targets.

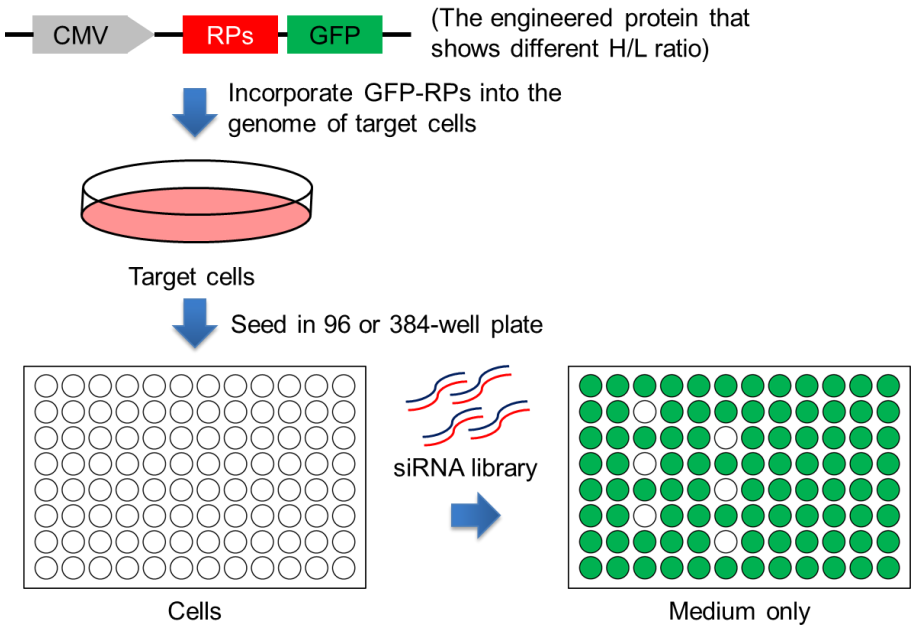

Figure 5.1. Identification of proteins that regulate the sorting of ribosomal proteins (RPs) into the exosomes by RNAi screening.

In Chapter 3, I described the identification of R-Ras2 as a SIRT6 lysine defatty-acylation target that contributes to SIRT6's tumor suppressor function. Interestingly, from the proteomics study where R-Ras2 is identified (**Figure 3.1b**), a few more metabolic enzymes were also identified as potential SIRT6 defatty-acylation targets (**Figure 3.1c**). Previous studies showed that SIRT6 regulates different metabolic processes such as glucose metabolism[2] and lipid homeostasis[3]. One interesting future direction to investigate is whether SIRT6 regulates these metabolic enzymes via defatty-acylation. This may further uncover the mechanisms by which SIRT6 serves as a cell metabolism regulator.

In Chapter 4, I described the KRas4a and KRas4b interactome study. KRas is a well-known tumor driver and plays important roles in numerous biological processes. Most current studies about KRas are mainly focused on one isoform KRas4b. But accumulating evidence suggests that KRas4a is also an important player in

tumorigenesis and possibly other biological processes.[4] To identify the shared and unique signaling pathways and biological functions of the two KRas isoforms, I performed state-dependent KRas4a and KRas4b interactome study. Some proteins were identified to specifically interact with only one isoform, such as v-ATPase a2 (interact with KRas4b) and eIF2Bδ (interact with KRas4b), whiles others interact with both KRas4a and KRas4b, such as mTOR. I further demonstrated that KRas4a has higher RAF1 interaction than KRas4b, and the increased RAF1-KRas4a interaction may lead to increased anchorage-independent cell growth in KRas4a transformed cells. Lastly, from the interactome study, mTOR was identified as a KRas4a/b interacting protein, and KRas4a/b forms a new mTOR complex without raptor or rictor.

The KRas4a and KRas4b interactome study reveals many previously unknown KRas4a and KRas4b interacting proteins that could play crucial roles in various biological processes. As mentioned earlier, v-ATPase a2 and eIF2Bδ were identified as KRas4b specific interacting proteins. These interactions were validated by co-immunoprecipitation in my thesis work. It will be interesting to further investigate the functional outputs of these interactions. v-ATPase functions to pump protons from cytosol to the late endosome and lysosome, and is also an essential component in mTORC1-mediated amino acid sensing. It is known that KRas4b is mainly localized on the plasma membrane to activate its downstream signaling[5]. The interactome study suggests that KRas4b may also localize on the late endosome and lysosome, and participate in v-ATPase related functions. eIF2B is the GEF for eIF2α[6], and both proteins are indispensable in protein translation initiation. The interaction between KRas4b and eIF2B indicates that KRas4b may function in translation initiation, which could be important for KRas-driven cancers because these cancers need more protein synthesis to maintain high proliferation rate.

In addition, the KRas4a and KRas4b interactome study identified many potential KRas effector proteins. Ras is known to recruit several GEFs to turn on other small GTPases, such as RIN (GEF for Rab), RalGDS (GEF for Ral), and Tiam1 (GEF for Rac)[7]. The KRas4a/b interactome identified Rap1GDS1 (GEF for Rap), ARFGEF3 (GEF for Arf), and FARP2 (GEF for Rho) as potential KRas4a/b effector proteins (**Figure 6.2**). This suggests that besides Rab, Ral, and Rac, KRas4a/b may also activate Rap, Arf, and Rho through recruiting these previously unknown effector proteins. Investigation of these interactions could reveal new signaling cascade of KRas4a/b.

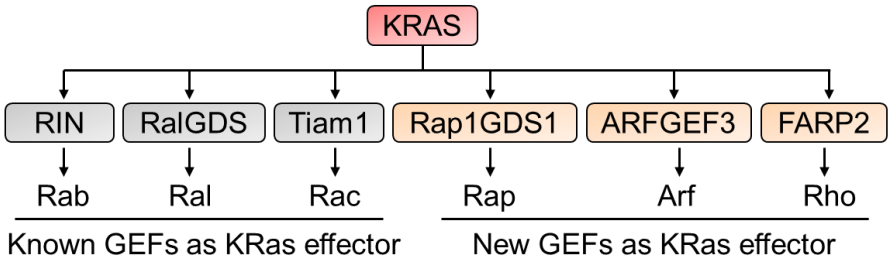

Figure 5.2. Potential KRas4a/b effector proteins that server as GEFs for other small GTPases.

In my thesis work, mTOR was identified as a KRas4a/b interacting protein. Several pieces of evidence together allow me to propose a unique KRas4a/b-mTOR complex model. In this model, KRas4a/b, mTOR, and mLST8 form a complex in the absence of raptor and rictor. However, the function of this complex is still unknown at this point. Since KRas4a/b-mTOR interaction does not seem to affect the phosphorylation of some well-studied mTOR substrates (**Figure 4.9**), it is likely that this new mTOR complex has different substrates from mTORC1 and mTORC2. To identify these new substrates, mTOR phosphorylome study with or without KRas4a/b can be performed. Knowing the substrates of KRas4a/b-mTOR complex could reveal the new signaling

functions of KRas and mTOR.

REFERENCES

1 Jiang, H. *et al.* SIRT6 regulates TNF-alpha secretion through hydrolysis of long-chain fatty acyl lysine. *Nature* **496**, 110-113, doi:10.1038/nature12038 (2013).

2 Zhong, L. *et al.* The histone deacetylase Sirt6 regulates glucose homeostasis via Hif1alpha. *Cell* **140**, 280-293, doi:10.1016/j.cell.2009.12.041 (2010).

3 Tao, R., Xiong, X., DePinho, R. A., Deng, C. X. & Dong, X. C. FoxO3 transcription factor and Sirt6 deacetylase regulate low density lipoprotein (LDL)-cholesterol homeostasis via control of the proprotein convertase subtilisin/kexin type 9 (Pcsk9) gene expression. *The Journal of biological chemistry* **288**, 29252-29259, doi:10.1074/jbc.M113.481473 (2013).

4 Tsai, F. D. *et al.* K-Ras4A splice variant is widely expressed in cancer and uses a hybrid membrane-targeting motif. *Proc Natl Acad Sci U S A* **112**, 779-784, doi:10.1073/pnas.1412811112 (2015).

5 Jang, H. *et al.* Mechanisms of membrane binding of small GTPase K-Ras4B farnesylated hypervariable region. *The Journal of biological chemistry* **290**, 9465-9477, doi:10.1074/jbc.M114.620724 (2015).

6 Kashiwagi, K. *et al.* Crystal structure of eukaryotic translation initiation factor 2B. *Nature* **531**, 122-125, doi:10.1038/nature16991 (2016).

7 Bos, J. L., Rehmann, H. & Wittinghofer, A. GEFs and GAPs: critical elements in the control of small G proteins. *Cell* **129**, 865-877, doi:10.1016/j.cell.2007.05.018 (2007).

APPENDIX A: PERMISSION FOR REPRODUCTION

Chapter 2: Reproduced with permission from Zhang, X. et al. Nat. Chem. Biol. 2016, 12, 614-620.

The publisher terms and conditions are available by accessing the website below:

http://www.nature.com/reprints/permission-requests.html

APPENDIX B: PERMISSION FOR REPRODUCTION

Chapter 3: Reproduced with permission from Zhang, X. et al. eLife 2017, 6, e25158.

The publisher terms and conditions are available by accessing the website below:

https://elifesciences.org/terms